INAUGURAL - DISSERTATION

zur Erlangung der Doktorwürde der Naturwissenschaftlich-Mathematischen Gesamtfakultät der Ruprecht-Karls-Universität Heidelberg

vorgelegt von:
Dipl. Chem. Franziska C. Schenk
geboren in: Würzburg

Tag der mündlichen Prüfung: 4. Mai 2016

Chemical Modification Strategies for the Preparation of Bioactive Interfaces

Gutachter:

Prof. Dr. Joachim P. Spatz

Prof. (apl.) Dr. Reiner Dahint

Abstract

Biomimetic systems and interfaces allow to understand and control cellular behavior in a well defined and reproducible manner. In this study three different strategies are developed to prepare such simplified, well-defined biomimetic materials. Firstly, a combination of click chemistry and gold thiol interactions allows the presentation of two distinct signaling molecules at controlled density and arrangement to investigate the cross-talk between two signaling molecules in cell culture. Secondly, the commonly used Ni^{2+}-NTA interaction with His_6-tagged proteins is substantially improved in its stability and inertness for protein immobilization on SAMs by replacing the Ni^{2+} ions with Co^{3+} in the complex. Thirdly, His_6-tagged proteins are stably tethered on TiO_2 nanoparticles for targeted delivery.

To produce dual functionalized gold nanostructured interfaces, first the presentation of a ligand of interest with azide functionality on glass substrates at controlled density is established. For this pirpose, alkyne terminated poly(ethylene glycol) (PEG) is covalently bound to glass through a silanization reaction and subsequently modified through copper catalyzed azide alkyne cycloaddition (CuAAC). The functionalization density can be statistically tuned through the coimmobilization of a methoxy-terminated PEG. The surface coating and its modification with the CuAAC is analyzed using fluorescence microscopy, XPS, an enzymatic digestion assay for the determination of the ligand density, QCM-D and in cell adhesion studies. This PEG coating is used in combination with the established gold nanostructured surfaces to generate orthogonally dual functionalized biomimetic interfaces where one of the ligands is attached to the PEG coating between the gold nanoparticles using the CuAAC and the second ligand is attached to the gold nanoparticles using the gold thiol interaction. These interfaces, which present two distinct ligands at controlled density and arrangement, are suitable to investigate the mutual influence of two signaling molecules on cell behavior. Exemplarily, the combined effect of the adhesion peptide cRGD and the synergy site PHSRN on REF fibroblast adhesion is investigated. While on neither of the monofunctionalized substrates the cells can attach, the cells adhere on the dual functionalized cRGD and PHSRN presenting interfaces.

The second part of this study deals with the stable immobilization of His-tagged proteins on NTA presenting surfaces using the cobalt(III) mediated interaction. The cobalt(III) complex is generated by first preforming the well-established cobalt(II) complex between NTA and His_6-tagged proteins and

the subsequent chemical oxidation of Co^{2+} to Co^{3+} with hydrogen peroxide. A comparison of the Ni(II) and Co(III) mediated interaction between NTA moieties and His_6-GFP reveals the lability of the Ni(II) and stability of the Co(III) complexes against high concentrations of competing ligands and washing off overtime. Further, also the resistance of the Co(III) mediated interaction against reducing agents is demonstrated. The oxidation step in this immobilization strategy can potentially harm the protein's activity and this has to be investigated case by case. To illustrate that this method can be used to immobilize functional protein, the His_6-tagged protein A is immobilized through the Co(III) mediated interaction and it is shown that the oxidation step dosen't influence the immunoglobulin binding activity.

In the third part the Co(III) mediated stable immobilization of His-tagged proteins is used to biofunctionalize TiO_2 nanoparticles. Here, the photocatalytic activity of TiO_2 is taken advantage of to perform the oxidation of Co(II) complexes between the chelating TETT surface coating on the TiO_2 nanoparticles and a His-tagged protein. The Co^{2+} ion loading capacity of the nanoparticles and their photocatalytic activity is characterized with a colorimetric assay, fluorescence studies using terephtahlic acid as radical detection reagent, absorbance measurements, DLS and zeta potential measurements proving the photo-mediated oxidation of coordinated Co^{2+} ions to Co^{3+}. Exemplarily, the stable immobilization of the model protein His_6-GFP and of the glycoprotein transferrin-His_6 is studied.

Kurzfassung

In den vergangenen Jahrzehnten wurden verschiedenste biomimetische Systeme zur Untersuchung grundlegender biologischer Vorgänge, zum Verständnis komplexer Zusammenhänge und zur gezielten Steuerung der Zellantwort entwickelt. Dennoch sind viele Fragestellungen unbeantwortet und der Bedarf an neuartigen biomimetischen Systemen zur Anwendung in der Grundlagenforschung und im biologischen sowie medizinischen Bereich ist ungebrochen. Im Rahmen dieser Studie werden drei unterschiedliche Funktionalisierungstrategien zur Herstellung biomimetischer Substrate verfolgt.

Im ersten Abschnitt wird die chemische Modifizierung endständiger Alkingruppen vor dem proteinabweisendem Hintergrund einer Polyethylenglycol (PEG) Monolage mit diversen organischen Aziden durch Kupfer-katalysierte Azid Alkin Cycloaddition (CuAAC) etabliert. Die Funktionalisierungdichte kann dabei je nach Bedarf durch simultane Verwendung eines zweiten PEGs mit endständiger Methoxygruppe angepasst werden. Die Oberflächenbeschichtung wird mittels Fluoreszenzmikroskopie, XPS, einer Analyse der Ligandendichte durch enzymatische Degradierung, QCM-D und einer Zelladhäsionsstudie charakterisiert. Durch Kombination dieses Ansatzes mit einem etabliertem Konzept zur Herstellung hexagonal angeordneter Goldnanopartikel entstehen dual funktionalisierte biomimetische Grenzflächen. Diese ermöglichen die Untersuchung der spezifischen Wechselwirkungen von Zellen mit zwei unterschiedlichen Signalmolekülen in definierter Konzentration und Anordnung, wie hier am Beispiel des Einflusses der Adhäsionssequenz RGD und der synergistischen Seite PHSRN auf das Adhäsionsverhalten von Fibroblasten gezeigt.

Im zweiten Abschnitt wird die Co(III) Ionen vermittelte stabile Anbindung von His_6-markierten Proteinen auf den Chelatliganden NTA präsentierenden Oberflächen abgehandelt. Die vorgeformten Co(II) Komplexe werden durch chemische Oxidation mit Wasserstoffperoxid in ihre entsprechenden Cobalt(III) Komplexe überführt. Ein Vergleich der Ni(II) und Co(III) vermittelten Wechselwirkung zwischen dem Chelatliganden und dem Protein offenbart die Labilität des ersteren und die Stabilität des letzteren gegenüber hohen Konzentrationen an konkurrierenden Komplexliganden. Mit Hinblick auf die Reversibilität der Oxidation der Cobaltzentren wird die Beständigkeit gegenüber Reduktionsmitteln untersucht und verifiziert. Ein wichtiger Aspekt ist darüberhinaus die Retention des zu immonbilisierenden Proteins in seiner biologisch aktiven Form. Dies ist besonders vor dem Hintergrund der chemischen Oxidation der Cobaltzentren und der Oxidationsanfälligkeit einiger Proteine zu bewerten.

Beispielhaft wird an dieser Stelle die Wechselwirkung von immobilisiertem Protein A mit Immunoglobulin betrachtet.

Der dritte Abschnitt der Studie fokussiert die Cobalt(III) vermittelte Anbindung von His-markierten Proteinen auf Titandioxid-Nanopartikeln unter Vorteilsnahme der photokatalytischen Eigenschaften von TiO_2 zur Oxidation vorgeformter Cobalt(II) Komplexe. Die Anbindung der His-markierten Proteinen erfolgt durch Co(II) vermittelte Wechselwirkung mit dem auf den TiO_2 Nanopartikeln angebundenem Chelator TETT und anschließende Photooxidation der vorgeformten Komplexe. Die Bindungskapazität für Co^{2+} Ionen und die photokatalytische Aktivität der TiO_2 Nanopartikel wird analysiert. Fluoreszenz-, Absorbanz- und Zeta-Potentialmessungen bestätigen die Oxidation oberflächennaher Co(II) Komplexe zu Co(III) durch Bestrahlung der Nanopartikel mit UV Licht. Dieses Konzept wird zur stabilen Anbindung von His-markierten Proteinen auf den TiO_2 Nanopartikel verwendet, wie hier exemplarisch für das Modellproteins His_6-GFP und das Glycoprotein Transferrin-His_6 dargestellt.

Danksagung

An dieser Stelle möchte ich die Gelegenheit nutzen all jenen zu danken, die zum Gelingen dieser Arbeit beigetragen haben.

Zuallererst möchte ich Prof. Joachim Spatz für sein Vertrauen und seine Unterstützung über die gesamte Zeit danken. Vielen Dank für die Gelegenheit dieses spannende, interdisziplinäre Thema verfolgen zu dürfen und all die Möglichkeiten die mir zur Verfügung standen.

Vielen herzlichen Dank auch an Prof. Reiner Dahint für seine bereitwillige Zusage Zweigutachter dieser Arbeit zu sein.

Mein besonderer Dank gilt Dr. Seraphine Wegner für die stete Unterstützung über all die Jahre hinweg, die Betreuung und konstruktive Diskussionen. Vielen Dank dir sowohl für die praktische Anleitung im Labor als auch für thematischen Erörterungen und das Korrekturlesen meiner Doktorarbeit. Und vor allem möchte ich dir für das angenehme und freundschaftliche Arbeitsklima danken. Nicht zu vergessen sind die schönen Gruppenausflüge und geselligen Abende.

Mein herzlicher Dank geht auch an die anderen Gruppenmitglieder der AG Wegner, die im Verlauf der Jahre erstaunlich gewachsen ist. Vielen Dank für die angenehme Arbeitsatmosphäre.

Des weiteren geht mein Dank an alle Spatzen und den "Heidelberger Zoo", mit dem zusammen die Arbeit immer unterhaltsam und lustig war und bei der Gesang - auch wenn ein Außenstehender es nur für schräge Geräusche halten möge - niemals fehlen durfte. Dir, liebes Böse möchte ich für alle deine Geduld bei meinen Fragen zu Biologie und Mikroskopie danken und deine stete Hilfsbereitschaft, wenn ich nicht mehr weiter wusste. Ganz lieben Dank an Christiane, die mich in jeder Situation aufgemuntert und mit Rat und Tat zur Seite stand. Ganz besonders möchte ich dir für deine Hilfe im Umgang mit LaTeX über die letzten Wochen und Monate hinweg danken und für das Korrekturlesen von Teilen dieser Arbeit. Dir, Julia, möchte ich für deine laute, schrille Art danken die stets sehr unterhaltsam war und das Korrekturlesen von Teilen dieser Arbeit in allerletzter Minute. Vielen Dank an all die anderen 'Zootiere', die das Arbeiten so angenehm gestaltet haben.

Vielen Dank auch an unsere beiden guten Seelen Sigrid und Helmi, die immer hilfsbereit und verständnisvoll waren, wenn ich mal eben schnell noch irgendetwas brauchte.

Auch möchte ich mich bei Tamas bedanken für seine Anleitung am AFM und all sein Wissen, das er immer gern mit einem teilt.

Nicht unerwähnt bleiben soll hier das Zutun von Janis, der mir mit der Bedienung des REM geholfen hat und an Maria Sycha und Kersten Hahn, die sich liebevoll der Präparation und Mikroskopie meiner TEM Proben angenommen haben. Vielen Dank an euch!

Nicht zuletzt möchte ich meiner Familie für die Unterstützung über all die Jahre hinweg während des Studium und der Promotion danken!

Abbreviations

A	absorbance
Ac	acetyl
aq	aqueous
BSA	bovine serum albumin
CME	cellulose mixed ester
Cp*	pentamethylcyclopentadienyl
CPS	counts per second
CuAAC	copper catalyzed azide alkyne cycloaddition
Da	dalton
DABCO	1,4-diazabicyclo[2.2.2]octane
DAPI	4',6-diamidino-2-phenylindole
dd water	doubly deionized water
DFT	density functional theory
DLS	dynamic light scattering
EDC	*N*-(3-dimethylaminopropyl)-*N'*-ethylcarbodiimide
DMEM	Dulbecco's modified eagle medium
DMF	*N*,*N*-dimethylformamide
E. coli	*Escherichia coli*
EDTA	ethylenediaminetetraacetic acid
EG	ethylene glycol
EM	electron microscopy
en	1,2-diaminoethane (ethylenediamine)
eq.	equivalent
EtOH	ethanol
eV	electronvolt
GFP	green fluorescent protein
HEDTA	*N*-(2-hydroxyethyl)ethylenediamine-*N*,*N'*,*N'*-triacetic acid
His	histidine
HRP	horseradish peroxidase
HS-cRGD	cyclic[RGDfK(3-mercaptopropionyl-aminohexanoic acid)]
HS-NTA	HS-$(CH_2)_{11}$-EG_3-NTA
2-HTA	2-hydroxyterephthalic acid
Hz	hertz [1/s]
IDA	iminodiacetic acid

YFP	yellow fluorescent protein
LB medium	lysogeny broth medium
Me	methyl
MOPS	3-(*N*-morpholino)propanesulfonic acid)
MWCO	molecular weight cut-off
NEAA	non-essential amino acid
NHC	N-heterocyclic carbene
NHS	*N*-hydroxysuccinimide
NMR	nuclear magnetic resonance spectroscopy
NTA	nitrilotriacetic acid
PBS	phosphate buffered saline
PEG	poly (ethylene glycol)
PFA	*para*-formaldehyde
Phe	phenylalanine
PHSRN	5 amino acid sequence proline-histidine-serine-arginine-asparagine
PLL-g-PEG	poly-*L*-lysine-graft-poly(ethylene glycol)
ppm	parts per million
PS	polystyrene
P2VP	poly(2-vinylpyridine)
QCM-D	quartz crystal microbalance with dissipation
REF	rat embryonic fibroblast
REF YFP-paxillin	yellow fluorescent protein labelled paxillin expressing rat embryonic fibroblasts
RGD	3 amino acid sequence arginine-glycine-aspartic acid
rt	room temperature
SAM	self assembled monolayer
SDS-PAGE	sodium dodecyl sulfate polyacrylamide gel electrophoresis
SEM	scanning electron microscopy
SHE	standard hydrogen electrode
TA	terephthalic acid
TBS-T	Tris buffer saline containing tween 20
TRITC	tetramethylrhodamine B isothiocyanate
UV	ultraviolet
vis	visible
vol%	volume precent
w/v%	weight/volume percent
XPS	X-ray photoelectron spectroscopy

Chemical structures

5/6-carboxyrhodamine 110-EG_3-azide

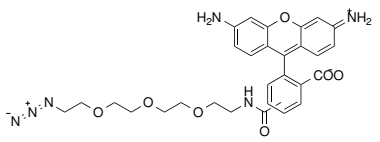

3-azidomethyl-5-iodopyridine

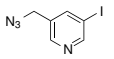

biotin-EG_3-azide

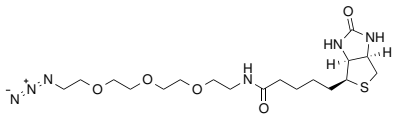

N^{α},N^{α}-bis(carboxymethyl)-*L*-azidolysine

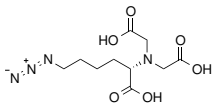

cyclic(RGDfE)K(N_3)-NH_2

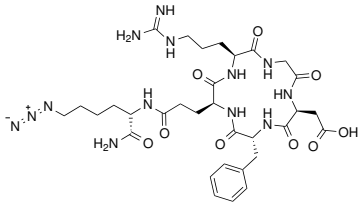

K(N_3)PHSRN

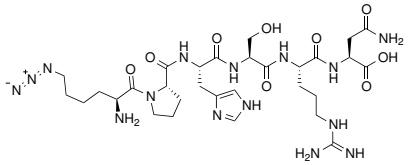

cyclic[RGDfK(3-mercaptopropionyl-aminohexanoic acid)]

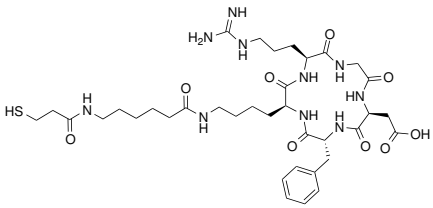

HS-$(CH_2)_{11}$-EG_3-NTA

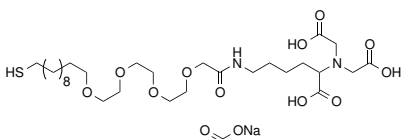

N-(trimethoxysilylpropyl)ethylene diamine triacetic acid trisodium salt

List of Figures

Contents

Chapter 1

Introduction

1.1 Immobilization strategies of bioactive molecules

Cells respond to their environment through highly complex interactions. These interactions between cells and their surrounding have not a unilateral but a bidirectional character meaning that not only the physical, chemical and biological properties of the environment influence the cell behavior by inducing diverse signaling cascades but also the cell can modify its environment actively. To investigate and understand the influence of individual factors much effort has been put into preparing simplified model systems.

In the last decades numerous biomimetic systems were developed using diverse immobilization strategies for the modification of substrates with proteins, peptides and small signaling molecules. The variety of different immobilization techniques can be classified into categories using criteria like the specificity and the bond stability, for example. Distinguishing between specific and nonspecific immobilization, as well as covalent and noncovalent tethering strategies results in the following four categories: I. nonspecific, noncovalent immobilization, II. nonspecific, covalent immobilization, III. specific, noncovalent immobilization, and IV. specific, covalent immobilization (Fig. 1.1).[3] The advantages and disadvantages of the different strategies are briefly discussed in the following section.

Nonspecific, noncovalent immobilization strategies are characterized by simple, unpretentious and cost-efficient methods. The best known procedure is the physical adsorption of proteins on substrates. The interaction between protein and surface is achieved through weak interactions like hydrophobic interactions, electrostatic interactions, van-der-Waals interactions and hydrogen bonds. However, this immobilization strategy results generally in a disordered arrangement of the protein on the surface and the orientation of the protein relative to the surface can not be controlled. Additionally, it is challenging to determine the number of accessible functional groups making it difficult to characterize such surfaces. Physisorption of proteins on surfaces also commonly leads to conformational changes up to partial or complete denaturation of the protein, which potentially causes a reduction or loss of protein activity

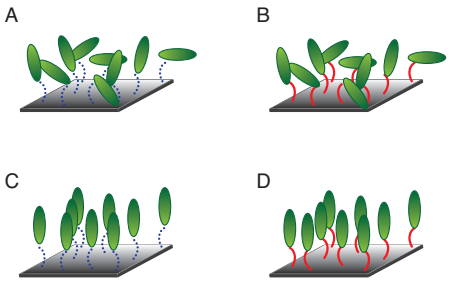

Figure 1.1: Schematic presentation of the different immobilization strategies. **A.** Nonspecific, noncovalent immobilization, **B.** nonspecific, covalent immobilization, **C.** site-specific, noncovalent immobilization, and **D.** site-specific, covalent immobilization. The ligand is symbolized through a green ellipse, noncovalent interactions as blue dotted lines and covalent bonds as red solid lines. Adopted from Redeker *et al.*[3]

as changes in the structure of the binding site or related regions occur. An additional drawback of the surface functionalization through physical adsorption is the tendency towards desorption of the protein over long-term incubation in liquid. Despite these disadvantages, this approach is successfully and widely used for the immobilization of different proteins. Particularly, extracellular matrix proteins like fibronectin are commonly adsorbed on surfaces mimicking the natural environment of cells for cell adhesion and migration studies[4, 5] and wound healing assays[6].

A more stable option for protein immobilization and surface modification are the **nonspecific, covalent immobilization** strategies. Methods belonging to this category profit from the higher stability due to the covalent binding of the ligand to the substrate. This requires, that the desired ligand has chemical functional groups which can be reacted with complementary moieties on the surface. Ideally, the coupling reaction conditions should resemble physiological conditions; this is particularly important for the immobilization of sensitive molecules like proteins. In numerous protein immobilization protocols the inherent functional groups of the amino acid side chains or the termini are used for covalent attachment. These include the amine groups (from lysine and the N-terminus), hydroxyl functionalities (from serine and threonine), thiol moieties (from cysteine) and carboxylic acids (from glutamic acid, asparitic acid and the C-terminus).[3, 7] The most commonly used methods include the coupling of amine groups either to *N*-hydroxysuccinimide (NHS) esters or carboxylic acids activated through *N*-(3-dimethylaminopropyl)-*N'*-ethylcarbodiimide (EDC), EDC/NHS or EDC/sulfo-NHS chemistry (Fig. 1.2). Thiols are widely immobilized on surfaces through nucleophilic addition to maleimides and vinyl sulfones, formation of disulfide bonds or nucleophilic substitution of haloacetyl groups. Carboxylic acids are activated with *N,N'*-dicyclohexylcarbodiimide (DCC) or EDC and coupled to amines. As a certain amino acid or functional group is normally multiple times present in a protein, random orientations of the protein on the surface are obtained with

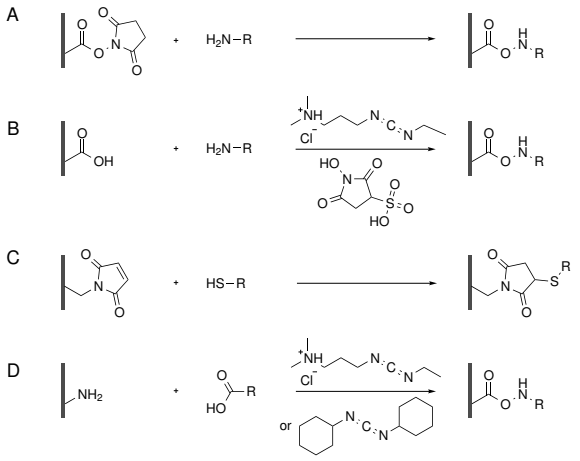

Figure 1.2: Nonspecific, covalent immobilization strategies. Coupling of a ligand with a primary amine to a **A.** NHS ester or **B.** EDC/sulfo-NHS activated carboxylic acid. **C.** Chemical conjugation of a sulfhydryl to a maleimide and **D.** activation of carboxylic acid with EDC or DCC for conjugation with an amine.

these immobilization strategies. Although, depending on the reaction partners and conditions a preferred orientation of the protein on the surface might be achieved.

In cases where it is important to control the orientation of the ligand on the surface site-specific immobilization strategies are demanded. **Specific, noncovalent immobilization** is based on the specific interaction of a functional moiety present uniquely in the ligand (or protein) with a complementary functionality at the substrate in a noncovalent manner. These immobilization strategies are generally more costly and time-consuming compared to the methods mentioned before due to the selective introduction of functional moieties into the ligand. Many approaches take advantage of affinity based interactions between complementary biomolecules like the interaction between antigens and antibodies, complementary DNA strands, (strept)avidin and biotin, or polyhistidine sequences and divalent metal ions (Fig. 1.3). For the antigen antibody interaction synthetic epitopes of antigens are designed and the recognition between these epitopes and corresponding antibodies are used for immobilization. Similarly, the highly specific interaction between complementary DNA strands through Watson-Crick base pairing[8] is exploited to link ligands to a surface. In the case of the (strept)avidin biotin interaction[9], (strept)avidin functions as an intermediary link between two biotin groups, of which one is attached to the surface and the other is part of the ligand that is immobilized. The interaction of divalent transition like metal ions like Ni^{2+}, Cu^{2+}, Zn^{2+} and Co^{2+} with polyhistidine tagged proteins is exploited for ligand immobilization on surfaces decorated with chelating groups like nitrilotriacetic acid (NTA). This immobilization strategy is particularly popular due to numerous libraries of His-tagged proteins and commercially available NTA modified small molecules

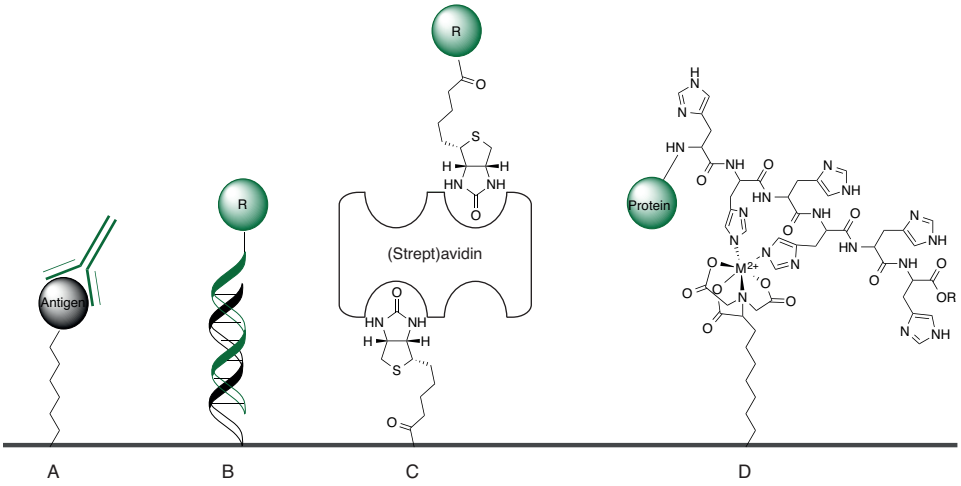

Figure 1.3: Site-specific, noncovalent interactions between **A.** antigen and antibody, **B.** complementary DNA strands, **C.** two biotinylated ligands through (strept)avidin and **D.** His_6-tagged protein and NTA through a divalent metal ion.

and materials. Whereas orientation of the ligand is achieved in a highly controlled manner the lifetime of the noncovalent interactions can be a drawback depending on the application. Affinity tag mediated interactions can also be used for a two step immobilization procedure, in which the ligand is first orientated on the surface through a noncovalent interaction and then covalently coupled to the surface in an orientated manner.[10]

Specific, covalent immobilization combines the control over the orientation of the ligand on the surface through the site-specific interaction and the high stability of the covalent bond. This approach requires the implementation a single functional group at a site-specific location in the ligand, which is coupled then to the reactive counterpart on the surface. For controlled immobilization the functional group should ideally be bioorthogonal, meaning that it dosen't compete or interfere with endogenous functional groups of the ligand and the reactive counterpart. In recent years the so called click chemistry concept[11] enjoys great popularity, especially because of the compatibility of the reactions with biological molecules like proteins and the (almost always) bioorthogonality of the functionalities used for immobilization. The click reactions include the copper-catalyzed or ring-strain promoted azide alkyne cycloaddition, Diels-Alder reactions, thiol ene reactions and Staudinger ligations. Further, for the immobilization of biomolecules, especially proteins, enzymatically mediated tethering is possible. In these approaches short peptide sequences that are recognized by a ligating enzyme are inserted in the protein and through catalytic reaction of the enzyme, the protein is covalently linked to the substrate with the complementary reaction partner. Also enzymes themselves can serve as a connecting link between proteins and the desired coupling partner. Therefore the protein of interest is fused to an enzyme which then

reacts with its (modified) substrate under formation of a covalent linkage. For example, the transpeptidase sortase connects two peptide fragments by cleaving a peptide bond in the enzyme recognition motif and forming a new peptide bond to the second peptide fragment via nucleophilic substitution. The SNAP-tag is an enzymatic tag which transfers an alkyl group from its substrate to an inherent cysteine residue and thereby links the attached protein to the desired label or surface through a thioether.[12] Analogously, the Halo-tag reacts with alkyl halide substrates under formation of a covalent ester bond. A crucial mutation in its catalytic site (substitution of His^{272} residue with Phe) results in the efficient and specific trapping of this reaction intermediate and prevents the bond dissociation through nucleophilic substitution.[13]

In literature countless examples are published taking advantage of one immobilization strategy or another to present biologically active molecules on a substrate and investigate the interaction with cells. However, for many cell receptor - ligand interactions cell adhesion is a prerequisite, which opens the need for biomimetic systems presenting more than one signaling molecule. This can be achieved by mixing the two desired ligands in a defined ratio and immobilizing both through the same coupling strategy. For example, Ochsenhirt *et al.* prepared Langmuir-Blodgett supported films from PEG-conjugated amphiphiles and two types of lipid-conjugated peptides containing either either the adhesion peptide RGD or the synergy site PHSRN and investigated the mutual influence of the peptides on cell spreading.[14] Similarly, activated titanium surfaces were first silanized with (3-chloropropyl)triethoxysilane and subsequently coupled to a mixture of two peptides through nucleophilic substitution by Chen *et al.*.[15] The gradual reduction of quinone presenting thiol SAMs on gold results in the formation of primary amines on the surface, which were used as anchoring points for proteins through a bifunctional NHS-maleimide linker by Lee *et al.*[16]. In this study, surfaces presenting two peptide gradients in opposed direction are developed. Azagarsamy *et al.*[17] utilized the simultaneous (cross)linking of two cysteine containing peptides either a RDGS and or a matrix metalloproteinase (MMP) degradable peptide sequence with an 4-arm PEG tetravinyl sulfone and prepared bifunctional hydrogels through Michael addition. The same group also developed off-stoichiometric hydrogels using an 4-arm PEG tetranorbornene and a peptide linker with two cysteines and an additional chymotrypsin cutting site through thiol ene reaction. The remaining norbornene functionalities are spatially photopatterend with a cysteine terminated RGDS by light induced thiol ene reaction. However, these systems for creating biomimetic substrates lack spatial control over the ligand distribution. Moreover, the average surface concentration of the two ligands can only be regulated with respect to each other. More recent approaches use two orthogonal coupling strategies for the immobilization of two signaling molecules. Thereby, independent control over the surface density of the two distinct ligands is achieved. For example, Ma *et al.* created two-dimensional gradients of two orthogonally reactive silanes on silicon or glass substrates and was capable to subsequent modify each separately through orthogonal click reactions (thiol ene reaction and azide alkyne coupling).[18] Further, Azagarsamy *et al.*[17] de-

veloped hydrogels by the strain promoted azide alkyne cycloaddition (SPAAC) of an azide terminated 4-arm PEG and a dicyclooctyne MMP degradeable peptide with an additional alkene functionality. Subsequently, the alkene groups are reacted with thiolated biomolecules through spatiotemporal photopatterning. Cai *et al.*[19] investigated the T-cell activation on bifunctional substrates mimicking the immunological synapse. AuPd nanodots on glass substrates are functionalized consecutively with a thiol biotin linker, streptavidin and a biotinylated UCHT1 Fab antibody, which interacts with the T-cell receptor. The PEG background is decorated with the His-tagged intercellular adhesion molecule-1 (ICAM-1) through Ni^{2+}-NTA groups. In a similar approach Declassian *et al.* probed T-cell activation on dual functionalized nanoarrays where the immunoreceptor stimulating antibody UCHT1 $F(ab')_2$ is immobilized on gold nanoparticels and the integrin ligand ICAM-1 is bound to biotinylated PLL-g-PEG through streptavidin.[20] Hudalla and Murphy[21] described the formation of ethylene glycol alkanethiolates SAMs presenting two orthogonally reactive functional groups, namely carboxylic acid and azide. These are orthogonally functionalized with an amine terminated peptide through EDC/NHS coupling and an alkyne terminated peptide though CuAAC, respectively and used to study the adhesion of stem cells. While some of these approaches benefit from the control over the spatial arrangement of the signaling molecule, the noncovalent tethering of one or the other ligand may result in limited stability of the surface coating. Other modification strategies with a statistical distribution of the signaling molecules over the substrate lack control over the spatial arrangement.

The following sections address the site-specific immobilization strategies relevant in the context of this work. First, the formation of self-assembled monolayers (SAMs) of thiols on gold is focused, followed by the concept of click chemistry and metal ion mediated immobilization of His-tagged proteins on surfaces presenting chelating groups.

1.2 Surface modification based on gold-thiol chemistry

1.2.1 Self assembly of thiols on gold

The interaction of thiols, thiolates and disulfides with gold surfaces is widely applied for surface modification for diverse application. To characterize the nature of the sulfur anchoring group and the interaction with the gold surface, experimental studies[22, 23] and theoretical calculations[24, 25] were preformed. The strong interaction of thiols on gold is based on the formation of thiolate-gold bonds with a covalent binding character; this requires the abstraction of a proton from the sulfhydryl functional group and leads to the generation of a thiyl radical ($RS\cdot$).[26, 27] In their protonated form thiols interacte with gold in a weaker, coordination bond like type through the long pair of the sulfur atom. Accordingly, the strength of the sulfur gold interaction depends on the experimental preparation conditions. The binding strength of single thiol gold

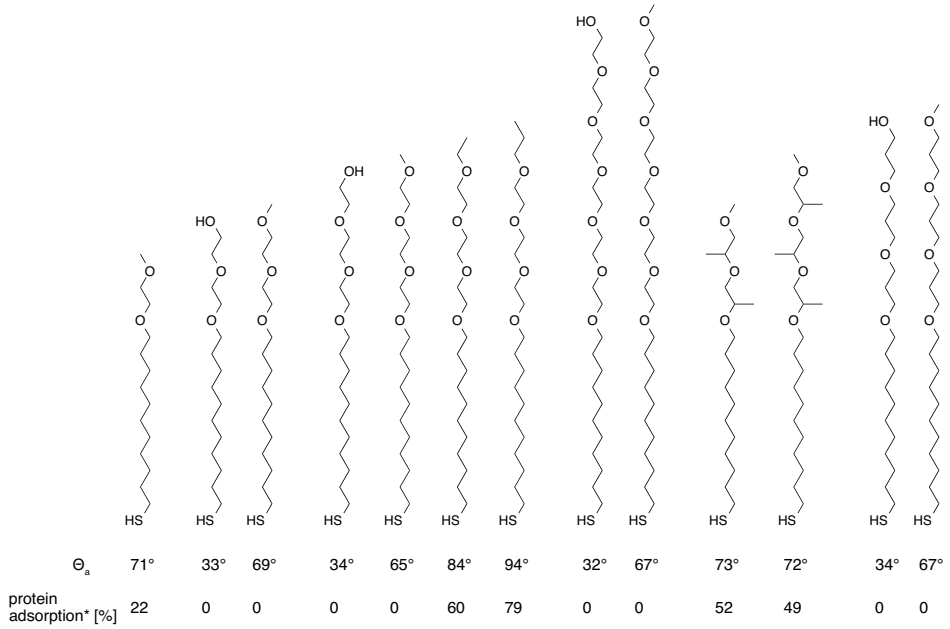

Figure 1.4: Advancing water contact angle Θ_a and relative protein adsorption on SAMs of the corresponding oligoether alkane thiol on gold according to Herrwerth *et al.*[29] (*Relative amount of adsorbed fibrinogen determined by ellipsometry and normalized to the amount of adsorbed protein on a hexadecanethiol SAM on gold).

interactions is enhanced on oxidized gold substrates or at higher pH.[23]

Adsorption of organic thiols from solution on gold surfaces results in the formation of monolayers by self assembly.[28] The value and utility of absorbed monolayers of thiols on gold is the inertness of metal gold, the well-ordered, orientated packing of alkanethiols on gold and the variability in the presentation of functional groups. The compatibility with functional groups is constrained to those that do not compete with the thiol in the coordination to gold or react with thiols and have a sufficiently low geometric dimensions not preventing the close packing. Thus, this reliable method is used for all kinds of surface coatings and for the preparation of biomimetic systems. Depending on the application it may be important to prevent nonspecific interactions with the surface coating.

In a detailed study by Herrwerth *et al.*[29] factors that contribute to protein resistance of oligoether SAMs are investigated (Fig. 1.4). Key aspects are the hydrophilicity of the internal and the terminal units as well as the lateral packing density. Protein resistance necessitates the coordination of water in the interior and on the surface of the polyether SAM. Further, for methoxy terminated oligo(ethylene glycol) alkanethiol SAMs on gold at least two ethylene glycol units are necessary to resist protein adsorption. The additional methyl groups of oligo(propylene glycol) prevent the formation of a dense SAM and thus, these SAMs are not passivating. Interestingly, SAMs with comparable

good passivating properties can be achieved by using either hydrophilic hydroxy terminated or hydrophobic methoxy terminated oligoether alkane thiols. Besides brushed SAMs of oligo(ethylene glycol) alkane thiols on gold, high molecular weight PEGs are used to prevent nonspecific protein adsorption. In contrast, the protein resistance of the PEGs[30] is based on steric repulsion between the protein and the PEG. Dehydration and confinement of the long polymer chains with high conformational freedom is energetically unfavored.

SAMs of functionalized alkanethiols on gold serve as a platform to investigate the influence of adsorbed protein or covalently attached bioactive peptides on cell behavior like cell adhesion, proliferation and differentiation.[31] Further, other extracellular matrix components like hyaluronon are immobilized on substrates through self-assembly of thiols on gold.[32]

1.2.2 Presenting ligands in defined order: gold nanostructured surfaces

Besides the formation of thiol SAMs on homogenous coated gold surfaces, the presentation of the desired ligand in defined structured areas with control on the nanoscale is achieved by nanolithography. The block copolymer micellar nanolithography (BCMN) established by Spatz and coworkers presents an ideal platform to investigate interactions of cells with specific ligands in defined order and variable spacings. With BCMN ordered gold nanoparticles in a quasi-hexagonal array are produced, where the particle size (hight) can be varied between 1 - 15 nm and the interparticle spacing between 30 - 250 nm.[33, 34] The technique is based on the self-assembly of block copolymer micelles, which are loaded with a metal salt. The block copolymer consists of a hydrophobic polystyrene (PS) and a hydrophilic poly(2-vinylpyridine) (P2VP) unit (Fig. 1.5) and is dissolved in a apolar solvent (typically toluene or *para*-xylene) at a concentration above the critical micelle concentration resulting in reverse micelles formation. According to their hydrophilicity/hydrophobicity the hydrophilic P2VP forms the core of the micelle which is surrounded by a hydrophobic PS layer. Subsequently, the hydrophilic core of the micelle is loaded with metal salts, like $HAuCl_4$.

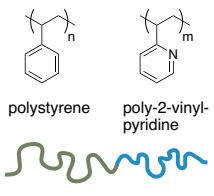

Figure 1.5: The diblock copolymer consists of a hydrophobic polystyrene block and a hydrophilic poly-2-vinylpyridine block.

The micelles are coated on a substrate by either dip coating or spin coating. For dip coating a freshly cleaned glass substrate is immersed into the micellar solution perpendicularly and retracted with constant velocity. In a first step

the hydrophilic P2VP probably covers the hydrophilic glass substrate followed by the adsorption of entire micelles during the retraction of the sample from the solution (Fig. 1.6).[35] Subsequently, the dried metal salt loaded micelles on the substrate are subjected to a plasma treatment. Thereby, all of the polymer is removed and the gold salt is reduced to elementary gold creating a quasi-hexagonal array of gold nanoparticles. The distance between individual adjacent gold nanoparticles can be adjusted from 30 to 250 nm through the choice of the diblock copolymer, especially the size of the hydrophobic PS unit[33, 36, 37], the total polymer concentration[34, 38] and the retraction velocity[34, 38, 39, 40]. Furthermore, the size of the gold nanoparticles can be varied from 1 to 15 nm according to the extend of the loading of the micellar core with metal salt.[41]

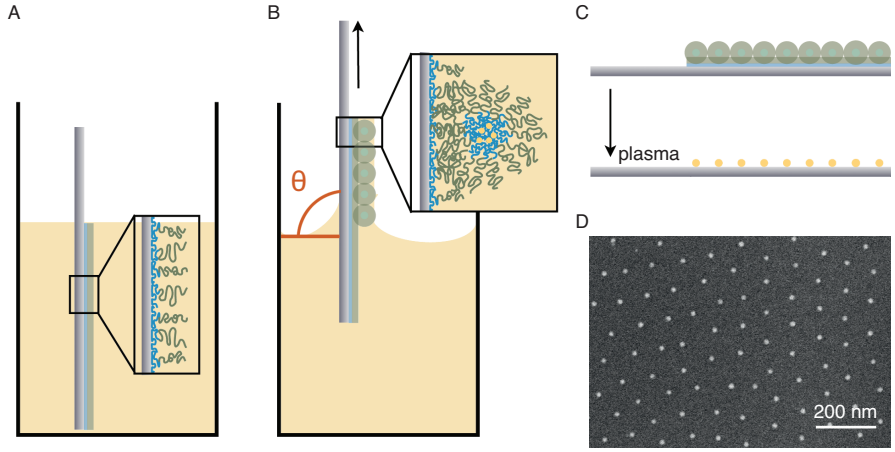

Figure 1.6: Preparation of gold nanostructured surfaces. **A.** The block copolymer adsorbs on the hydrophilic glass surfaces by its hydrophilic P2VP unit. **B.** Upon perpendicular retraction ($\theta = 90°$) of the glass substrate from the solution the solvent evaporates and the gold ion loaded block copolymer micelles arrange in a quasi-hexagonal order on the surface. **C.** The dried surfaces are treated with hydrogen plasma to remove the remaining polymer and reduce the metal ions to elementary gold leaving gold nanoparticles in a quasi-hexagonal array on the substrate behind. **D.** Scanning electron micrograph of quasi-hexagonal arranged gold nanoparticles with an average interparticle distance of 100 nm on a glass substrate. Adopted from H. Boehm[35].

These arrays of gold nanoparticles on different substrates are particularly suitable for cell adhesion studies. The gold nanoparticles serve as anchoring points for specific cell receptor ligands with thiol functional groups for immobilization in a defined arrangement by gold thiol chemistry. For this purpose, RGD containing ligands and peptidomimetics are used, which interact with cells via their integrins. Integrins are transmembrane proteins consisting of a α and β subunit that link to the cytoskeleton and are involved in the environmental sensing, cell adhesion, migration and proliferation.[42] In addition, unspecific interactions between cells or proteins and the substrate are prevented through a protein repellent PEG coating[43] in the intermediate space between the nanoparticles, which is covalently attached to the glass substrate.

The small size of the gold nanoparticles <10 nm provides a unique platform to investigate cellular adhesion. Although several signaling molecules bind to a single gold nanoparticle only one integrin receptor can interact with the signaling molecules per nanoparticle due to the spatial dimension of the integrin receptor, which is 8 -12 nm.[44] These distinctive features of this platform are used in the investigation of integrin mediated adhesion[44], with focus on cell spreading and molecular composition of focal adhesion complexes[45] and focal adhesion dynamics[46]. These studies reveal stable integrin mediated cell adhesion along with the development of mature focal adhesions on surfaces with an interparticle distance of 58 nm but not at higher distances (73 nm, 110 nm or 108 nm). Furthermore, combining the BCMN technique with classical e-beam lithography allows to produce micro-nanostructured surfaces. These surfaces are used to determine the minimum number of activated integrins required for cell adhesion and focal contacts to form.[47] On the other hand, gradients in the interparticle distance of gold nanoparticles are produced with BCMN by altering the retraction speed. Such surfaces are used to investigate the sensitivity of the cells towards ligand gradients and the effect of these on cell polarization.[38, 39]

1.3 Click chemistry

1.3.1 The conceptional background

The concept of "click chemistry"[11] coined by H. Kolb, M. Finn and K. Sharpless encompasses a class of efficient chemical reactions for the synthesis from modular blocks (mainly through heteroatom links C-X-C) inspired by nature. Criteria for the classification of a reaction as such include the modular character, wide scope of application, high yields and stereospecificity. Therefore, processes require simple reaction conditions (ideally insensitive to oxygen or water), readily available starting reagents, the use of either no or benign (like water) or easy to remove solvents and simple product isolation (and purification) by nonchromatographic methods from harmless byproducts. In order to meet this criteria click reactions are characterized through a high thermodynamic driving force (usually greater than 20 kcal/mol). The spectrum of click reactions comprises ring-opening reactions of strained heterocyclic electrophiles (for example epoxides, aziridines,) through nucleophilic substitution, 'non-aldol' type carbonyl chemistry, oxidative additions to unsaturated C-C bonds (such as epoxidation and dihydroxylation) and cycloadditions of unsaturated species like 1,3-dipolar cycloadditions and Diels-Alder reactions (Fig. 1.7).

Particularly efficient are pure fusion processes in which no byproducts are formed and which therefore have highest atom economy. These include, among others, the previously mentioned nucleophilic ring-opening reactions and cycloadditions. The nucleophilic opening of strained rings is stereospecific, often highly regioselective and nearly quantitative. Particularly, three membered ring systems are preferred due to the disfavored competing elimination process Ad-

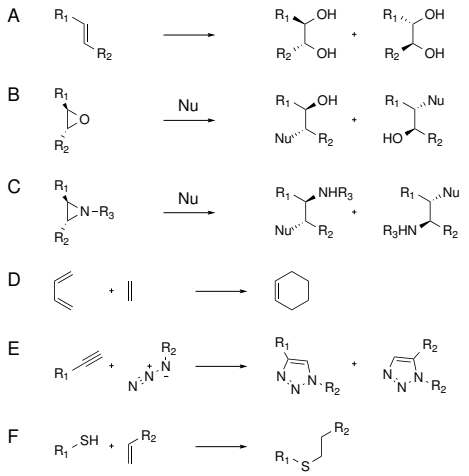

Figure 1.7: Exemplary click reactions showing the **A.** dihydroxylation of olefins, nucleophilic opening of ring-strained **B.** epoxides and **C.** aziridines, **D.** the Diels-Alder reaction, **E.** the Huisgen 1,3-dipolar cycloaddition and **F** (radicalic or base/nucleophile-mediated) the thiol ene reaction.

ditionally, regioselectivity can be adjusted in such reactions by the choice of the solvent and the substitution pattern of aziridines and aziridinium ions. The fusion of two unsaturated compounds (containing heteroatoms) in cycloaddition reactions through the formation of new σ bonds (without breaking already existing σ bonds) results in easy and convenient synthesis for a broad range of 5- and 6-membered heterocycles.

Click chemistry is widely used in many fields of research to produce biocompatible materials including polymerdesign[48], polymer and material science [49], manufacturing of cell culture scaffolds[17], biofunctionalization of substrates[50] and labeling of biomolecules[51] (such as proteins, sugars, lipids, DNA and RNA).

1.3.2 Copper catalyzed azide alkyne cycloaddition

The copper catalyzed azide alkyne cycloaddition is a variant of the Huisgen 1,3-dipolar cycloaddition using Cu(I) as catalyst. Its easy implementation, good yields and high tolerance towards functional groups and solvents contributes to its popularity in wide areas of chemistry. In contrast to the uncatalyzed reaction, in this process solely the 1,4-disubstituted 1,2,3-triazole is formed but not the 1,5-disubstituted regioisomer. The Cu(I) catalyst promotes a non-concerted, complex, multistage reaction sequence, with an strongly increase in the reaction rate (10^7-10^8 fold rate acceleration compared to the uncatalyzed, thermal process[52]).

A first DFT study by Himo *et al.* proposed a reaction mechanism that involves mononuclear copper complexes as active species in the catalytic cycle.[52] In this mechanism, a Cu(I) acetylide is formed (via a π-alkyne copper complex intermediate), followed by the coordination of the azide to the copper atom

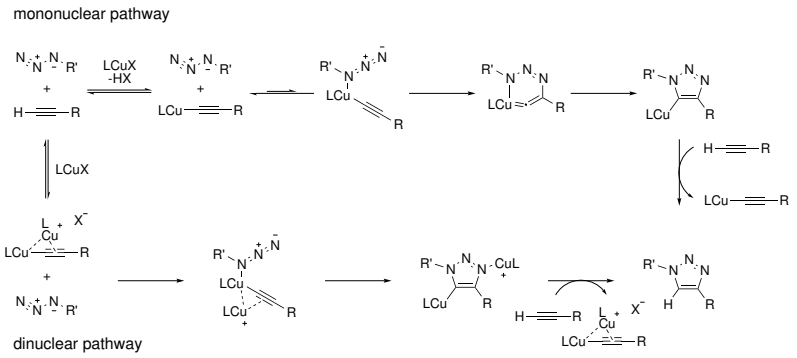

Figure 1.8: Postulated mechanism for CuAAC reaction. Although both pathways are involved in the CuAAC reaction mechanism the dinuclear pathway is favored over the mononuclear. Adapted from Makarem *et al.*[53] and Jin *et al.*[54]

through its nitrogen proximal to carbon (Fig. 1.8). In the key step a C-N bond is formed between the terminal nitrogen of the azide and the β-carbon of the copper(I) acetylide resulting in a six-membered metallacycle. Ring contraction leads to a 5-triazoyl copper intermediate and the triazol is released through proteolysis. However, a more recent DFT study by Hein and Forkin indicate the contribution of dinuclear Cu(I) acetylides in the reaction mechanism.[55] Lately, Makarem *et al.*[53] investigated the coordination mode of copper atoms and acetylide ligands of an isolated, molecularly defined dicationic hexa-NHC octacopper hexaacetylide clusterkomplex by x-ray diffraction. This cluster serves as catalyst resting state, which releases dinuclear copper species upon addition of acid. The dinuclear copper species has higher catalytic activity in CuAAC than to the cluster itself supporting the identification of dinuclear copper complexes as catalytically active species. Furthermore, Jin *et al.*[54] succeeded in the isolation of a cationic π,σ-bis(copper) acetylide and a 3,5-dimetallated-1,2,3-triazole complex as key intermediates in the reaction cycle. Although both mononuclear and dinuclear copper species are involved in the catalytic cycles, the dinuclear pathway is favored (Fig. 1.8).

Besides the Cu(I) catalyzed reaction there are other catalyzed versions of the [3+2] Huisgen 1,3-dipolar cycloaddition like the ring-strain promoted alternative and the ruthenium catalyzed reaction. For the strain promoted version cyclooctyne derivatives are used instead of linear alkynes and these provide the necessary ring strain (due to bond angle deformation) for the rapid reaction process yielding both regioisomers.[[56]] As opposed to the copper catalyzed conversion the ruthenium catalyzed reaction using Cp*RuCl(PPh_3) as catalyst results in the formation of the complementary regioisomer, a 1,5-disubstituted 1,2,3-triazole.[[57]] Further, not only terminal alkynes but also internal alkynes can be converted into the corresponding 1,4,5-trisubstituted 1,2,3-triazoles through ruthenium catalyzed azide alkyne cycloaddition.

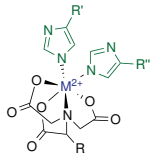

Figure 1.9: Illustration of NTA-M^{2+}-His_2 complex. The chelator NTA (black) binds to four coordination sites of the divalent metal ion M^{2+} (blue) and the histidine ligands (green) to two other coordination sites.

1.4 Metal ion mediated interactions as a tool for ligand and protein immobilization

1.4.1 The interaction of polyhistidine with Ni^{2+}-NTA complexes

The interaction of histidine rich protein regions or implemented short polyhistidine sequences with divalent metal ions (Ni^{2+}, Cu^{2+}, Zn^{2+}, Co^{2+}) is taken advantage of for the (temporarily) immobilization of the protein on chelator presenting substrates. In 1975 Porath *et al.* established protein purification based on the interaction between proteins and divalent metal ions (Cu^{2+}, Zn^{2+}, Ni^{2+}, Mn^{2+}) coordinated by the surface bound chelator iminodiacetic acid (IDA).[58] In this context, Hochuli *et al.* developed a nitrilotriacetic acid (NTA) based chelator with beneficial properties for reversible protein binding, namely a sufficient tight anchoring of the metal ion and adequate free coordination sites for protein binding.[59] Moreover, fusion of a oligohistidine tags to the protein of interest enhances the selective interaction.[60]. The most frequently used approach is based on the interplay between His_6-tagged proteins, NTA as chelator and Ni^{2+} as mediator ions. In these complexes four of the six coordination sites of the Ni^{2+} ion are occupied by the three carboxylic acid functional groups and the tertiary amine of the NTA. The remaining two coordination sites are coordinated through imidazole nitrogens from the histidine side chains (Fig. 1.9).

In addition to the commonly used interaction between His_6-tagged proteins and NTA strategies based on other types of His-tags[61, 62] and multi NTA tethers[63, 64, 65] have been explored. For example, in a systematic study by Knecht *et al.*[61] the binding affinity of linear oligohistidine peptides in dependence of the number of histidine amino acids and the arrangement of histidine in histidine-alanine peptides has been investigated.In this study, the lowest dissociation constant and therefore highest affinity is measured for His_6 (K_d = 14 nM). However, as the length of the oligohistidine increases more pronounced rebinding effects are observed. Thus, for stable protein immobilization a longer histidine tag (His_{10}) with moderate dissociation constant might be advantageous. Further, this study reveals a preferred binding of two histidines in the i and $i+2$ or $i+5$ position of the His_6 ligand to Ni^{2+}-NTA.

Complementarily, the affinity between His_6 or His_{10} and NTA is increased

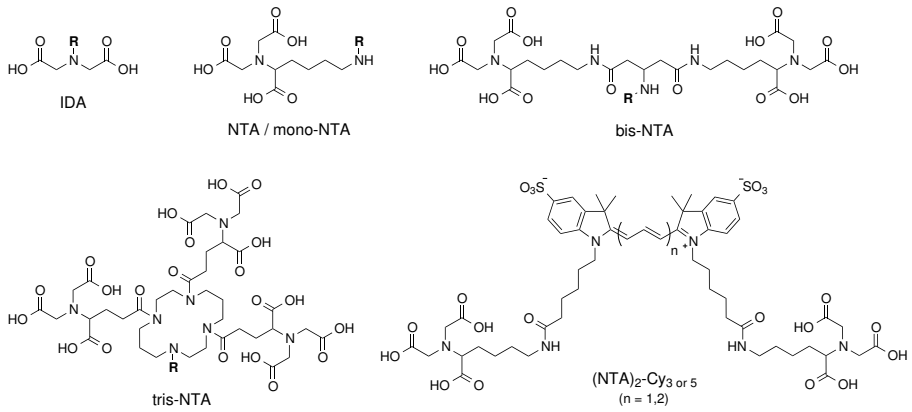

Figure 1.10: Chemical structures of complex chelators IDA and NTA derivatives with one, two or three NTA moieties. Mono-NTA, bis-NTA and tris-NTA from Lata *et al.*[64] and $(NTA)_2$-$Cy_{3\ or\ 5}$ from Kapanidis *et al.*[63].

by multi NTA tethers (Fig. 1.10). Kapanidis *et al.* obtained higher affinity ligands and simultaneously fluorescence labeling of the protein by linking of two NTA moieties through fluorophores.[63] Lata *et al.*[64] developed "recognition units" with 1, 2, 3 or 4 NTA moieties (referred as "mono-NTA", "bis-NTA", "tris-NTA" and "tetrakis-NTA") and an additional functional group (primary amine, carbonyl diamine and secondary amine) for further functionalization or tethering. An significantly increased stability is observed for the "tris-NTA" (K_d = 2.1 nM and 0.14 nM for His_6- and His_{10}-protein, respectively) compared to "mono-NTA" (K_d = 13 mM and 5 mM, respectively). This increase in stability can be ascribed to the increased number of available coordinating donor atoms. However, for even higher multivalency a decrease in affinity is observed due to the loss of entropy through the restriction on conformational freedom.

The metal ion mediated interaction between histidine rich sequences and chelating agents is used for a broad range of applications including protein purification[66], fluorescent labeling of proteins[63], structural studies of protein complexes[65], live cell protein labeling[67] and protein immobilization on surfaces and lipid bilayers[68].

1.4.2 Cobalt coordination chemistry

Cobalt has a series of stable oxidation states in different cobalt compounds. Cobalt complexes often include Co(II) or Co(III) species. While Co(III) complexes with a d^6 electron configuration are characterized by octahedral geometry and almost all are diamagnetic low-spin complexes with $t_{2g}^6 e_g^0$ configuration; most Co(II) species with d^7 electron configuration have either octahedral or tetrahedral geometry and almost all are high-spin complexes with $t_{2g}^5 e_g^2$ and $e_g^4 t_{2g}^3$ electron configuration, respectively (Fig. 1.11).[69] According to the spectrochemical series of the ligand field theory, the ligand field splitting increases

with increasing oxidation state of the metal center.[70] Thus, the ligand field splitting is more pronounced for Co(III) ions compared to the corresponding Co(II) complexes and octahedral complex geometry is favored. Additionally, the low-spin configuration is favored for Co(III) due to the high ligand field stabilization energy. Contrary, the less pronounced ligand field splitting for Co(II) results in the formation of octahedral and tetrahedral complexes with often high spin configuration.

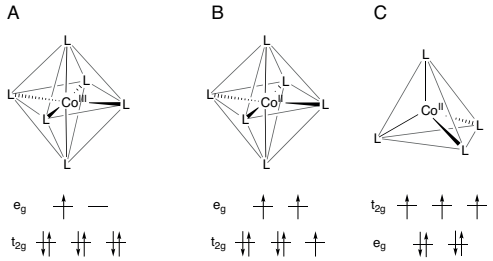

Figure 1.11: Geometry and electron configuration of an **A.** octahedral low spin Co^{3+}, **B.** octahedral high spin Co^{2+} and **C.** tetrahedral Co^{2+} complex.

Besides various preferences of Co(II) and Co(III) ions for certain coordination geometries and spin states, the kinetic and thermodynamic properties of their complexes differ. Kinetically Co(II) and Co(III) complexes show significant differences in the ligand exchange rates in their primary coordination sphere. For example, the water exchange rate at 25 °C of the Co(III) complexes $[Co(NH_3)_5(H_2O)]^{3+}$, $[Co(CN)_5(H_2O)]^{2-}$, *cis*-$[Co(en)_2(H_2O)_2]^{3+}$ and *trans*-$[Co(en)_2(H_2O)_2]^{3+}$ are $5.7 \cdot 10^{-6}$ s^{-1}, $5.9 \cdot 10^{-4}$ s^{-1}, $7.5 \cdot 10^{-6}$ s^{-1} and $1.1 \cdot 10^{-5}$ s^{-1}, respectively.[71] In comparison, the Co(II) complexes with $t_{2g}^5 e_g^2$ electron configuration $[Co(H_2O)_6]^{2+}$, $[Co(MeOH)_6]^{2+}$, $[Co(MeCN)_6]^{2+}$ and $[Co(en)_3]^{2+}$ have ligand exchange rates at 25 °C of $3.2 \cdot 10^6$ s^{-1}, $1.8 \cdot 10^4$ s^{-1}, $3.4 \cdot 10^5$ s^{-1} and $5.4 \cdot 10^3$ s^{-1}, respectively.[71] Similarly, the ligand exchange rates of the corresponding Ni(II) complexes with $t_{2g}^6 e_g^2$ configuration $[Ni(H_2O)_6]^{2+}$, $[Ni(MeOH)_6]^{2+}$, $[Ni(MeCN)_6]^{2+}$ and $[Ni(en)_3]^{2+}$ are $3.2 \cdot 10^4$ s^{-1}, $1.0 \cdot 10^3$ s^{-1}, $2.8 \cdot 10^3$ s^{-1} and $2.0 \cdot 10^1$ s^{-1}.[71] Although, a direct comparison of the values for the Co(II) and Co(III) species is not possible due to their various ligands, the significant difference over many orders of magnitude of the ligand exchanges rates emphasizes the difference of Co(II) and Co(III) complexes in terms of their kinetics. The ligand exchanges proceeds several orders of magnitude slower in the case of Co(III) complexes compared to Co(II) complexes. While the reaction rate is in the microsecond regime for Co(II) complexes, the exchange of a water ligand takes minutes to days for the Co(III) complexes. Moreover, a comparison of the data for equivalent Co(II) and Ni(II) complexes verifies similar exchange kinetics, though the ligand exchange is one to two orders of magnitude faster in the case of Co(II).

Thermodynamically Co(II) and Co(III) complexes show significant differences in stability. For instance, the stability constants of the cobalt complexes of the hexadentate $EDTA^{4-}$ ligand are log $K_{[Co^{II}(EDTA)]^{2-}} = 16.03$[72]/16.1[73]

and log $K_{[Co^{III}(EDTA)]^-} = 40.92$[72]/41.1[73]. In comparison, the stability constants of the triacetato $HEDTA^{3-}$ complexes are log $K_{[Co^{II}(HEDTA)(H_2O)]^-} = 14.8$ and log $K_{[Co^{III}(HEDTA)(H_2O)]} = 37.5$.[72] The tridentate ligand IDA^{2-} forms Co(II) and Co(III) complexes with stability constants of log $K_{[Co^{II}(IDA)_2]^{2-}} = 6.95$ and log $K_{[Co^{II}(IDA)_2]^-} = 29.6$, respectively.[73] The hexaamine cobalt complexes $[Co(NH_3)_6]^{2+/3+}$ have stability constants of log $K_{[Co^{II}(NH_3)_6]^{+2}} = 5$ and log $K_{[Co^{III}(NH_3)_6]}{}^{+3} = 35$.[69] In all these examples, the stability constant of the corresponding Co(III) complex surpasses that of the Co(II) complex. Further, the data show a particularly high complex stability with increasing quantity of available coordinating sites in multidentate ligands (chelate effect) for both the Co(II) and the Co(III) complexes.

Chapter 2

Results and Discussion

2.1 Part I: Biomimetic interfaces through click chemistry

The results and the discussion treated in the following chapter are published by Schenk *et al.*.[74]

In recent years countless approaches for surface modifications to create biomimetic systems have been published for the purpose of understanding biological issues. Among others, click reactions are particularly popular functionalization methods due to their mild reaction conditions and biocompatibility. The aim of this chapter is to establish a biomimetic substrate coating, which can be modified with high flexibility through copper catalyzed azide alkyne 1,3-dipolar cycloaddition (CuAAC) and which ensures specific interactions due to the protein repellent properties of a underlying poly(ethylene glycol) (PEG) layer. Towards this end, a clickable PEG-alkyne which is immobilized on glass and SiO_2 substrates with a terminal functional alkyne moiety for further modifications through CuAAC is developed. Due to increasing popularity of click reactions various prefabcricated as well as custom-made reaction partners are commercially available allowing for a wide scope of this approach. Furthermore, the clickable PEG-alkyne can be used with the establish preparation of gold nanostructured surfaces by BCMN to create dual functionalized biomimetic interfaces. The orthogonality of the functionalization of the PEG-alkyne through CuAAC and the gold nanoparticles through gold thiol interaction allows for the defined presentation of two ligands of interest.

2.1.1 Preparation and characterization of monofunctionalized substrates

For the functionalization with a broad range of azide containing molecules through CuAAC and covalent attachment through silanization a PEG with a terminal alkyne and a terminal silyl ether moiety (PEG-alkyne) is used. The PEG-alkyne is synthesized adopting the protocol for the synthesis of other silyl ether terminated PEGs.[43] A linear PEG with a terminal alkyne group and a

terminal primary amine is condensed with 3-(triethoxy)silylpropyl isocyanate in a nucleophilic addition (Fig. 2.1).

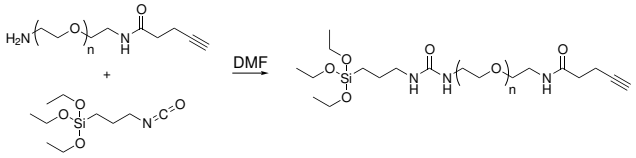

Figure 2.1: Synthesis of $(CH_3CH_2O)_3$Si-PEG3000-alkyne (PEG-alkyne) through condensation reaction of the amino terminated H_2N-PEG3000-alkyne with 3-(Triethoxy)silylpropyl isocyanate.

The obtained PEG-alkyne is bound covalently to substrates like glass or any other SiO_2 surface through nucleophilic substitution at the silyl ether moiety in the presence of catalytic amounts of triethyl amine (Fig. 2.2). In a second step the alkyne moieties of the PEG monolayer are modified with an azide compound of interest in a CuAAC resulting in the stereoselective formation of the corresponding 1,4-disubstituted 1,2,3-triazole. Furthermore, this functionalization method allows to tune the ligand density on the surface by using a mixture with defined molar ratios of the PEG-alkyne and a methoxy terminated PEG (PEG2000)[43] in the surface coating reaction. In the following, the specified mole fractions of PEG-alkyne represent the mole fraction of PEG-alkyne in solution in the silanization reaction.

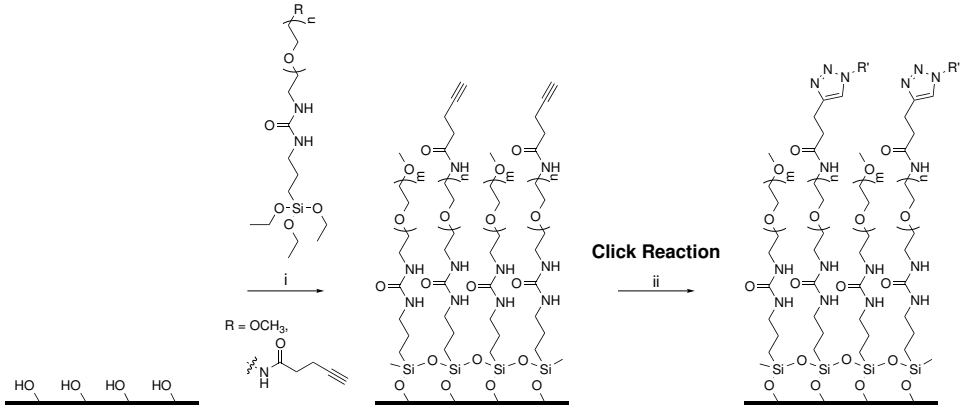

Figure 2.2: Surface coating with silyl ether terminated PEGs and subsequent functionalization through CuAAC with diverse azides. PEG-alkyne and $(CH_3CH_2O)_3$Si-PEG2000 (PEG2000) are used in different molar ratios to obtain PEG monolayers with various functional group densities. i. NEt_3, toluene, 80 °C, overnight ii. $CuSO_4$, *L*-ascorbic acid, Tris (pH 8.5), azide-R', 2h, rt. Adopted from [74].

In a first experiment PEG coated glass substrates with varying mole fractions of PEG-alkyne (0, 25, 50, 75, 100% PEG-alkyne) are reacted with a small fluorophore, 5/6-carboxyrhodamine 110-EG_3-azide. The surfaces fluorescence

intensity of the homogenous coated surfaces is quantified by fluorescence microscopy (Fig. 2.3). As expected the surface fluorescence intensity increases with increasing mole fraction of PEG-alkyne with some saturation behavior at high PEG-alkyne density. Marginal fluorescence intensity is detected on pure PEG2000 coated surfaces lacking the alkyne moieties essential for the CuAAC reaction.

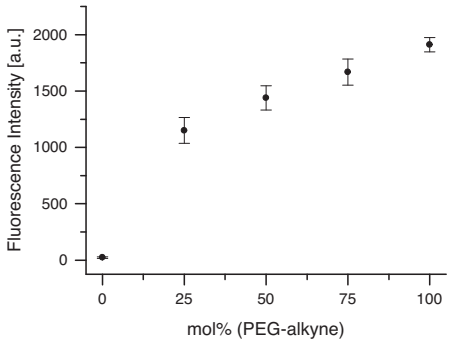

Figure 2.3: Surface fluorescence intensity on glass substrates silanized with PEG layers containing varying molar ratios of PEG-alkyne to PEG2000 after CuAAC reaction with 5/6-carboxyrhodamine 110-EG_3-azide. The mean and standard deviation for n = 3 (50, 75mol% PEG-alkyne) or n = 4 (0, 25, 100 mol% PEG-alkyne) samples is shown. Adopted from [74].

Further, to confirm the transformation of the alkyne moieties on the surface in the CuAAC, 3-azidomethyl-5-iodopyridine is used as a reaction partner on PEG surfaces with different alkyne densities. X-ray photoelectron spectra reveal a qualitative increase of the iodine signal (I 5d peak) with rising mole fraction of PEG-alkyne (Fig. 2.4). The shoulder at lower binding energies in the carbon signal (C 1s peak), which is more pronounced on surfaces with increasing amount of PEG-alkyne, confirms the presence of new carbon species originating from the 3-azidomethyl-5-iodopyridine moiety and the formation of the triazole ring. Correspondingly, the changes in the nitrogen signal (N 1s) of a surface coated with PEG-alkyne after the CuAAC with 3-azidomethyl-5-iodopyridine indicate the formation of the triazole ring[75]. Whereas only one nitrogen species is present on the surface before the CuAAC reaction (according to the chemical structure of the PEG-alkyne), four different species are identified after the reaction. Two of the three additional nitrogen species belong to the triazole ring formed in the reaction and one to the pyridine nitrogen of the reaction partner. The fit for the measured nitrogen signal for these four chemically different nitrogen species (402.5, 401.4, 399.7 and 398.9 eV), setting a fixed ratio of 1:2:1 for the area under the peak for the middle triazole nitrogen (N=**N**-N, 402.5 eV), the outer triazole nitrogens (**N**-N=**N**, 401.4 eV) and the pyridine nitrogen (C-**N**=C, 398.9 eV) (according to the chemical structure) results in calculated peak areas of 5.2, 10.4, 21.0 and 5.2 eV·CPS from higher to lower binding energy. Taken into account the chemical structure of the PEG-

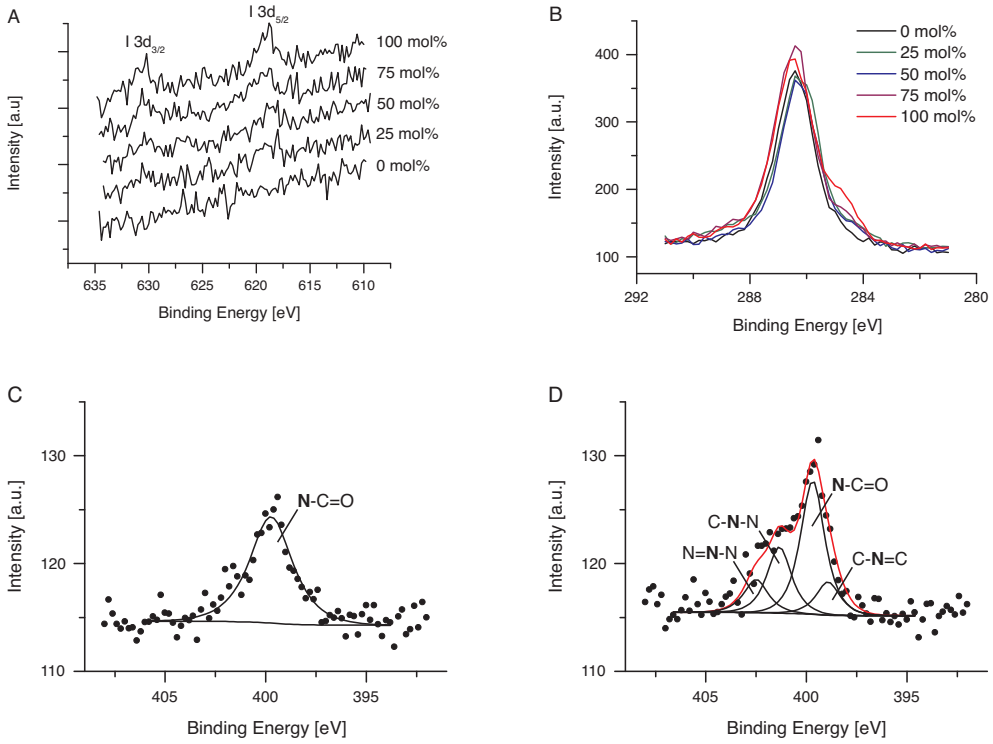

Figure 2.4: X-ray photoelectron spectra from **A.** the I 3d (spectra are shown with a offset) and **B.** the C 1s region from PEG monolayers with different PEG-alkyne to PEG2000 composition modified through CuAAC with 3-azidomethyl-5-iodopyridine. The N 1s signal of a pure PEG-alkyne monolayer on a glass substrate **C.** bafore and **D.** after the CuAAC with 3-azidomethyl-5-iodopyridine. The spectra are calibrated with respect to the C 1s signal for ethylene glycol (286.4 eV).[76] The measured data of the N 1s signal (filled circles) are fitted to chemical different nitrogen species (black line) contributing to the envelope (red line). As published in [74].

alkyne a conversion rate of 74% of the surface alkyne groups is estimated.

The density of ligand attached to the surfaces by CuAAC reaction is determined adopting a approach from Barber *et al.*.[77] This fluorescence based characterization method takes advantage of the selectivity and sensitivity of enzymatic proteolysis of an surface immobilized peptide for the release of a fluorescently labeled fragment. Glass surfaces with different molar ratios of PEG-alkyne and PEG2000 are therefore clicked with a peptide that is labeled with a fluorophore and contains an α-chymotrypsin cutting site, Ac-K(N_3)GGNGEPRGDTYRAYK(fluorescein)GG-NH_2. The surfaces are treated with α-chymotrypsin for enzymatic digestion of the surface bound peptide which releases the fluorescent labeled peptide fragment. The amount of the released peptide fragment is quantified by fluorescence intensity measurements and the peptide density on the surface before enzymatic digestion is calculated using a standard of known concentration of the same digested protein (Fig.

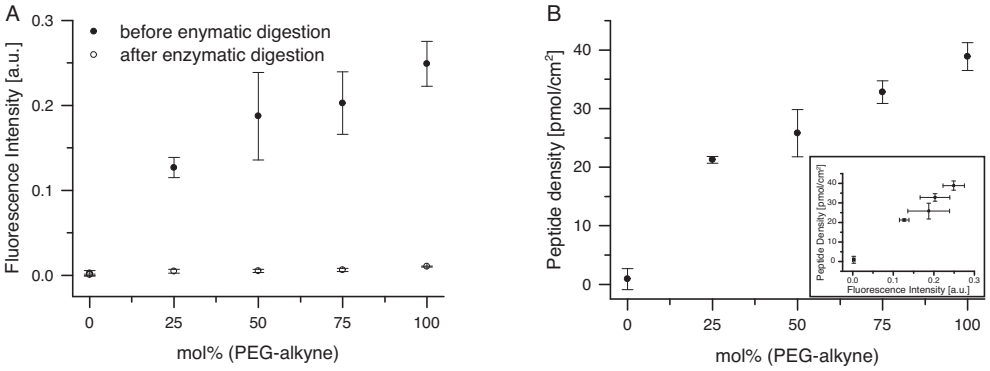

Figure 2.5: Ligand density quantification by enzymatic digestion. PEG-alkyne/PEG2000 films are modified with a fluorecently labeled peptide containing a α-chymotrypsin digestion site. The fluorescence **A.** on the surface before and after enzymatic digestion through α-chymotrypsin and **B.** in solution is measured. Inset: Plot of the determined peptide density against surface fluorescence intensity before enzymatic digestion. Data points represent the mean and the standard deviation of n = 4 samples. Adopted from [74].

2.5). From these measurements a correlation between the surface functionalization density and the amount of PEG-alkyne in the silanization reaction is obtained. Using PEG monolayers with varying mole fractions of PEG-alkyne the ligand density can be tuned from 0.9 pmol/cm^2 for pure PEG2000 coatings up to 38.9 pmol/cm^2 for pure PEG-alkyne coatings. Complementary to these measurements, the surface fluorescence intensity before and after the enzymatic digestion is determined. In agreement with the previous characterizations the density of immobilized ligand on the surface after CuAAC increases with increasing mole fraction of PEG-alkyne in the PEG layer which is visualized by the rise in the fluorescence intensity on the surface before enzymatic digestion. Moreover, fluorescence intensity measurements on the surfaces after enzymatic digestion reveal negligible fluorescence intensity confirming that the digestion is complete. Furthermore, peptide densities measured in solution and fluorescence intensities on surfaces show a linear correlation proving the approach is quantitative.

In the field of biomaterials a frequently used method for the immobilization of bioactive ligands on substrates is the noncovalent biotin (strept)avidin interaction. To broaden the scope of the developed PEG-alkyne coating, it is also possible to combine these two immobilization strategies. For this purpose, SiO_2 sensors are coated with a PEG layers containing different molar ratios of PEG-alkyne and PEG2000 (0, 25, 50, 75 and 100 mol% PEG-alkyne) and the alkyne functionalities are coupled to biotin-EG_3-azide (biotin-azide) in a CuAAC reaction. To quantify the binding of streptavidin (from *Streptomyces avidinii*, recombinant expressed in *Escherichia coli*) to biotin functionalized substrates in real time quartz crystal microbalance with dissipation monitoring (QCM-D) is used. The sensors are first equilibrated with PBS, then a solution

Table 2.1: The specific interaction of streptavidin with biotinylated PEG coated substrates is monitored by QCM-D. SiO_2 sensors are silanized using different ratios of PEG2000 and PEG-alkyne and subsequently modified through CuAAC reaction with biotin-azide. The sensors are first equilibrated with PBS. Then, streptavidin is passed over the sensors and unspecific bound protein is removed in a following wash with PBS. The changes in 7th resonance frequency represent the mean and the standard deviation of n = 3 measurements. Adopted from [74].

mol% (PEG-alkyne)	$\Delta f_n/n$ [Hz] (n = 7)
0	0.2 ± 0.4
25	-12.7 ± 3.1
50	-25.4 ± 4.0
75	-31.8 ± 5.1
100	-40.1 ± 3.3

of streptavidin in PBS is passed over the sensors before unspecific bound streptavidin is removed in a further washing step with PBS. The resulting binding curves show changes in resonance frequencies to different extent depending on the composition of the PEG layer (Tab. 2.1). Marginally changes in resonance frequency are observed on a pure PEG2000 coating subjected to the CuAAC reaction conditions with biotin-azide upon addition of streptavidin. This finding proves that there are no unspecific interactions between the streptavidin and the passivating PEG layer. In comparison, surfaces coated with various amounts of PEG-alkyne and functionalized with biotin show large decreases in resonance frequencies up on incubation with streptavidin due to the specific biotin streptavidin interaction. As expected, the amount of adsorbed streptavidin increases with increasing functionalization density of biotin.

To specifically understand the effect of an immobilized bioactive molecule on cell behavior, it is important to avoid unspecific interactions with the substrate. To investigate unspecific adsorption of proteins, bovine serum albumin (BSA) is used as a model protein. SiO_2 sensors for QCM-D are coated with a PEGalkyne monolayer and subjected to different concentrations of BSA (Fig. 2.6). While the addition of 0.01 w/v% BSA in PBS causes no observable changes in resonance frequency, 0.1 w/V% BSA results in a little decrease and for 1 w/v% and 5 w/v% BSA this decrease is even more pronounced. In all cases the resonance frequency returns immediately to the baseline frequency upon washing with buffer, which proves, that the protein is not adsorbed unspecifically on the surface. The observed changes in resonance frequency are causes by differing viscoelastic properties of the high concentrated protein solutions. The protein repellent properties of PEG-alkyne are very comparable to those measured for the methoxy terminated and slightly shorter PEG2000.[43]

Another key issue is if copper or copper ions remain on the surface after the CuAAC reaction, which in high concentrations could cause cell toxicity and prevent the application of this approach in the preparation of biomimetic

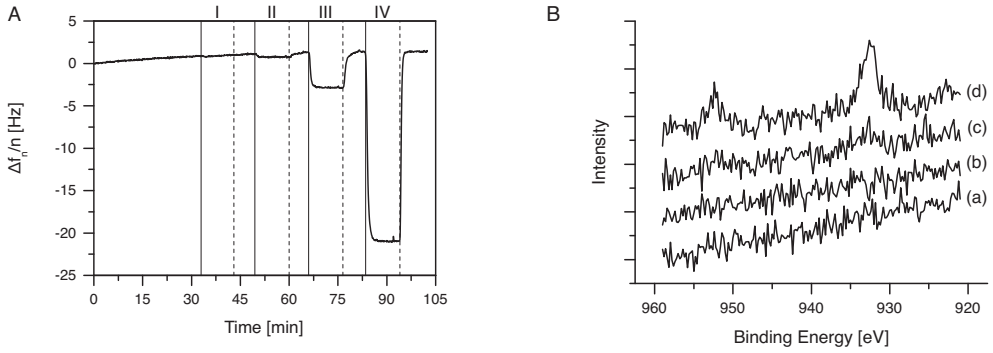

Figure 2.6: A. The protein repellent properties of a PEG-alkyne monolayer investigated by QCM-D. After equilibration with PBS increasing concentrations of BSA in PBS (I. 0.01 w/V%, II. 0.1 w/v%, III. 1 w/v% and IV. 5 w/v%) are passed over PEG-alkyne coated SiO_2 sensor (indicated by solid lines) alternated with rinsing steps with PBS (dotted lines). Exemplarily the curve of the 7th frequency is shown. **B.** XPS of the Cu 2p region of for a PEG-alkyne monolayer (a) without further treatment, (b) subjected to CuAAC reaction conditions without azide-R, (c) functionalized with NTA groups through CuAAC reaction with N^{α},N^{α}-bis(carboxymethyl)-*L*-azido-lysine hydrochloride and (d) functionalized with Cu^{2+} ion loaded NTA groups. As published in [74].

substrates. To investigate this point, comparative XPS spectra of different PEG surfaces are taken to analyze the amount of remaining copper on the surface (Fig. 2.6). On the one hand, a pure PEG-alkyne monolayer and a PEG-alkyne monolayer subjected to the CuAAC reaction conditions but without any azide as reaction partner is analyzed. On the other hand, a PEG-alkyne monolayer clicked with N^{α},N^{α}-bis(carboxymethyl)-*L*-azido-lysine hydrochloride (azide-NTA) is investigated, where the unintentionally bound copper ions are removed with EDTA. As a positive control such a NTA modified PEG-alkyne monolayer is loaded with Cu^{2+} ions. Both the pure PEG-alkyne monolayer and the PEG-alkyne treated by click reaction conditions (without any azide) don't give a copper signal (Cu 2p) in the XPS. The PEG-alkyne surface modified with NTA shows a little copper signal compared to the signal detected from the NTA modified PEG-alkyne monolayer loaded with Cu^{2+} ions. In summary, there is only very little copper remaining on the surface after the CuAAC reaction making this approach suitable for cell culture studies on biomimetic substartes.

In recent years, versatile biomimetic systems have been used to study the cell adhesion on extracellular matrix proteins such as fibronectin. In particular, the role and influence of the tripeptide adhesion sequence RGD from the 10th domain of fibronectin has been investigated. Here, the developed PEG-alkyne coating is used to investigate the correlation between the RGD density and the adhesion behavior of rat embryonic fibroblasts expressing YFP labeled paxillin (REF YFP-paxillin). Therefore, the short peptide sequence cyclic(RGDfE)K(N_3)-NH_2 (azide-cRGD) with an azide functionality is linked

to PEG monolayers on glass substrates containing different mole fractions of PEG-alkyne (0, 0.01, 0.1, 1, 10, 100 mol% PEG-alkyne). REF YFP-paxillin cells are seeded on the samples at a defined density and cultured for 4 h. The density of adherent cells and their spreading area is evaluated from fluorescence images of the stained cell nuclei and actin cytoskeleton, respectively (Fig. 2.7). This data clearly show that only very few REF YFP-paxillin can attach to substrates only coated with the passivating PEG layer independent of the molar ratio of PEG-alkyne and PEG2000. In comparison to this the density of adherent REF YFP-paxillin on PEG monolayers modified through the CuAAC reaction and presenting the cRGD sequence is strongly dependent on the functionalization density. While the REF YFP-paxillin density on a pure PEG2000 layer and the lowest functionalized PEG layer (0.01 mol% PEG-alkyne) are very low, the number of attached cells rises with increasing mole fraction of PEG-alkyne and thus increasing cRGD density, up to 1 mol%. At higher concentrations of cRGD saturation in the cell density is reached with about 15.6 cells/mm^2 (for 1 mol% PEG-alkyne). At the same time the spreading area of the REF YFP-paxillin fibroblasts depends on the cRGD density. While a moderate spreading of REF YFP-paxillin is observed on substrates presenting 0.1 mol% cRGD, the average spreading area of the cells is twice as high for substrates presenting 1 mol% cRGD and higher. Thus, a minimal cRGD density of 0.1 mol% is required to promote cell attachment, while after reaching the saturation level at 1 mol% a even higher cRGD density shows no significant influence on the here evaluated cell adhesion criteria cell density and spreading area.

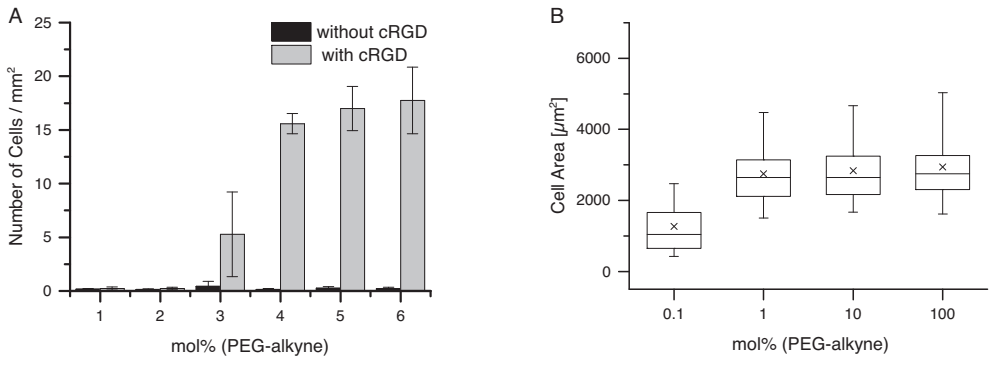

Figure 2.7: Characterization of REF YFP-paxillin cell adhesion on PEG coated glass substrates with varying cRGD functionalization densities. **A.** The density of adherent cells on PEG monolayers functionalized with cRGD or without cRGD. The bar graph represents the mean and standard deviation of three independent samples. **B.** Spreading area of the adherent cells on PEG monolayers modified with cRGD. The boxes show the 2nd and 3rd quartile of the data points and the whiskers the 95-5% interval; x represents the mean of the data. For the different RGD densities (0.1, 1, 10 and 100 mol%) the spreading area of n = 207, 436, 467 and 395 cells is analyzed. As published in [74].

In the last decades numerous systems for presenting cell adhesion molecules, such as the RGD peptide, in varying densities have been developed highlighting the complexity and sensitivity of cell adhesion.[78] Whether a cell attaches (or adheres) to a synthetic substrate or not depends, among others, on the topography[79], mechanical properties of the substrate[80, 81], spatial arrangement of the adhesion ligand[47],dynamic changes in ligand presentation[82], the ligand concentration[50, 83, 84], and the cell type.

Cell adhesion molecules in form of lipopetides with a RGD sequence incorporated into supported lipid monolayers promote maximum adhesion of nonspreading KG-1a cells at 0.5 mol% RGD (4.2 pmol/cm^2).[85] In comparison to this, with the same setup, lower RGD densities of 0.02 mol% RGD (170 fmol/cm^2) are required for near-maximal human umbilical vein endothelial cell (HUVEC) adhesion and 0.5 mol% RGD (4.2 pmol/cm^2) for maximal cell spreading. Likewise, Hudalla *et al.* showed that on thiol-ethylene glycol SAMs on gold modified through click chemistry with RGD a functionalization density of 0.01 mol% RGD (calculated intermolecular RGD spacing of 36 nm) is sufficient for human mesenchymal stem cell (hMSC) attachment and 0.1 mol% (calculated intermolecular RGD spacing of 11 nm) for hMSC spreading and focal adhesion complex formation.[86] At the same time the density of adherent cells as well as their spreading area increases with rising RGD functionalization concentration. In a study by Orgovan *et al.* the HeLa cell adhesion kinetics on supported PLL-*g*-PEG/PLL-*g*-PEG-RGD layers were investigated.[87] Maximal cell adhesion and spreading is observed at 25 mol% RGD modified PLL-*g*-PEG (correlating with a average ligand-ligand distance of 10 nm). On the other hand, in a study by Arnold *et al.* on hexagonal arrays of gold nanoparticles functionalized with c(RGDfK)-thiol and a passivation PEG layer in the intermediate space, effective cell adhesion is observed at interparticle spacings $\leq$ 58 nm for MC3T3 osteoblasts, B16 melanocytes, REF52 fibroblasts and 3T3 fibroblasts, while cell adhesion, spreading and focal adhesion formation were aberrant for interparticle spacings $\geq$ 73 nm.[44] Cavalcanti-Adam *et al.* used the same approach to investigate the focal adhesion assembly and dynamics with REF52 fibroblasts. Colocalization of the focal adhesion proteins vinculin and zyxin and the coupling of the focal adhesion clusters with actin stress fibers, along with the transition from transient focal contacts to mature focal adhesions only occur on surfaces with an interparticle distance of 58 nm but not at higher distances.[45, 46]

The observations from the presented study correlate well with the results from the literature. A cRGD density of 0.1 mol% is sufficient to support cell attachment and weak spreading and maximum cell adhesion and spreading is observed with cRGD densities $\geq$ 1 mol%. Assuming a hexagonal close packing and a homogenous distribution of the cRGD modified PEG molecules the average spacing between two adjacent cRGD moieties is:

$$d_{\text{RGD-RGD}} = \sqrt{2/(\sqrt{3} * N_{\text{A}} * \rho_{\text{RGD}})}$$

Taking into account a ligand density of 21.9 pmol/cm^2 for a surface with 25 mol% PEG-alkyne (as determined with the α-chymotrypsin digestion as-

say), this equation results in an average distance of two neighboring cRGD moieties of 47 nm and 15 nm for 0.1 mol% and 1 mol% PEG-alkyne, respectively. The slight differences to the results of the other studies can be attributed to differences in cell types, the chemical structure of the adhesion ligands and the immobilization and presentation strategy of the RGD.

2.1.2 Dual functionalized nanostructured biomimetic interfaces

The approach presented here based on the modification of immobilized PEG-alkyne monolayers by click chemistry can be also combined with the gold nanoparticle arrays mentioned above. Thereby dual functionalized substrates are created presenting two different ligands in a controlled manner. The resulting dual functionalized surfaces can be generated due to the chemical orthogonality of the two functionalization strategies and profit from the flexibility in ligand choice. Further advantages are the controlled spatial presentation of the ligand immobilized on the gold nanoparticles and the passivating properties of the PEG monolayer in the intermediate space.

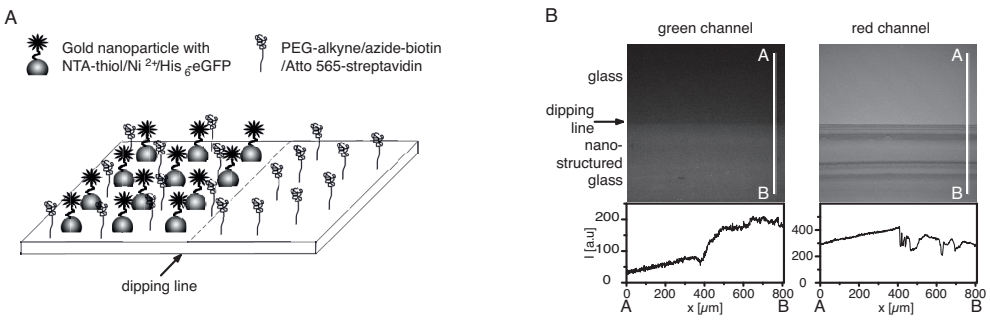

Figure 2.8: A. Schematic presentation of dual fluorophore functionalized substrates. The glass surface is partially nanostructured with gold nanoparticles (left side) and completely coated with a PEG-alkyne layer. The PEG-alkyne monolayer is first modified with biotin through CuAAC with biotin-azide and subsequently fluorescently labeled with streptavidin (Atto565-streptavidin). The gold nanoparticles are modified with thiol-NTA linkers and the NTA moieties are loaded with Ni^{2+} ions and with His_6-tagged GFP. **B.** Fluorescence images (top) and intensity line profiles (bottom) of the dual fluorophore labeled half gold nanostructured surface. The fluorescence images and the line profiles from A to B visualize that the gold nanoparticle coupled fluorophore (green channel) is restricted to the nanostructured area and the PEG-alkyne coupled fluorophore (red channel) is homogeneously distributed over the hole sample. Adopted from [74].

As a proof of concept nanostructured surfaces are first dual functionalized with two distinct fluorophores. To this end, glass surfaces that are half nanopatterned with hexagonally arranged gold nanoparticles are produced by block copolymer micellar nanolithography (BCMN). The intermediate space between the nanoparticels and the unpatterned area of the glass surface is coated with clickable PEG-alkyne; the gold nanoparticles protrude from the

surrounding PEG layer. First, the PEG-alkyne is coupled to biotin through CuAAC reaction with biotin-azide and subsequently to a Atto565 fluorescently labeled strepatvidin. Taking advantage of the gold-thiol interaction the gold nanoparticles are modified with a thiol-NTA linker and loaded with Ni^{2+} ions followed by the binding of His_6-tagged green fluorescent protein (GFP). Fluorescence images of a partially nanostructured glass surfaces proof the dual labeling based on the two orthogonal functionalization strategies (Fig. 2.8). The red fluorescent Atto565 dye coupled to the PEG layer through the specific biotin-streptavidin interaction is distributed homogenously over the hole sample, whereas the detection of the green fluorescent GFP coupled to the gold nanoparticles through interaction with Ni^{2+}-NTA is restricted to the nanostructured area. Thus, each of the two functionalization steps only takes place with the intended reaction partner.

2.1.3 Effect of the adhesion peptide cRGD and the synergy site PHSRN on cellular adhesion

These dual functionalized biomimetic substrates can be used to study the crosstalk between two different bioactive molecules. In particular, the $\alpha_5\beta_1$ integrin mediated cell adhesion to fibronectin is considered. Among other protein side chains a short 5 amino acid sequence, PHSRN, from the 9th domain of fibronectin type III plays a key role in the synergistic enhancement of $\alpha_5\beta_1$ integrin mediated cell adhesion to the RGD sequence in the 10th domain of fibronectin type III. [88, 89] Hitherto it is still under discussion whether the two peptide sequences RGD and PHSRN, located on the adjacent domains 9 and 10 of fibronectin type III, are acting synergistically or competitively in integrin mediated cell adhesion. So far, there is published experimental data supporting a synergetic binding of the two peptide sequences to two epitopes of a single integrin receptor as well as a competitive interaction of the two peptides with a common site (or to allosterically related sites).

Cell adhesion studies by Feng *et al.*[90] on SAMs of peptide terminated alkanethiols revealed that baby hamster kidney (BHK), 3T3 and IMR 90 cells can attach to SAMs presenting either GRGDS or PHSRN, although the cell spreading, actin stress filaments and focal adhesions are less pronounced or lacking on PHSRN presenting monolayers. Further, antibody blocking studies and competitive adhesion assays suggest a competitive binding of the two peptides to the $\alpha_5\beta_1$ integrin, whereas the RGD peptide binds with a higher affinity than the PHSRN peptide to the integrin. In an additional study by Eisenberg *et al.*[91] on SAMs of alkanethiols presenting fibronectin domains (instead of short peptides) the presence of the 9th domain, which contains the PHSRN sequence, shows an effect on BHK cell attachment (but not on spreading) at low densities of protein (0.0001-0.001%) but not at high densities ($\geq$ 0.01%). In addition, the cell adhesion to the 10th domain is inhibited in the presence of soluble RGD or PHSRN peptides advocating a competitive binding of PHSRN and RGD.

On the other hand, studies show a synergistic effect in the presence of

both the RGD and the PHSRN sequence, whereas PHSRN rarely supports cell adhesion on its own. Aota *et al.*[88] showed that the synergistic site PHSRN of fibronectin enhances cell spreading of HT-1080 cells. Ochsenhirt *et al.*[14] used Langmuir-Blodgett supported films of linear or looped peptide amphiphiles to investigate the effect of RGD secondary structure and PHSRN on cell adhesion and spreading of HUVEC cells. In this study it is shown that PHRSN dosen't support cell adhesion on its own, but a significant increase in cell spreading is observed when both peptides are presented in a 1:1 ratio at each 25 mol%. A recent study by Lee *et al.*[16] on thiol SAMs on gold with opposed peptides gradients revealed that NIH3T3 cell adhesion depends on both on the ratio of the two peptides RGD and PHSRN and the total peptide density. PHSRN alone rarely supports cell attachment, but in combination with RGD either a synergistic or competitive effect is observed depending on the ratio of the two peptides. A 1:1 ratio of RGD and PHSRN results in increased cell attachment, whereas any other ratio of RGD to PHSRN leads to reduced cell attachment compared to RGD alone. Further, the synergistic effect of RGD and PHSRN (1:1 ratio) is more pronounced on surfaces with low total peptide density.

The presented method for creating dual functionalized biomimetic substrates is used to investigate the mutual influence of the cRGD and PHSRN peptide on cell adhesion of rat embryonic fibroblasts (REF52). This approach profits from the fact that not only the statistical density of the first ligand coupled to the PEG-alkyne by click reaction can be controlled, but also that the arrangement of the second ligand linked to the gold nanoparticles can be adjusted with high spatial resolution. Furthermore, the PEG monolayer prevents nonspecific interactions of the cells with the underlying substrate. Nanostructured substrates with an interparticle distance of 100 ± 15 nm are chosen as REF52 cell attachment and spreading is reduced on surfaces where the distance between two adjacent RGD ligands attached to the gold nanoparticles exceeds 58 nm.[44] The glass in the intermediate space between the gold nanopaticles is coated with a PEG layer with varying mole fractions of PEG-alkyne (0, 0.1, 1, 10 mol% PEG-alkyne) and the terminal alkyne functionalities are coupled to K(N_3)PHSRN through click reaction. In a second step the gold nanoparticles are optionally decorated with a cRGD that contains a free thiol group for immobilization (HS-cRGD). The cell adhesion of REF52 cells is evaluated after 4 h cultivation on these surfaces based on fluorescence images of the DAPI stained nuclei and phalloidin-TRITC stained actin (Fig. 2.9). While limited cell attachment is observed for substrates solely functionalized with one of the two peptide sequences (cRGD without PHSRN or 10 mol% PHSRN without cRGD) and for substrates presenting cRGD and 0.1 mol% PHSRN, the number of cells increases with increasing PHSRN density. Moderate cell attachment is detected on substrates functionalized with cRGD and 1 mol% PHSRN. A further increase of the PHSRN density to 10 mol% results in a striking increase in the adherent cell density. Fluorescent stainings of the adhesion peptides vinculin and paxillin show focal adhesion formation and actin filaments on dual functionalized surfaces presenting cRGD and 10 mol% PHSRN, but not on monofunctionalized substrates with cRGD only. Thus, effective attachment of

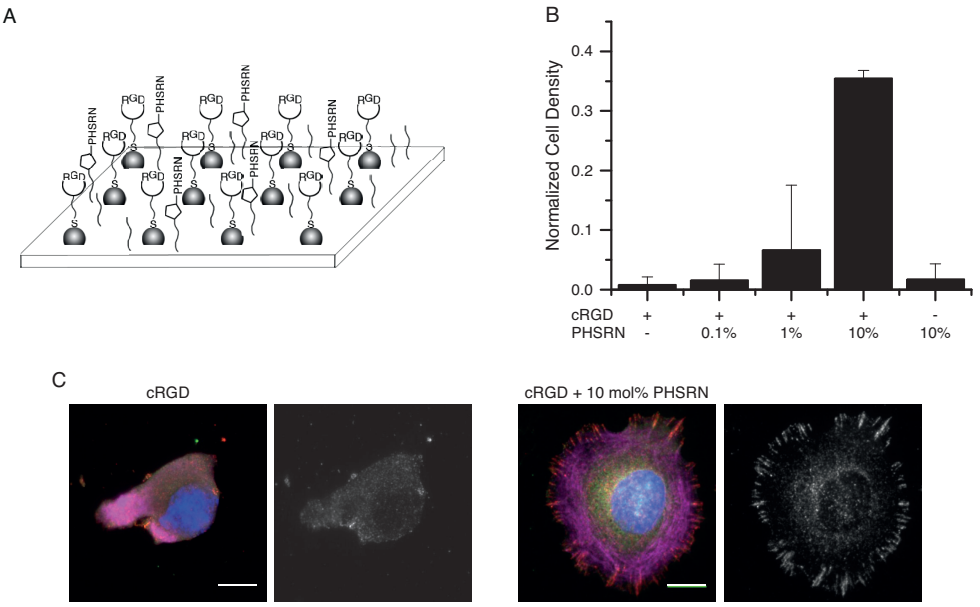

Figure 2.9: A. Schematic presentation of dual peptide functionalized substrates. The nanostructured glass surface is coated with a PEG monolayer comprising varying mole fractions of PEG-alkyne. The terminal alkyne moieties are coupled to K(N_3)PHSRN through CuAAC reaction. The gold nanoparticles serve as anchoring point to present the second thiolated peptide sequence cRGD. **B.** Density of adherent cells (normalized to the seeded cell density) on gold nanostructured substrates (interparticle distance: 100 ± 15 nm) presenting cRGD and/or PHSRN at varying densities. **C.** Fluorescence images of REF52 on nanostructured surfaces functionalized with cRGD or cRGD and 10 mol% PHSRN. The nucleus is shown in blue, actin in magenta, vinculin in green and paxillin in red. Grey images visualize localization of paxillin. The scale bar is 10 µm. As partially published in [74].

REF52 cells is only observed in the presence of both the cRGD and the PHSRN ligand at appropriate concentration. At first glance, the results of the cell adhesion on the dual functionalized substrates support a synergistic effect of the two peptides on REF52 cell attachment as cells only adhere well to the substrate in the presence of both peptides but not when only either cRGD or PHSRN is present. However, the results can also be reconciled with a competitive binding mechanism following the line of arguments of Eisenberg *et al.*[91]. Considering the lower binding affinity of PHSRN to $\alpha_5\beta_1$[90] and the in total higher peptide density on substrates presenting both peptides (cRGD, 10 mol% PHSRN) enhances the probability of ligand cell interactions during attachment.

Thus, the approach established in this work serves as a platform for cell adhesion studies presenting two signaling ligands in defined spatial arrangement. In summary, the preparation of clickable PEG-alkyne monolayers and their subsequent modification with varying azide containing compounds is shown. The effective conversion through the CuAAC reaction is visualized by fluorescence

microscopy, XPS, QCM-D and a cell adhesion assay and the ligand density is quantified in an enzymatic digestion assay. The density of the functional ligand is adjusted through coimmobilization of an inert methoxy terminated PEG2000. The tailored ratio of PEG-alkyne and PEG2000 used in the solution for the formation of the PEG film on the substrate by self-assembly correlates well with the functionalization density detected on the surface after the modification through CuAAC. Furthermore, in combination with established gold nanostructured surfaces the clickable PEG-alkyne allows for the preparation dual functionalized interfaces presenting two distinct ligands in controlled density and arrangement. As a proof of principle, a partially nanostructured surfaces is labeled orthogonally with two distinct fluorophores. Moreover, this platform is used for the investigation of the mutual influence of cRGD and PHSRN on integrin mediated cell adhesion.

2.2 Part II: Co(III) as mediator ion to immobilize His-tagged proteins on NTA functionalized surfaces

The line of argument and parts of the results of the following chapter are published by Wegner *et al.*[92].

One of the most commonly used techniques for the immobilization of proteins relies on the Ni^{2+} mediated interaction of NTA and His-tagged proteins. The His-tag sequence can be easily introduced in a protein at the desired position and due to the popularity of this approach to purify proteins large libraries of His-tagged proteins exist. However, the reversible binding kinetics, which are desired in protein purification, can be disadvantageous depending on the application. For stable protein immobilization, for example, higher thermodynamic stability and lower kinetic lability of the coordination complex is desirable. Increased stability between the His-tag and the metal ion coordinated NTA moiety can be achieved by replacing the bridging Ni^{2+} ion with Co^{3+}[93].Opposed to the divalent transition metal ions Ni^{2+} and Co^{2+}, which have similar kinetic and thermodynamic properties, Co^{3+} complexes are characterized by significant higher thermodynamic stability and kinetic inertness. The low ligand exchange kinetics of Co(III) complexes favor the application in the labeling of proteins[93], mechanistic studies of enzymes[94, 95], drug delivery[96] and tethering of His-tagged peptides to lipid bilayers[97]. In this study the applicability of the Co(III) mediated interaction between NTA functionalities and His-tagged proteins for stable protein immobilization is investigated. Due to the thermodynamic and kinetic properties of Co^{3+} the complex is formed in a two step procedure comprising first the formation of the appropriate Co(II) complex and subsequent the oxidation of the metal ion to Co(III). The diverse kinetic and thermodynamic properties of Ni^{2+}, Co^{2+} and Co^{3+} ions enable the reversible or stable immobilization of His-tagged proteins depending on the metal ion which mediates the interactions of NTA and His-tagged proteins.

2.2.1 Comparison of the Co(III), Co(II) and Ni(II) mediated interaction between NTA and His_6-GFP

The binding between NTA, different metal ions and His_6-GFP is investigated time-resolved by QCM-D (Fig. 2.10). For this study cobalt and nickel ions are used for comparison as cobalt has two stable oxidation states (+2 and +3) and nickel only one (+2). First, a SAM of thiol-NTA is formed on a gold surface and the NTA moieties are loaded with the corresponding divalent metal ion (Co^{2+} or Ni^{2+}). Subsequently the His_6-GFP is coordinated. Subsequently, the His_6-GFP is passed over these surfaces so that it can coordinate. To obtain the Co(III) mediated interaction, Co^{2+} are chemically oxidized to Co^{3+} using 10 mM hydrogen peroxide. To access the difference in stability, the surfaces are washed with high concentrations of imidazole (250 mM). The curves of the Co(III), Co(II) and Ni(II) mediated interactions differ significantly. While for the Co(III) mediated interaction the washing with imidazole results in only

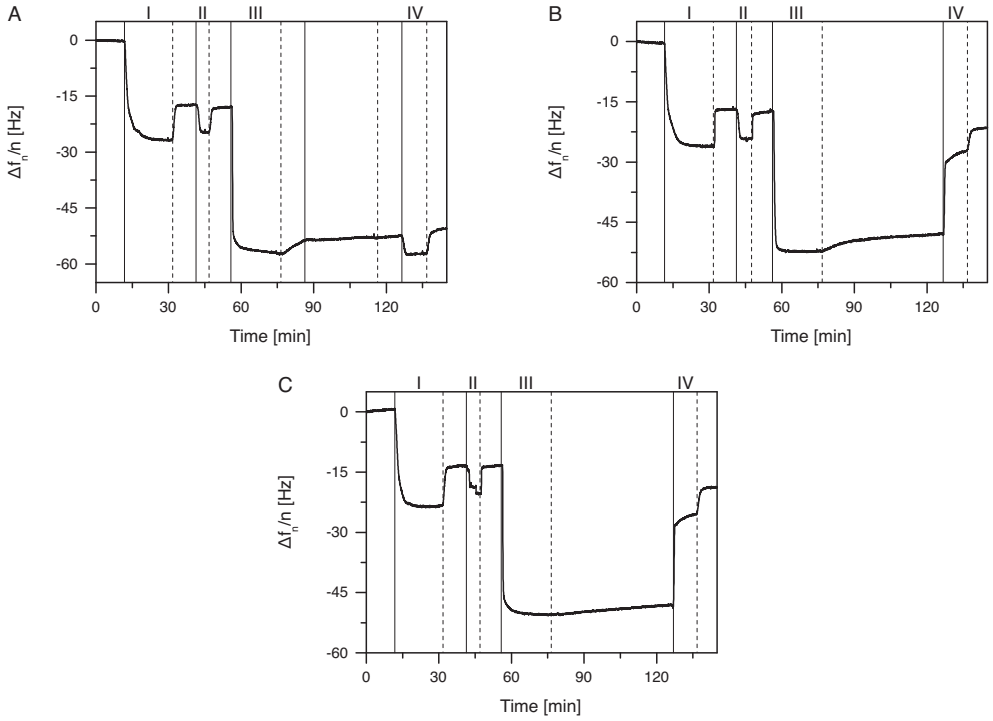

Figure 2.10: A. Co(III) and **B.** Co(II) and **C.** Ni(II) mediated interaction between NTA and His_6-GFP. First, a SAM of thiol-NTA is formed on a gold substrate (I). The NTA functionalities are loaded with A. Co^{2+} and B. Ni^{2+} ions (II) followed by the coordination of His_6-GFP (III). The Co(II) complexes are oxidized to Co(III) using hydrogen peroxide (IV). Subsequently, imidazole is directed over the surface (V) . Afterwards, the sensor is once more incubated with His_6-GFP (III) and washed with imidazole (V). Vertical lines are added for clarity displaying the addition of the reagents (solid lines) and the return to the buffer solution (dashed lines). QCM-D curves illustrate the 7th resonance frequency.

marginal frequency changes, nearly complete removal of the protein is observed for the Co(II) and Ni(II) mediated interaction indicated by the strong increase in the resonance frequency. Opposed to Co(III), ligand exchange reactions proceed quickly on the Co(II) and Ni(II) complexes resulting in the release of the protein in the presence of high imidazole concentrations. Small resonance frequency differences after protein binding and release might be attributed to either some unspecific binding or in the case of the Co(II) mediated interaction to partial oxidation of the metal ions to more stable Co(III). In comparison to the reversible binding via Co(II) or Ni(II), the Co(III) mediated interaction resists high concentrations of competing ligand. Thus, the higher stability of the Co(III) mediated interaction compared to the Co(II) or Ni(II) mediated one predestines it for stable protein immobilization.

S. Wegner[92] obtained similar results when performing analogous experiments with an protein repellent PEG monolayer on SiO_2 instead of the OEG

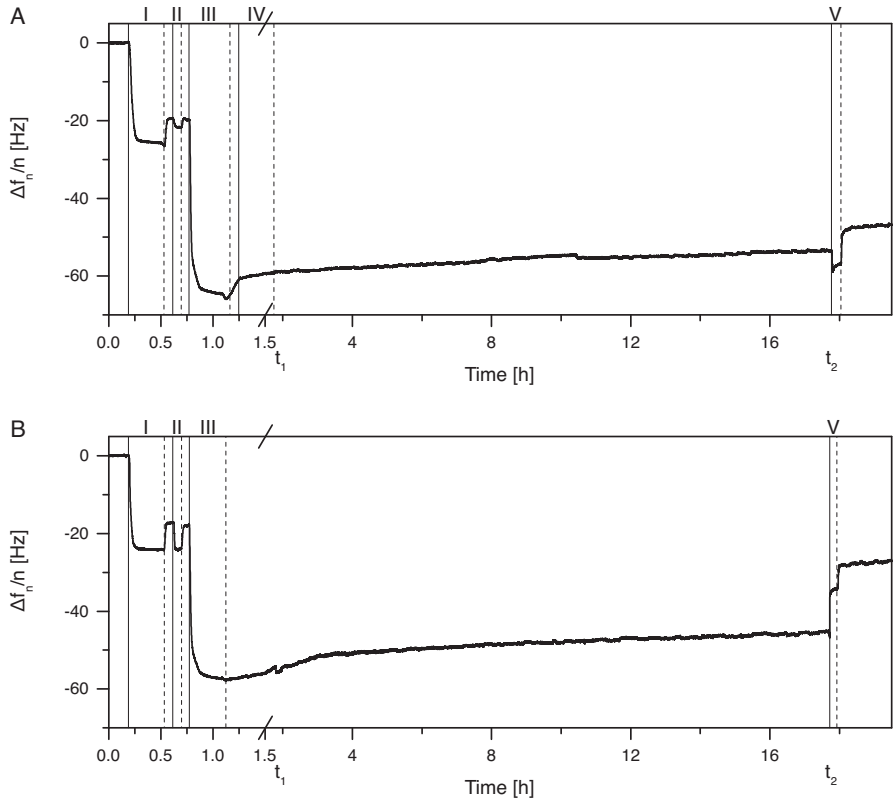

Figure 2.11: The long-term stability of the **A.** Co^{3+} and **B.** Ni^{2+} mediated protein immobilization. The measurement is performed at a flow rate of 100 µL/min at 37 °C. Following chemicals in Tris-NaCl buffer are washed over to the sensor surface at vertical solid lines: I. 50 µM thiol-NTA, II. 100 mM $CoCl_2$ or 100 mM $NiCl_2$, III. 5 µM His_6-GFP, IV. 10 mM H_2O_2, V. 250 mM imidazole. Washing steps with Tris-NaCl buffer are indicated with vertical dashed lines. An exemplary QCM-D curve of the 7th resonance frequency is illustrated.

monolayer on gold. Therefore, SiO_2 sensors are coated with PEG-alkyne and functionalized with azide-NTA through CuAAC reaction as described in chapter 2.1. The NTA moieties are loaded with either Co^{2+} or Ni^{2+} ions and His_6-GFP is coordinated. Hydrogen peroxide treatment leads to the oxidation of Co(II) to Co(III). Here, too the resistance of the Co(III) mediated interaction and the lability of Ni(II) mediated interaction against high concentrations of imidazole and EDTA is observed. Further, due to the longer PEG no unspecific adsorption of the protein on the surface is detected. Moreover, the specificity of the interaction is demonstrated as the His_6-GFP protein dosen't bind to the surface when the cobalt centers are oxidized to Co(III) beforehand. For comparison the Co(II) mediated interaction is considered. The curve shows partial protein release upon addition of imidazole indicating the partly oxidation of the cobalt centers due to oxidative species in the buffer solution. Furthermore, the applicability of this approach for the stable immobilization of His-tagged

proteins on lipid bilayers presenting NTA moieties is investigated. It is shown, that the oxidation step with hydrogen peroxide dosen't affect the integrity of the lipid bilayer and that the protein is stably immobilized.

2.2.2 Long-term stability of the Co(III) mediated interaction in comparison to the Ni(II) mediated interaction

Wegner *et al.*[93] has shown that the NTA-Co^{III}-His_6 complexes have a higher stability against competing ligands like imidazole and EDTA compared to the corresponding Co^{II} complexes. This arises the question if this is also the case for the Co(III) mediated surface immobilization strategy presented here.

Table 2.2: Long-term stability of Co^{III} and Ni^{II} mediated protein immobilization. Resonance frequency changes attributed to His_6GFP adsorption directly after the oxidation step (t_1) and after extended washing (t_2) are determined in consideration of the frequency change upon formation of the metal ion loaded NTA SAM. Further, the average change in resonance frequency per hour ($\Delta(\Delta f_n/n)/\Delta t$) and the relative change in resonance frequency per hour (normalized to the amount of initially bound protein) are shown. The average values represent the mean and the standard deviation of the n = 3 measurements.

		Co(III)		Ni(II)	
		single exp.	average	single exp.	average
$\Delta f_n/n$ (GFP) [Hz]	t_1	-38.9 ± 0.3 -40.1 ± 0.2 -39.3 ± 0.2	-39.4 ± 0.6	-35.3 ± 0.4 -36.9 ± 0.7 -36.7 ± 0.2	-36.3 ± 0.9
	t_2	-40.2 ± 0.2 -33.9 ± 0.2 -33.9 ± 0.2	-36.0 ± 3.6	-26.2 ± 0.4 -27.2 ± 0.2 -32.2 ± 0.1	-28.5 ± 3.2
$\Delta(\Delta f_n/n)/\Delta t$ [10^{-2} Hz/h]		-8.1 ± 2.3 38.7 ± 1.6 33.8 ± 1.5	21.5 ± 25.7	57.5 ± 3.5 61.5 ± 4.4 28.9 ± 1.4	49.3 ± 17.8
rel. frequency change/Δt [10^{-3}/h]		2.1[a] -9.7[a] -8.6[a]	-5.4 ± 6.5	-16.3[a] -16.6[a] -7.9[a]	-13.6 ± 5.0

[a] Errors calculated from standard deviation of the measured frequency changes are negligible small ($\leq 8*10^{-5}$/h)

To investigate the long-term stability of the NTA-Co^{III}-His_6 and NTA-Ni^{II}-His_6 complexes by QCM-D a thiol-NTA linker is used to form a SAM on a gold sensor, the NTA groups are loaded with the desired mediator ion and the model protein His_6-GFP is immobilized on the surface following the protocol above. For comparative purposes Ni^{2+} is used as a mediator ion and not Co^{2+} due to the possible partial oxidation of the cobalt ions on the surface over time. Tris-NaCl buffer is passed over the sensors' surface in an extended washing step

(16 h) with a relative high constant flow rate of 100 µL/min at 37 °C (Fig. 2.11). The temperature of 37 °C is chosen due to its relevance in biological systems and cell culture. The relative increase in frequency change during this washing step is evaluated (Tab. 2.2). It is assumed that the observed frequency changes are solely due to the amount of protein detaching through ligand exchange. The results indicate a slightly different binding mode for the Co(III) mediated interaction compared to Ni(II) as the amount of initially bound protein differ slightly. Further, the release of His^6-GFP upon excessive washing is more pronounced for Ni(II) immobilized protein compared to Co(III), which is twice as high. This is particular obvious from the relative frequency change which is $-13.6 \cdot 10^{-3}$/h for Ni(II) and $-5.4 \cdot 10^{-3}$/h for Co(III). Thus, the Co(III) mediated interaction between NTA and His_6-GFP features higher long-term stability compared to Ni(II).

2.2.3 Influence of the oxidation step with hydrogen peroxide on the functionality and activity of the immobilized protein

A potential concern about this immobilization strategy may be the impairment of the protein and its functionality through the oxidation step. Therefore, the integrity of immobilized protein A with an N terminal His-tag and its interaction with immunoglobulin is investigated. For comparison the interaction between the NTA moiety and the His-tag is either mediated through Co^{3+}, Co^{2+} or Ni^{2+} ions (Fig. 2.12). First, a SAM of thiol-NTA on a gold surface is formed followed by the loading of the NTA moieties with the appropriate metal ion (Co^{2+} or Ni^{2+}). The protein A fragment is bound to the surface over its His-tag. Optionally, the Co^{2+} ions are chemically oxidized to Co^{3+} using 10 mM H_2O_2. The antibody binding capacity of the immobilized protein A is investigated using an anti-BSA antibody. First of all, the protein A is active in all three cases and shows significant antibody binding for the Co^{3+}, Co^{2+} and Ni^{2+} ion based immobilization. Nevertheless there are some differences in the binding curves. On the one hand, the binding curves for the protein A differ for the Co(II) and the Ni(II) mediated immobilization. The binding on Co(II) is characterized by a strong decease in frequency, passing through a minimum and reaching a saturation level, whereas on Ni(II) the decrease merges in saturation. Second, the binding kinetics for the antibody vary on the different surfaces. Initially a strong decay in frequency is observed independent from the mediator ion. However, the frequency change merges in a linear decay for Co(III) and Ni(II) mediated immobilization, whereas it reaches saturation for Co(II) in the observed time frame. Finally, the three different surface coatings respond differently to high concentrations of imidazole. Upon addition of high concentrations of imidazole the resonance frequency does not show a significant alteration for the Co(III) mediated protein immobilization and only a slight increase is observed for Co(II). In comparison a strong and sharp increase in resonance frequency is detected for the Ni(II) mediated interaction. For the Co(II) mediated interaction the curve progression might be explained by par-

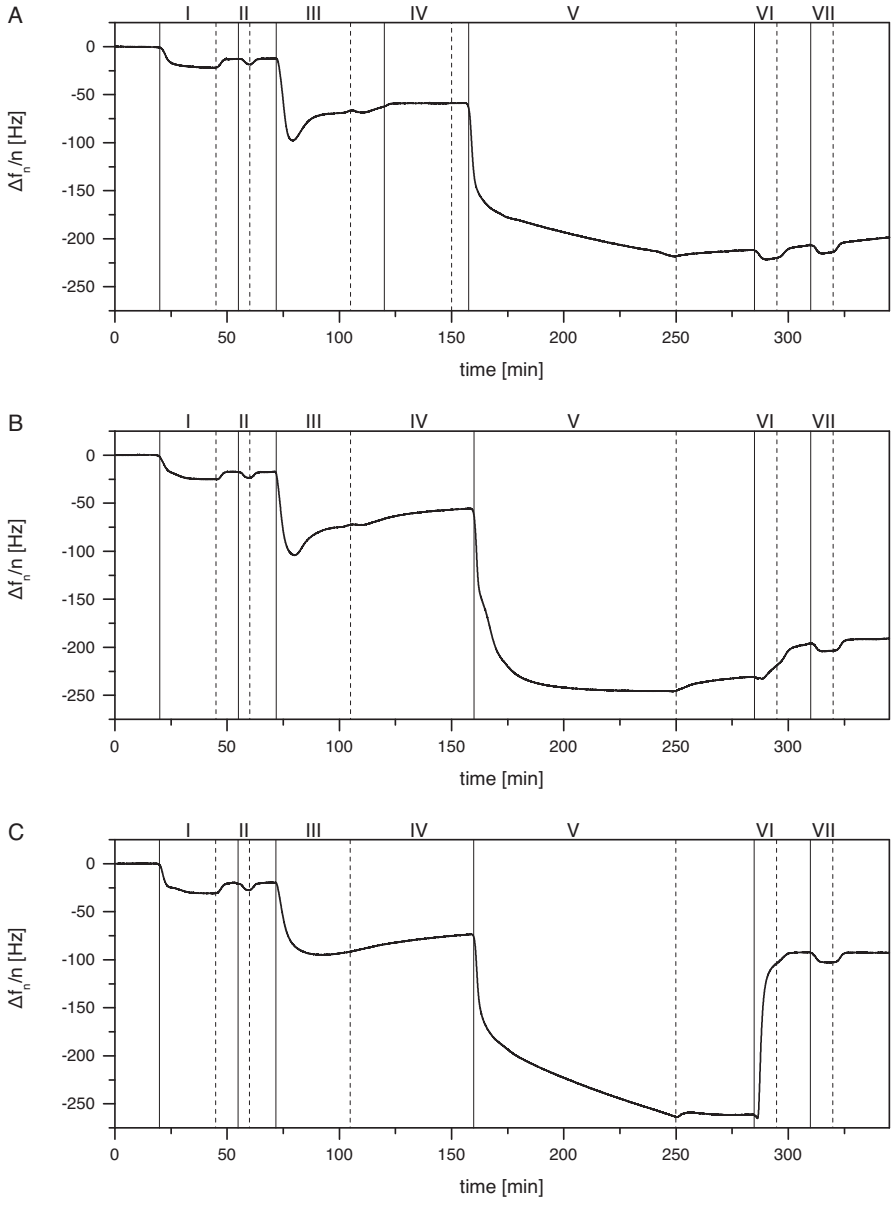

Figure 2.12: The influence of the oxidation step on protein A activity is monitored by QCM-D. A His-tagged protein A is bound to NTA by either **A.** Co^{3+}, **B.** Co^{2+} or **C.** Ni^{2+} and the interaction with an anti-BSA antibody is investigated. Following reagents in Tris-NaCl buffer are washed over the sensor's surface at vertical solid lines: I. 50 µM thiol-NTA, II. 100 mM $CoCl_2$ or 100 mM $NiCl_2$, III. 0.07 mg/mL His_6-protein A, IV. 10 mM H_2O_2, V. 0.30 mg/mL anti-BSA antibody VI. 250 mM imidazole, and VII. 50 mM EDTA (pH 7.4). The return to the Tris-NaCl buffer solution is indicated by vertical dashed lines.

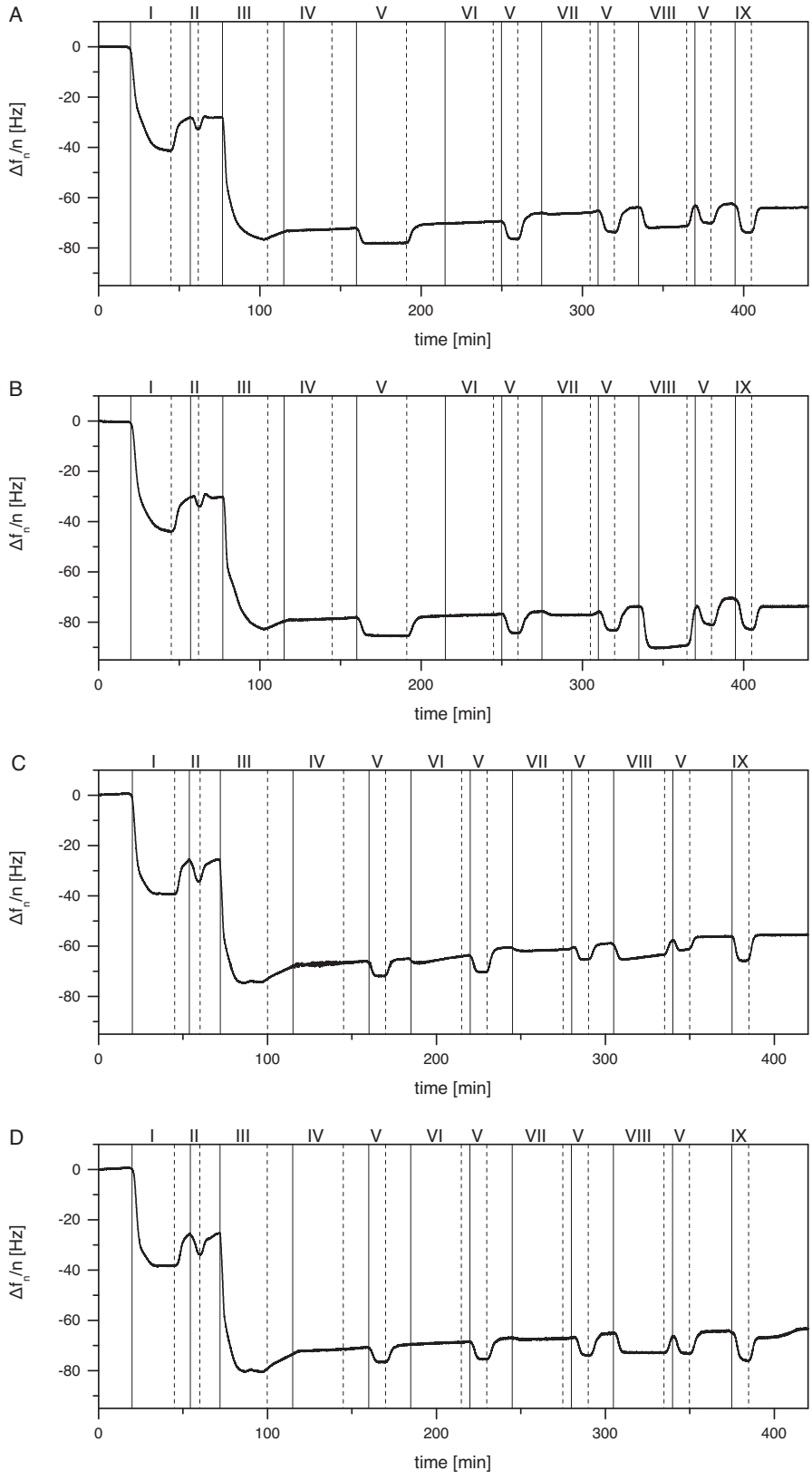
A
B
C
D
I
II
III
IV
V
VI
V
VII
V
VIII
V
IX
0
-20
-40
-60
-80
Δf /n [Hz]
n
0
100
200
300
400
time [min]

Figure 2.13: The chemical resistance of the Co(III) mediated immobilization of His_6-GFP on thiol-NTA SAMs on gold surfaces against the reducing agents **A.** ascorbic acid (pH 7.4), **B.** tris(2-carboxyethyl)phosphin (pH 7.4), **C.** dithiothreitol and **D.** sodium sulfite is monitored by QCM-D. The vertical lines indicate the direction of a reagent over the sensor surface (solid line) and the subsequent return to the Tris-NaCl buffer (dotted line).The measurement includes the addition of the following components in Tris-NaCl buffer to the sensor surface (indicated by vertical solid lines). I. 50 µM thiol-NTA, II. 100 mM $CoCl_2$, III. 5 µM His_6-GFP, IV. 10 mM H_2O_2, V. 250 mM imidazole, VI. 1 mM reducing agent, VII. 10 mM reducing agent, VIII. 100 mM reducing agent, and IX. 50 mM EDTA (pH 7.4). After the addition of the respective reagent the system is changed back to the Tris-NaCl buffer solution (indicated by vertical dashed lines).

tial oxidation of surface bound Co(II) to Co(III) through oxidative species in the buffer solution. Noteworthy, the curve progression for the Ni(II) mediated interaction indicates some unspecific binding. Nonetheless, it can be concluded that in the specific case of protein A, the protein function is not affected by the oxidation step.

2.2.4 Resistance of the Co(III) mediated immobilization to reducing agents

In this section the reversibility of the oxidation step of the Co(III) mediated His_6-protein immobilization is considered. The influence of the four different reducing agents ascorbic acid, tris(2-carboxyethyl)phosphin (TCEP), dithiothreitol (DTT), and sodium sulfite, which are commonly used in biochemistry, is investigated (Fig. 2.13). For this purpose different concentrations of reducing agents are passed over NTA-Co^{III}-His_6-GFP surfaces for the same time frame as the hydrogen peroxide for the oxidation step. After formation of an NTA modified SAM on gold sensors, the loading of the NTA with divalent cobalt ions and the binding of His_6-GFP, the Co(II) ions are oxidized to Co(III) with hydrogen peroxide following the procedure described above. First, a washing step with high concentrations of imidazole proves that all cobalt ions are oxidized as no frequency change is observed. Afterwards, the surfaces are incubated with the appropriate reducing agent in increasing concentrations (1 mM, 10 mM, 100 mM) separated by washing steps with first Tris-NaCl buffer, second imidazole and finally Tris-NaCl buffer in order to determine wether the reducing agent has an influence on the immobilized protein. For all four reducing agents no significant changes in the resonance frequency are noticed. Only a slight shift is observed, most pronounced in the case of ascorbic acid and DTT. But since these shifts are not stronger at very high concentrations of reducing agent (100 mM), it can be concluded that the majority of the surface bound Co(III) complexes are not reduced to Co(II). This high resistance of the Co(III) mediated immobilization of His-tagged proteins towards reducing agents enables the application of this immobilization strategy for stable and

inert surface modification.

In conclusion, the stable immobilization of His-tagged proteins exemplarily His_6-GFP on NTA functionalized SAMs through Co(III) is presented. The strategy comprises first the formation of $Co^{II}(NTA)(His_6)$ complexes and the subsequent oxidation of the Co(II) centers to Co(III). The Co(III) mediated interaction features higher resistance towards imidazole and higher long-term stability to washing off. Further, the chemical oxidation with hydrogen peroxide, which might be problematic for protien functionality and activity, dosen't affect the antibody binding of protein A. Moreover, the resistivity of the Co(III) mediated interaction towards reducing agents is validated.

2.3 Part III: Photochemical immobilization of His-tagged proteins onto TiO_2 nanoparticles

Complementary to studies that examine the influence of external factors on cell behavior by exposing cells to synthetic biomimetic substrates and three-dimensional scaffolds, the internal effect caused by the uptake of biofunctionalized nanocomposites is also of interest. Different kinds of modified nanoparticles as well as polymer and biomolecule based nanocomposites have been developed for targeted delivery. The uptake behavior depends on the biochemical properties of the nanoparticles and can be adjusted by changing the surface hydrophobicity/hydrophilicity and specific modifications with receptor specific ligands addressing a certain uptake mechanism. Diverse materials like mesoporous silica, carbon nanostructures (fullerenes, carbon nanotubes) and metals (Au, Ag, Fe) as well as metalloid and metal oxides (SiO_2, TiO_2, Fe_3O_4) are developed with applications in material science, catalysis, environmental purification (air and water), self-cleaning surfaces, biological technology and medicine. In particular, in biomedical research nanoparticles are used for the labeling of target molecules of cells and imaging[98] and targeted delivery of anticancer drugs [99].

In this study TiO_2 nanoparticles with a biocompatible coating are prepared. One of the most commonly used methods for the functionalization of titanium dioxide is the silanization of the surface with organofunctional alkoxysilanes. Further, the surface chemistry of TiO_2 nanoparticles smaller than 20nm is characterized by surface and corner defects, which are very reactive towards bidentale ligands.[100] For example, TiO_2 nanoparticles are functionalized with phosphonic acids[101], carboxylic and dicarboxylic acids[102] and catechols[103]. A noteworthy property of TiO_2 nanoparticles is their photocatalytic activity[104, 105, 106]. According to the band model for semiconductors TiO_2 possesses a band gap (the energy gap between the highest filled valence

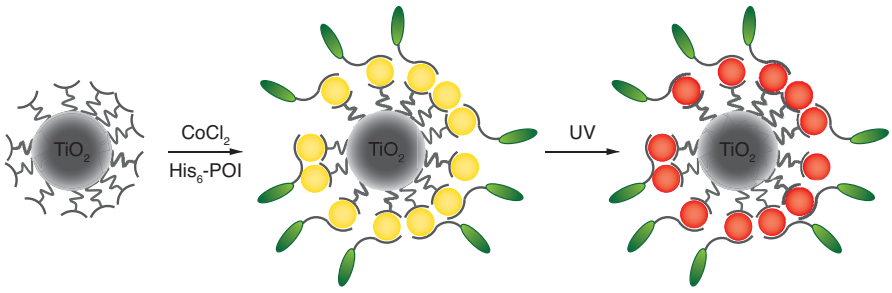

Figure 2.14: Co(III) mediated immobilization of the protein of interest on TETT coated TiO_2 nanoparticles. The chelating TETT groups on the nanoparticles' surface are loaded with Co^{2+} ions (yellow circle) and the protein of interest (green ellipse) is coordinated through its His_6-tag. The Co(II) centers are oxidized through UV illumination of the TiO_2 nanoparticles to Co(III) (red circle).

band and the lowest vacant conduction band) of 3.2 eV. Thus, excitation with UV irradiation leads to the generation of electron - hole pairs; the lifetime of the excited state, which is in the nanosecond regime, is sufficient for charge transfer to species adsorbed on the surface and formation of radicals. Doping TiO_2 with a metal, a nonmetal or a combination of metal and nonmetal like for example cobalt-carbon-sulfur co-doped anatase TiO_2 nanoparticles[107] and Fe_3O_4-TiO_2 core-shell nanoparicles[108] as well as the discovery of a substoichiometric titanium terminated anatase surface[109] facilitates the preparation of visible light responsive photocatalysts with a reduced band gab and an associated absorbance in the visible range of the spectrum.

In this part of the study advantage is taken of the photocatalytic properties of TiO_2 nanoparticles for the stable immobilization of His-tagged proteins through Co(III) complexes. Particularly, the conversion of a preformed Co(II) coordination complex between TiO_2 nanoparticles coated with a chelating ligand and a His-tagged protein into the corresponding Co(III) complex is aimed (Fig. 2.14). Consequently, the kinetic and thermodynamic properties of the complex are altered. The kinetic inertness and thermodynamic stability of Co(III) complexes can be beneficial in biomedical application where the stable coating and immobilization of nanoparticles with protein shells is desired.

2.3.1 Synthesis and characterization of TiO_2-TETT nanoparticles

TiO_2 nanoparticles functionalized with an organic layer of *N*-(Trimethoxysilylpropyl) ethylene diamine triacetic acid (TETT) are synthesized according to the procedure published by Qin *et al.* [110]. Briefly, the nanoparticles are prepared in a two step synthesis comprising first the formation of oleic acid stabilized TiO_2 nanoparticles and second the surface modification with TETT (Fig.

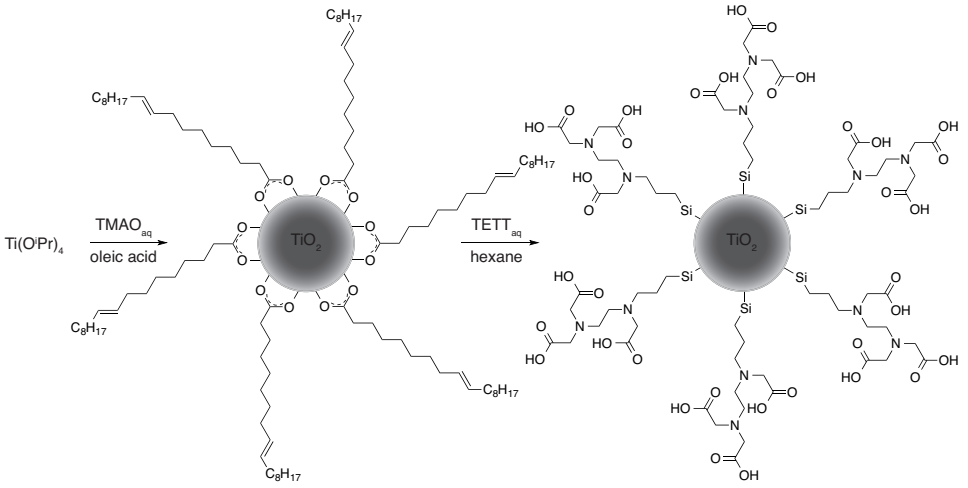

Figure 2.15: Synthesis of TETT coated TiO_2 nanoparticles in a two step procedure according to Qin *et al.*[110].

2.15). The hydrolysis of titanium(IV) isopropoxide in oleic acid results in the formation TiO_2 nanorods with anatase crystal structure; the shape and aspect ratio of the nanoparticles can be controlled by tuning their growth kinetics.[101] The replacement of the oleic acid capping with TETT alters the surface polarity and yields the water dispersibile TiO_2-TETT nanoparticles.

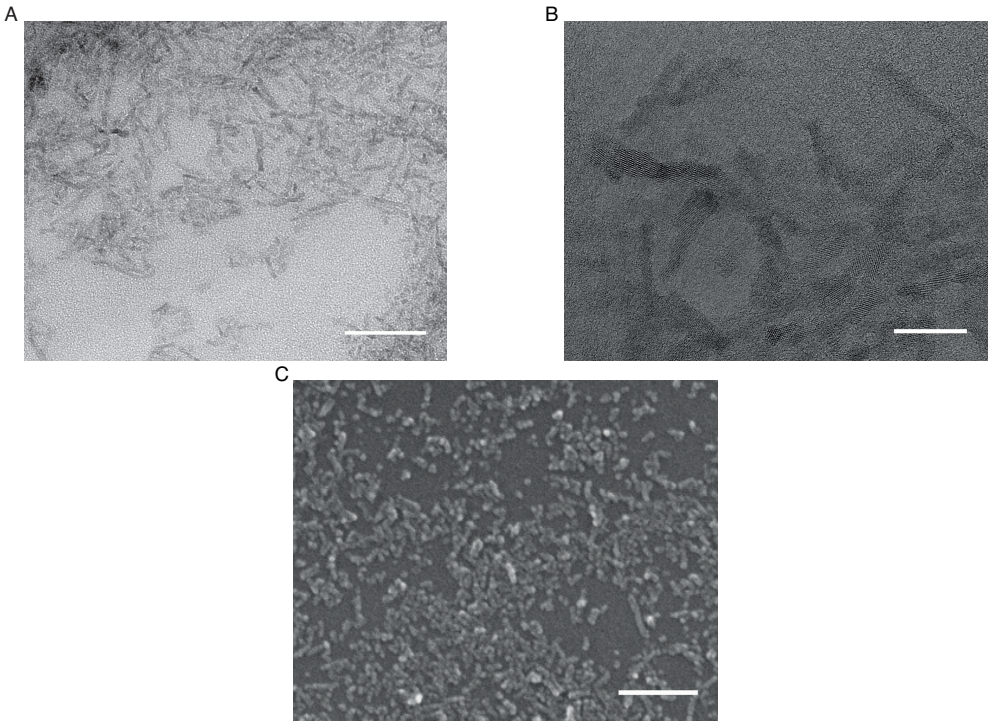

Figure 2.16: Characterization of TiO_2-TETT nanoparticles by **A.** TEM, **B.** high resolution TEM and **C.** SEM. The high resolution TEM image shows the crystalline strutucre of the TiO_2-TETT nanoparticles. The scale bars represent A. 50 nm, B. 15 nm and C. 150 nm

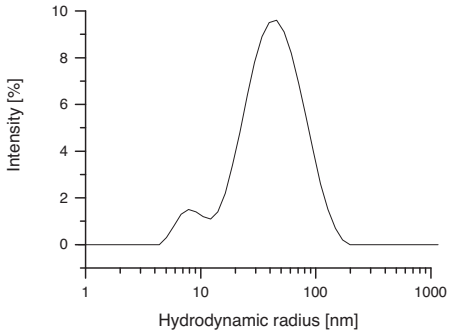

Figure 2.17: Size distribution of an aqueous suspension of TiO_2-TETT nanoparticles measured by DLS. An exemplary spectra is shown.

The synthesized TiO_2-TETT nanoparticles are characterized by transmission electron microscopy (TEM) and scanning electron microscopy (SEM) imaging (Fig. 2.16). As previously reported[110] the nanoparticles are rod shaped and a few nanometers in size. The hydrodynamic radius of the TiO_2-TETT nanoparticles is measured by dynamic light scattering (Fig. 2.17). Two local maxima in the intensity are detected at a hydrodynamic radius of 7.8 nm and 45.6 nm, respectively.

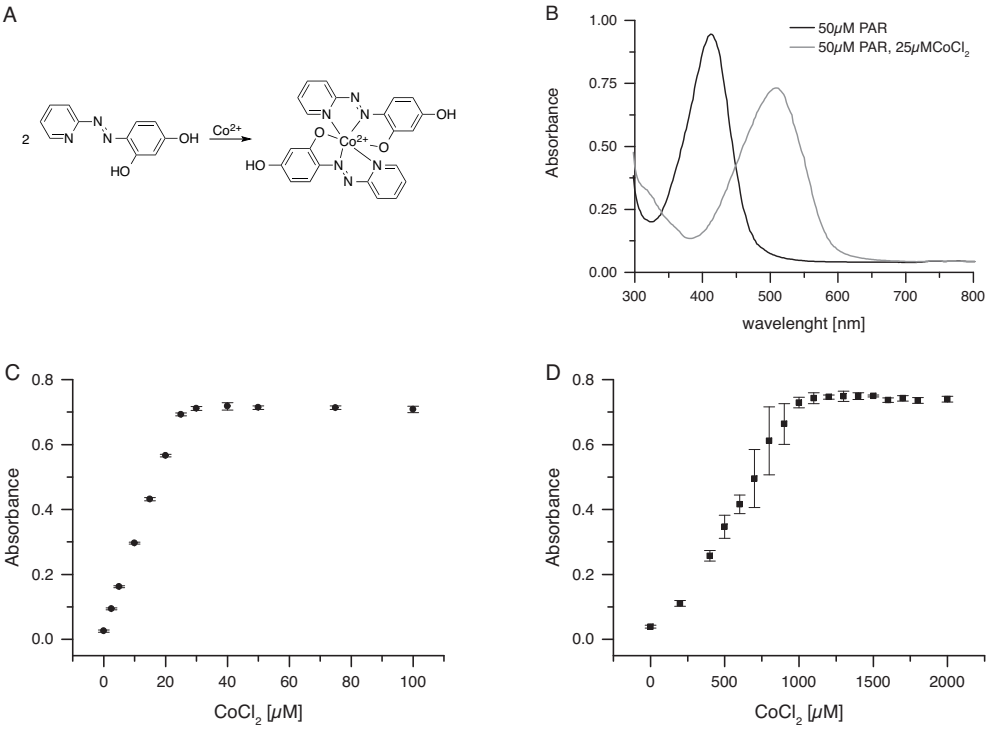

Figure 2.18: Colorimetric detection of Co^{2+} ions with 4-(2-pyridylazo)-resorcinol. **A.** The complexation of Co^{2+} ions by the chelating ligand results in a **B.** red shift of the absorbance spectra. Titration of 50 µM PAR against $CoCl_2$ in 10 mM Tris buffer **C.** in the absence or **D.** in the presence of 1 mg/mL TiO_2-TETT nanoparticles. The absorbance at $\lambda = 508$ nm is measured, background corrected by the absorbance of the 10 mM Tris buffer and averaged (mean and standard deviation) over 3 experiments.

The organic TETT coating of the nanoparticles is suitable for modifications based on coordination chemistry due to the multidentate ligand structure. The Co(II) binding capacity of the TiO_2-TETT nanoparticles is determined by titration of TiO_2-TETT with different $CoCl_2$ concentrations in the presence of the metallochromic indicator 4-(2-pyridylazo)resorcinol (PAR) (Fig. 2.18). The tridentate ligand PAR binds to a variety of divalent transition metal ions in a 2:1 complex through the pyridyl nitrogen, the distal nitrogen of the azo moiety, and the 3-phenolate oxygen of the resorcinol moiety. [111, 112, 113] The metal ion complexation results in a red shift of the absorbance spectra maximum from

412 nm to 508 nm for Co(II). The shift in the absorbance maximum is visible by a color change of the aqueous solution from yellow to red.

Absorbance measurements of PAR with different $CoCl_2$ concentrations confirm the formation of a 2:1 ligand to metal centre complex and show saturation in the absorbance at half the concentration of the PAR ligand (50 µM PAR, 25 µM $CoCl_2$). In contrast, when the same titration is performed in the presence of 1 mg/mL TiO_2-TETT nanoparticles, the saturation in the absorbance spectra is achieved at significantly higher $CoCl_2$ concentration (1.03 mM $CoCl_2$; determined as the intersection of two linear fits in the range of 0.2 - 1.0 mM and 1.1 - 2.0 mM $CoCl_2$, respectively). This shows that except for the low concentration of Co^{2+} ions complexed by PAR (25 µM), the remaining Co^{2+} ions are coordinated through the polydentate TETT ligand immobilized on the TiO_2 -TETT nanoparticles. To ensure that all added cobalt ions are complexed by the TETT ligand and that there are no free cobalt ions in the solutions, a ratio of 1 mM $CoCl_2$ per 1 mg/mL TiO_2-TETT is used throughout all following experiments.

2.3.2 Photochemical characterization of TiO_2-TETT nanoparticles

Consecutively, the photoactivity the TiO_2-TETT nanoparticles under UV light irradiation and the photooxidation of Co^{2+} ions is investigated. To demonstrate the photoactivity of these nanoparticles, solutions containing TiO_2-TETT nanoparticles with and without $CoCl_2$ are exposed to either UV light (254 nm or 365 nm) or ambient light using terephthalic acid (TA) as a detection reagent for hydroxyl radical formation. The non-fluorescent TA reacts in a free radical mediated aromatic hydroxylation with hydroxyl radicals to form only one monohydroxylated isomer, 2-hydroxyterephthalic acid (2-HTA), which is fluorescent.[114] Fluorescence intensity measurements of solutions containing the TiO_2-TETT nanoparticles with and without $CoCl_2$ that are irradiated with 254 nm UV light show increasing fluorescence intensity with increasing illumination time (Fig. 2.19). However, a significant lower 2-HTA formation over time is noticed for the TiO_2-TETT solution with $CoCl_2$ indicating the reaction of Co^{2+} ions with some generated radicals to potentially form Co^{3+} ions. In comparison, TiO_2-TETT nanoparticle solutions with and without $CoCl_2$ exposed to ambient light do not exhibit any detectable fluorescence regardless of the illumination duration over 4 h. Likewise, when irradiating a $CoCl_2$ solution without TiO_2-TETT nanaoparticels with 254 nm UV light no 2-HTA is produced, which clearly points out that the TiO_2-TETT nanoparticles cause the radical formation through their photoactivity.

Similar results are obtained when performing the identical experiment under a 365 nm UV source instead of a 254 nm UV lamp (Fig. 2.19). The TiO_2-TETT nanoparticles with and without $CoCl_2$ can also generate hydroxyl radicals under 365 nm UV light as the 2-HTA fluorescence increases over time. Here, once again the presence of the $CoCl_2$ leads to a lower concentration of 2-HTA formed by aromatic hydroxylation at the respective times. The dif-

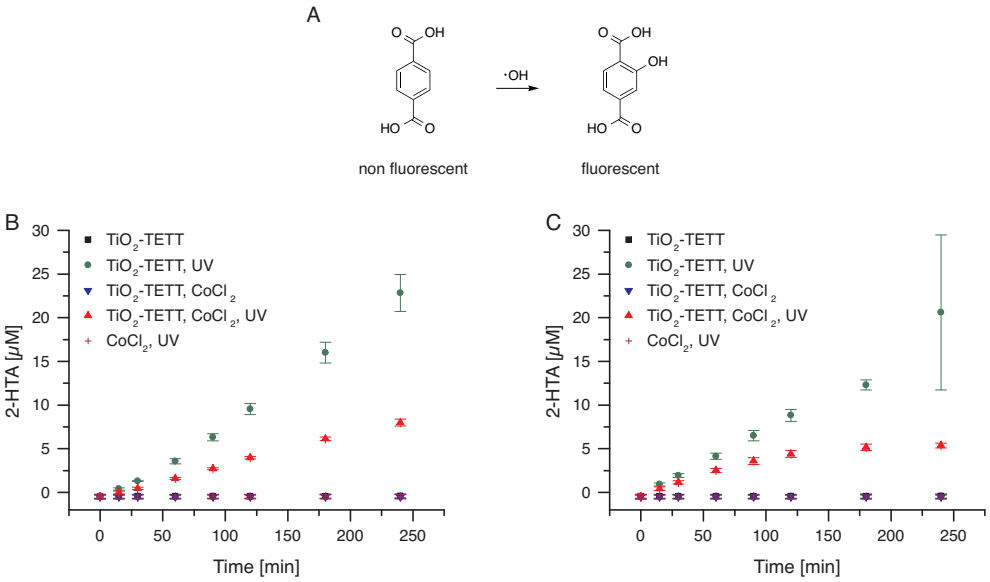

Figure 2.19: A. Radical oxidation of terephthalic acid to 2-hydroxyterephthalic acid. Photoactivity of TiO_2-TETT nanoparticles under illumination at **B.** 254 nm and **C.** 365 nm. Time-dependent fluorescence intensity measurements of 2-hydroxyterephthalic acid (λ_{ex} = 315 nm, λ_{em} = 425 nm) formed by TiO_2-TETT nanoparticle mediated photooxidation of terephthalic acid. Solutions of TiO_2-TETT nanoaprticles without or loaded with $CoCl_2$ in Tris buffer (pH 7.4) supplemented with terephthalic acid are illuminated with ambient light or UV light (**B.** 254 nm, **C.** 365 nm) for different time points. As a control $CoCl_2$ in Tris buffer pH 7.4 supplemented with terephthalic acid is used and exposed to UV light. Data represent the mean and the standard deviation of the concentration of produced 2-hydroxyterephthalic acid from 4 independent experiment. Points of the data series 1 (TiO_2-TETT) , 3 (TiO_2-TETT with $CoCl_2$) and 5 ($CoCl_2$, UV) overlap partially. Due to the illustration some error bars are not visible.

ference in the 2-HTA generation points to the oxidation of the TETT ligand complexed Co^{2+} to Co^{3+} ions. In this case also the TiO_2-TETT solution with and without $CoCl_2$ exposed to ambient light as well as the $CoCl_2$ solution (without TiO_2-TETT nanoparticles) irradiated with 365 nm UV light do not produce detectable amounts of 2-HTA at any of the points in time within the considered timeframe.

Complementary to the 2-HTA fluorescence intensity measurements, which monitor the photoactivity of the TiO_2-TETT nanoparticles, the absorbance of the corresponding solutions is analyzed to follow the formation of Co^{3+} species, which exhibit a prominent absorption in the visible range of the spectrum. The local maximum in the absorbance spectra is at λ = 550 nm (Fig. 2.20). Indeed, the absorbance at λ = 550 nm for samples with TiO_2-TETT nanoparticles and $CoCl_2$ that are treated with UV light (either 254 nm or 365 nm) increases over time. While the absorbance for samples treated with 254 nm UV light reaches

saturation within 3-4 h of illumination, samples treated with 365 nm UV light require longer illumination for measurable absorbance at 550 nm and do not reach saturation within the considered time frame. Moreover, an increase in the absorbance of the TiO_2-TETT nanoparticle solution without $CoCl_2$ is observed upon exposure to UV light after 4 h with the 254 nm light source and after 3 h with the 365 nm light source. This rise in absorbance is accompanied by an optically visible turbidity of the respective solutions due to the agglomeration and precipitation of the TiO_2-TETT nanoparticles. TiO_2-TETT nanoparticle samples exposed to ambient light without and with $CoCl_2$ as well as $CoCl_2$ without nanoparticles either treated with 254 nm or 365 nm UV light do not show any change in the absorbance (Fig. 2.20).

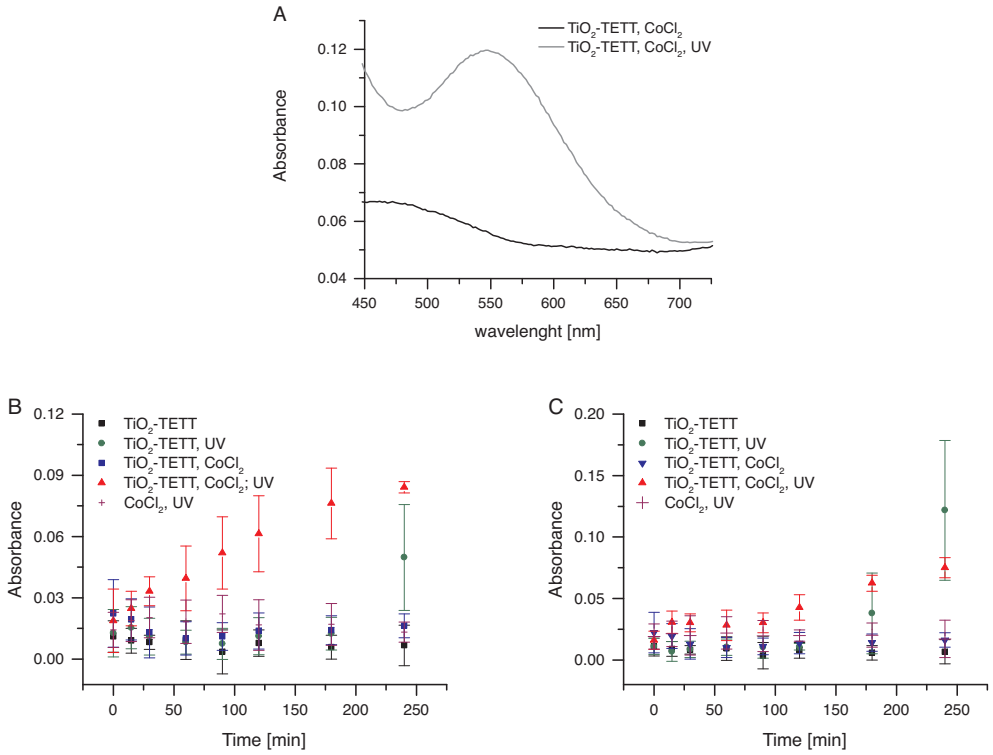

Figure 2.20: Photoactivity of TiO_2-TETT nanoparticles under UV irradiation. **A.** Absorbance spectra of a solution containing TiO_2-TETT nanoparticles and $CoCl_2$ before and after 254 nm UV irradiation for 4 h. Time dependent absorbance measurements of Co(III) species at $\lambda = 550$ nm are performed. The sample solutions are either exposed to ambient light or **B.** 254 nm or **C.** 365 nm UV light. The absorbance of Tris buffer is subtracted from the measured values. Data points show the mean values and standard deviations of n = 4-7 independent experiments.

From these results it can be concluded that the photoactivity of the TiO_2-TETT nanoparticles can be utilized to photochemically oxidize Co^{2+} to Co^{3+}. The photochemical oxidation requires the balance between sufficient irradiation

for satisfactory oxidation of the Co(II) centers to Co(III) and agglomeration of the nanoparticles at too high radiation doses. For further experiments and stable immobilization of His-tagged proteins on the TiO_2-TETT nanoparticles, 3 h exposure to the 254 nm UV light are used as optimal parameters to obtain an almost complete oxidation of the cobalt ions and no agglomeration of the nanoparticles.

Assuming that solely Co(III) complexes contribute to the absorbance at $\lambda = 550$ nm and that the oxidation of the Co^{2+} ions immobilized on the TiO_2-TETT nanoparticles to Co^{3+} is complete once reaching the saturation level, the absorbance approximately corresponds to 1mM Co^{3+} complex, which formed after 3 - 4 h of 254 nm UV illumination. In comparison to the oxidized cobalt ions, only low concentrations of 2-HTA are produced under the same conditions in the same time frame (16.8 µM and 7.4 µM 2HTA after 3 h of UV illumination in the absence and presence of $CoCl_2$, respectively). This prominent deviation in the concentrations of the two resulting oxidation products, Co^{3+} and 2-HTA, can be attributed to differing quantum yields of the different active oxidant species involved in the particular oxidation process. While the formation of the fluorescent 2-HTA during the photocatalytic reaction results from the specific reaction of hydroxyl radicals with TA, oxidative reactions on TiO_2 especially occur by photogenerated holes.[115, 116]

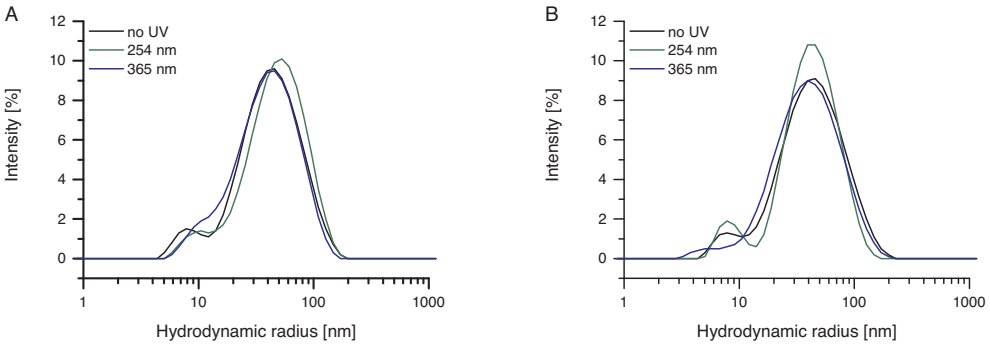

Figure 2.21: The size distribution of **A.** TiO_2-TETT nanoparticles and **B.** TiO_2-TETT nanoparticles loaded with Co^{2+} ions measured by DLS. The sample solutions are exposed to UV light (254 nm or 365 nm) for 3 h. Data show exemplary spectra.

Further, the size distribution of the TiO_2 nanoparticles before and after illumination with UV light in the presence or absence of $CoCl_2$ is analyzed by DLS. As illustrated by exemplary spectra (Fig. 2.21) the illumination of the TiO_2-TETT nanoparticles in Tris-NaCl buffer with either the 254 nm or 365 nm UV light for 3 h causes no significant change in the size distribution. However, the visually observed turbidity after 3 h exposure to 365 nm UV light (see above) can not be located in the spectra. This might be potentially due to the sedimentation of large agglomerates. Further, in the case of Co^{2+} loaded nanoparticles neither 254 nm nor 365 nm UV irradiation affect significantly

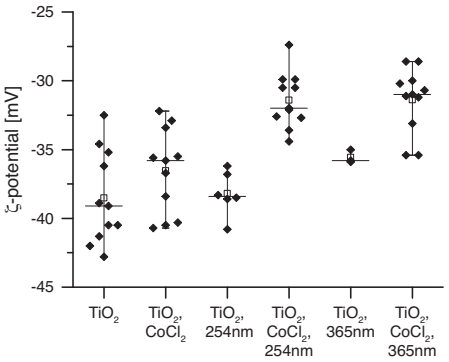

Figure 2.22: ζ-potential of 1 mg/mL TiO_2-TETT nanoparticles in 10 mM Tris buffer in the presence or absence of 1 mM $CoCl_2$. Sample solutions are either exposed to 254 nm or 365 nm UV light for 3 h. Data points originate from three independent experiments except for TiO_2, 254 nm (two samples) and TiO_2, 365 nm (one sample). Median (-) and mean(x) are displayed.

the size distribution of the nanoparticles. Finally, the loading of the organic TETT coating with Co^{2+} ions has marginal effect on the hydrodynamic radius of the nanopatricles.

Additionally, the ζ-potential of the TiO_2-TETT nanoparticles under the conditions mentioned before are quantified (Fig. 2.22). TiO_2-TETT nanoparticles in aqueous Tris-NaCl buffer have on average a ζ-potential of -38.5 mV. In comparision, the ζ-potential of Co^{2+} loaded nanoparticles (-36.5 mV) is increased due to the coordination of positively charged Co^{2+} ions to the chelating organic coating. There is no significant change in the ζ-potential of pure TiO_2-TETT nanoparticles upon illumination with 254 nm UV light. However, exposure of the TiO_2-TETT nanoparticles to 365 nm UV light induces a moderate increase in the ζ-potential. In consideration of the absorbance measurements the changes in the ζ-potential may be associated with alterations in the structure of the nanoparticles. Furthermore, the illumination of Co^{2+} loaded TiO_2-TETT nanoparticles with either 254 nm or 365 nm UV light results in a significant increase of the ζ-potentials (-31.4 mV for both). This further supports the oxidation of the coordinated Co^{2+} to the corresponding Co^{2+} complexes accompanied by a positive charging of the nanoparticle surface.

2.3.3 Protein immobilization using His_6-GFP as a model protein

After confirming the cobalt binding capacity, the photoactivity of the TETT coated TiO_2 nanoparticles and the TiO_2 mediated photochemical oxidation of surface bound Co^{2+} to Co^{3+}, His_6-GFP is used as a model protein for stable protein immobilization on the TiO_2-TETT nanoparticels through photochemical oxidation of the corresponding Co^{2+} complex. TiO_2-TETT nanoparticles are loaded with Co^{2+} ions and His_6-GFP is linked through the coordina-

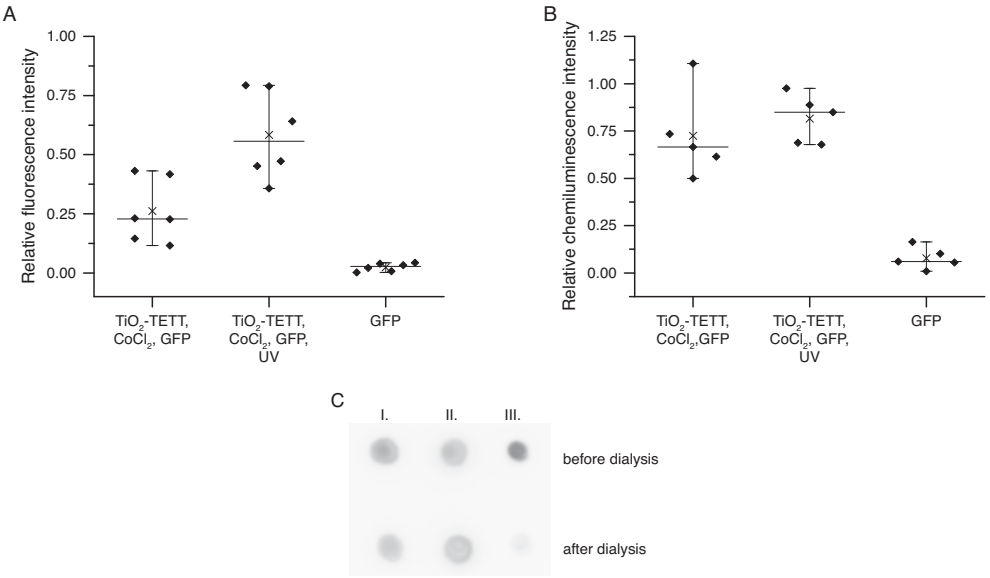

Figure 2.23: Relative amount of protein immobilized on TiO_2-TETT nanoparticles analyzed by **A.** fluorescence intensity measurements and **B.** indirect immunochemiluminescence assay. The $[Co^{II}(TETT\text{-}TiO_2)(His_6\text{-}GFP)]$ complex is preformed (I.) and oxidized photochemically by 254 nm UV irradiation (II.). Afterwards the protein solutions are dialyzed against Tris-NaCl buffer to remove all unbound protein. A pure protein solution is used as a dialysis control (III.). The presented values are background corrected (fluorescence of the Tris-NaCl buffer and grey value of the nitrocellulose membrane, respectively) and normalized to the appropriate value before dialysis. Data points originate from 6 (fluorescence measurements) and 3 (chemiluminescence assay) technical replicates. In the scatter plot the median (-) and the mean (x) are marked. **C.** Representative image of the indirect immunochemiluminescence assay.

tion complex. The protein loaded nanoparticles are either exposed to ambient light or UV light for 3 h. Subsequently, the solutions are dialyzed against the buffer to remove all unbound protein by means of a dialysis membrane with a molecular weight cut-off (MWCO) noticeable larger than the protein itself (MWCO = 100 kDa, MW(His_6-GFP) = 26.8 kDa). To determine the amount of protein immobilized on the nanoparticles, the relative amounts of GFP before and after dialysis is measured by fluorescence and an indirect chemiluminescence assay (Fig. 2.23).

The relative fluorescence intensities highlight the significantly increased amount of protein bound to the nanoparticles for the 254 nm UV treated sample compared to the non-irradiated sample. Here, the UV treatment results in the oxidation of the initially formed TETT-Co^{II}-His_6-GFP complexes to the corresponding Co(III) complexes and yields a kinetically inert immobilization through the Co^{3+} mediator ion. Comparatively, in the unoxidized case the amount of protein bound to the nanoparticles is decreased as the protein washes off over time due to the kinetic lability and lower thermodynamic sta-

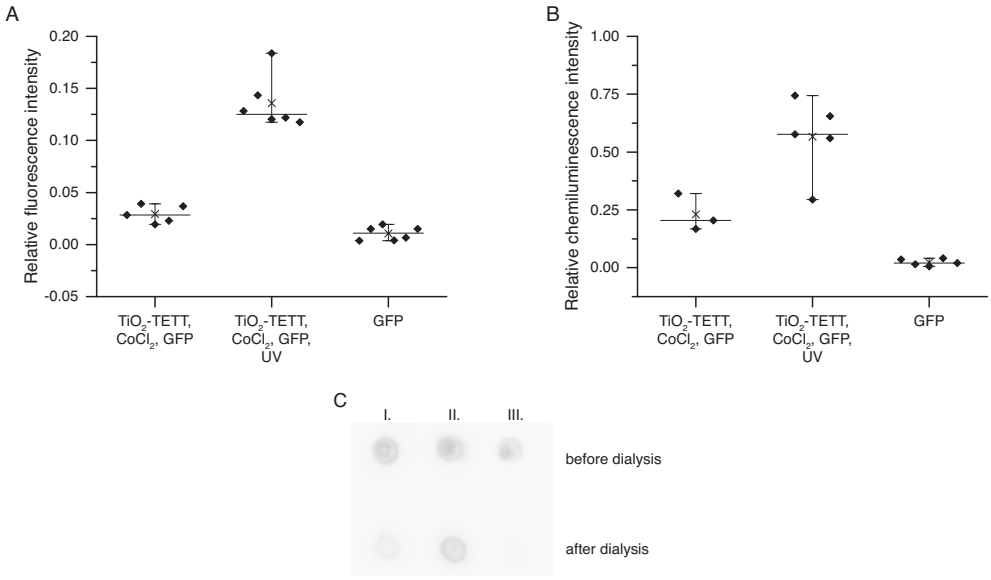

Figure 2.24: Relative amount of GFP immobilized on TiO_2-TETT nanoparticles determined by **A.** fluorescence intensity measurements and **B.** indirect immunochemiluminescence assay. TiO_2-TETT nanoparticles, $CoCl_2$ and His_6-GFP are mixed to form the corresponding Co(II) mediated complex (I.). Optionally, the solution is treated with UV light to convert the Co(II) complex into the Co(III) complex (II.). Further a protein solution without nanoparticels and $CoCl_2$ is used as a control (III.) Unattached protein is removed by dialysis against Tris-NaCl buffer containing imidazole. Values are background corrected (fluorescence of the Tris-NaCl buffer and grey value of the nitrocellulose membrane, respectively) and normalized to the appropriate value before dialysis. Data points present 5-6 (fluorescence measurements) and 2-3 (chemiluminescence assay) technical replicates.The median (-) and the mean (x) are indicated. **C.** Representative image showing the amount of protein detected by the indirect immunochemiluminescence assay.

bility of the Co(II) complex. In comparison, the indirect immunochemiluminescence assay shows a less clear result. Although a stronger signal and therefore higher protein amount is detected in the case of the UV treated solution, the difference between the oxidized and the non-oxidized sample is considerable less pronounced. Consistently, with both methods only a weak signal at background level is detected for a pure His_6-GFP solution, which proves that all unbound protein diffused through the dialysis membrane. At the same time, it verifies that the detected signals for the GFP loaded nanoparticles originates from protein specifically immobilized on the nanoparticles through complex chemistry.

Performing the experiment under the same conditions except for the use of an imidazole containing buffer in the dialysis step yields qualitatively similar results even though there are quantitative differences (Fig. 2.24). Imidazole is a monodentate complex ligand and competes at high concentrations with the multidentate His-tag of the protein resulting in the release of loosely bound

protein. In this experiment, both relative fluorescence intensity measurements and indirect immunochemiluminescence assay yield a significant higher signal for UV treated TiO_2-TETT nanoparticles loaded with His_6 -GFP compared to the non-oxidized case. A higher amount of protein is retained on the oxidized nanoparticles due to the photooxidation of the Co(II) to the corresponding Co(III) complexes and accompanied changes in kinetic and thermodynamic properties of the complex. In the non-oxidized case a large fraction of the protein is washed off from the nanoparticles over time through ligand exchange with imidazole. Here, again a dialysis control containing His_6 -GFP shows very limited quantities of protein in both the relative fluorescence measurement and the indirect immunochemiluminescence assay. This confirms the removal of all unbound protein from the solutions through dialysis. Comparing the results to those obtained with the Tris-NaCl buffer the amount of surface immobilized GFP is less in the case of the buffer containing imidazole for both analysis strategies. The high concentration of imidazole leads to competitive ligand exchange reactions releasing the His-tagged GFP from the particle surface. This affects primary the weakly bound Co^{2+} mediated interaction between the TETT chelator and the His-tagged protein, but also the more stable Co^{3+} mediated interaction to some extent.

Summarily, although the two quantification methods show the same trend for the different samples for both the Tris-NaCl and the Tris-NaCl buffer containing imidazole they differ in quantities (note the varying scalings of the graphs). Direct measurements of the relative fluorescence intensities of the GFP generally exhibit lower protein concentrations compared to the results determined by indirect immunochemoluminescence assay. Especially, for the buffer containing imidazole the protein amount specified by fluorescence measurements is substantially lower than by chemiluminescence. Both techniques have their advantages and drawbacks that have to be considered. While the fluorescence intensity measurement is a direct detection method, the indirect immunochemiluminescence approach bases on the interaction of a primary antibody with the protein and the subsequently binding of a secondary antibody conjugated to horseradish peroxidase producing enhanced chemiluminescence by luminol. Generally, indirect analysis assays are inherently more prone to errors compared to direct methods. On the other hand, the treatment of the fluorescent protein GFP with UV light is a critical point as proteins have an intrinsic absorption in the UV range (280 nm).

Concluding, the His-tagged protein is stably attached to TiO_2 nanoparticles via the TETT surface coating. In a study by Qin *et al.* the TiO_2-TETT nanoparticles are employed for investigating the effect of the loading mode of the chemotherapeutic doxorubicin on cellular delivery.[110] The doxorubicin is either non-covalently bound to the TiO_2-TETT nanoparticles through electrostatic interaction or via covalent conjugation of the primary amine of doxorubicin to the carboxylic acid functionalities through EDC/NHS coupling. The non-covalent, electrostatic interaction is unspecific, whereas the covalent linking results - in this case - in site-specific immobilization. However, for more complex target molecule with more than one primary amine acting as nucle-

ophile the EDC/NHS coupling strategy leads to disorientated arrangement of the ligand. In comparison, this approach allows for the site-specific immobilization of proteins on the surfaces of the nanoparticles as protein engineering facilitates the fusion of the His-tag to the protein of interest in the desired position. Further, the thermodynamic and kinetic properties of the Co(III) complex constitute to the high stability of the system.

2.3.4 Uptake of transferrin decorated TiO_2-TETT nanoparticles

As a first proof of principle the bioactive and targeting protein transferrin is immobilized on TiO_2-TETT nanoparticels and the cellular uptake is visualized. For the purpose of quantification and localization of the protein the human transferrin with C-terminal His-tag is labeled with a fluorescent dye. The coupling is achieved by covalent attachment of primary amines of the protein to the NHS functionalized chromophore Atto647N-NHS. The optically visible color of the solution and the absorbance spectrum of the reaction product proves the successful labeling.

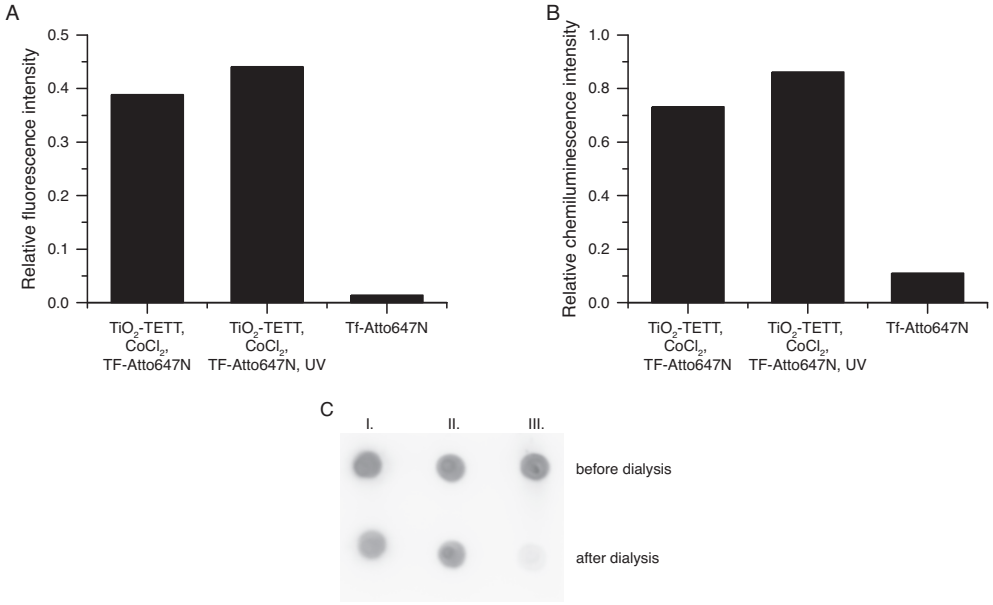

Figure 2.25: Fluorescently labeled His_6-tagged transferrin (Tf-Atto647N) immobilized on TiO_2 nanoparticles. **A.** Relative protein amounts after dialysis determined by fluorescence intensity measurements (λ_{ex} = 644 nm, λ_{em} = 669 nm). The fluorescence intensity values are corrected by the fluorescence intensity of the Tris-NaCl buffer and normalized to fluorescence intensities before dialysis. **B.** Corresponding values for the samples in A. determined by an indirect immunochemiluminescence assay. **C.** Photograph of the indirect chemiluminescence assay. I. TiO_2-TETT, $CoCl_2$, Tf-Atto647N, II. TiO_2-TETT, $CoCl_2$, Tf-Atto647N - exposed to 254 nm UV light for 3 h, III. Tf-Atto647N

For the photooxidation mediated immobilization fluorescently labeled hu-

man transferrin with the C-terminal His-tag is bound to the titanium dioxide nanoparticles through Co(II) (as for the immobilization of His_6-GFP on TiO_2-TETT nanoparticles). The transferrin loaded TiO_2 nanoparticles are exposed to 254 nm UV light for 3 h to oxidize the Co^{2+} mediator ions to Co^{3+}. Unbound protein is subsequently removed from the solution by dialysis (dialysis membrane: MWCO = 300 kDa, MW(Transferrin-His_6) = 76 kDa). Also here the amount of immobilized protein is quantified by the relative fluorescence intensity measurement and an indirect immunochemiluminescence assay (Fig. 2.25). Preliminary results of both techniques show that His-tagged transferrin is immobilized on the nanoparticles. But only slightly higher protein amount is observed on the TiO_2-TETT nanoparticles exposed to UV radiation compared to the non-irradiated sample. Consistently, only a very weak signal is measured for the control sample where the protein is not bound to nanoparticles proving efficient removal of free transferrin by dialysis. Here too, the qualitative tendency is identical, but disparity is observed in quantity. Again, direct fluorescence measurements yield lower values compared to the indirect chemiluminescence based method. Reasons for this discrepancy are the same as mentioned above.

The cellular uptake behavior of the transferrin coated TiO_2 nanoparticles is studied using two different human cell lines, hFF and panc-1. The two cell types are selected due to their difference in the expression levels of the transferrin receptor. To confirm this, the expression pattern is analyzed through a Western blot, a technique based on the separation of proteins according to their mass and the detection of the protein of interest by an indirect immunochemiluminescence assay. As a control the β-actin expression level is considered. The Western blot (Fig. 2.26) highlights a significant discrepancy in the amount of transferrin receptor for hFF and panc-1 cells; the signal for panc-1 is more pronounced. Yet, the protein amount of β-actin is similar in both cases. Thus, the higher expression level of the transferrin receptor level in panc-1 compared to hFF is evidenced.

Adherent panc-1 and hFF cells are incubated with transferrin coated TiO_2-TETT nanoparticles for 15 h and the cellular uptake of the nanoparticles is visualized by fluorescence microscopy (Fig. 2.26). In both cell types agglomerates of transferrin coated nanoparticles are found on the cell surface. Moreover, clear individual events of nanoparticles or small clusters of nanoparticles inside the cell are observed in panc-1 cells. However, the spread hFF fibroblasts have a low expansion in z direction (perpendicular to the surface). Thus, an unambiguous assignment of nanoparticles attached on the cell surface and inside the cell can not be made. Further, significant agglomeration of the transferrin coated TiO_2-TETT nanoparticles complicates the detection of signals from smaller clusters. Therefore, optimization of the experiment details is required to obtain meaningful results. Noteworthy factors include the nanoparticle concentration, incubation medium, incubation duration and the starving of cells prior/during the the experiment. Control experiments are required to establish a correlation of the protein coating of the nanoparticles and cellular uptake behavior. At best, a direct comparison of the cellular uptake is made in the

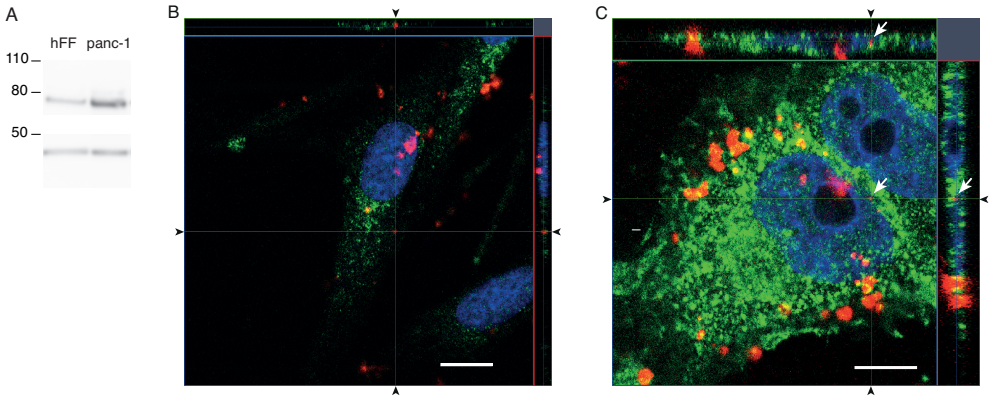

Figure 2.26: A. Western blot of hFF and panc-1 showing the transferrin receptor and β-actin band. Confocal fluorescence images of **B.** hFF and **C.** panc-1 cells. Tf-Atto647N coated TiO_2 nanoparticles are illustrated in red, the transferrin receptor in green and cell nuclei in blue. The images show a section in the xy plane and the projections along the axis (indicated by black arrow heads) in z plane on the top and right side, respectively. Internalized Tf-Atto647N coated TiO_2-TETT nanoparticles are indicated by white arrows. Scale bars represent B. 10 µm and C. 7.5 µm.

same cell line at two different transferrin receptor expression levels (over or down regulated by transfection, gene knock down or blocking). Further, the conservation of the protein's activity after the oxidation has to be considered.

In summary, the synthesis and functionalization of titanium dioxide nanoparticles with His-tagged protein through Co(II) and Co(III) is established. In this respect, the TiO_2-TETT nanoparticles are loaded with Co^{2+} ions and His-tagged protein is coordinated to open coordination sites of the mediator ion. Further, the Co^{2+} mediator ions are photooxidized to Co^{3+} through irradiation of the titanium dioxide with UV light affecting the thermodynamic and kinetic properties of the complex. Thus, the Co(III) mediated interaction conduces for the stable attachment of proteins on the TiO_2 nanoparticles. The applicability of this approach is demonstrated with the model protein His_6-GFP and His_6-tagged human transferrin.

Chapter 3

Summary and Outlook

In the scope of this study distinct chemical modifaction strategies of surfaces functionalization with biomolecules are investigated. For this purpose three different approaches are pursued, dealing with the surface modification through CuAAC click reaction, the stabilization of protein immobilization for surface bound preformed NTA-Co^{II}-His-tag complexes through chemical oxidation and the stable immobilization of His-tagged proteins on titanium dioxide nanoparticles through photochemical oxidation of the corresponding Co(II) complex. While the first strategy uses covalent linking of the ligand of interest on the surface, the latter two are based on coordination chemistry. However, the Co(III) mediated interaction is characterized through high thermodynamic stability and kinetic inertness.

The first section of this study deals with the covalent coating of glass and glass-like substrates with a protein repellent PEG with a functional alkyne moiety. In a second step, the available alkyne groups are modified with a variety of organic azides by CuAAC. The density of alkyne moieties on the interface can be tuned by mixing with a second inert PEG2000. These interfaces are characterized with different approaches including fluorescence microscopy, XPS, ligand density determination through enzymatic digestion, QCM-D and a cell adhesion assay. Consistently, a good correlation between the molar ratios of the two PEGs in solution in the silanization reaction and the surface functionalization density is obtained. Further, the formation of 1,4-disubstituted 1,2,3-triazoles is confirmed by the nitrogen XPS signal. The density of coupled ligand determined by the enzymatic digestion assay is 38.9 pmol/cm^2 for a pure PEG-alkyne monolayer. The cell adhesion assay reveals that a density of 0.1 - 1 mol% of the adhesion ligand cRGD is sufficient for REF YFP-paxillin cell adhesion. Furthermore, dual functionalized biointerfaces are established by combination of the click chemistry based approach with gold nanostructured substrates prepared by BCMN. The gold nanoparticles serve as anchoring point for a second thiolated ligand whose density and spatial arrangement can be controlled in defined manner. Yet, unspecific interactions between the interface and biomolecules or cells are prevented by the protein repellent PEG layer. As a proof of principle a partially nanostructured surface is labeled with two distinct fluorophores verifying the orthogonality of the coupling strategies

based on CuAAC and the gold thiol interaction. The dual functionalized interfaces are utilized to investigate the interplay of the adhesion sequence cRGD and the synergy site PHSRN on fibroblast adhesion. While monofunctionalization with either cRGD (attached to gold nanoparticles with an interparticle spacing of 100 nm) or PHSRN (bound to 10 mol% PEG-alkyne) at the corresponding densities do not promote cell attachment, the dual functionalization with both peptides results in a superior effect on cell attachment. The orthogonality of the two functionalization strategies facilitates not only the presentation of adhesion promoting ligands but also nonadhesive signaling molecules to investigate the interplay between two different receptors. For example, the influence of the growth factor bone morphogenetic protein 2 (BMP 2) and cell adhesive peptides like cRGD on cell adhesion dynamics and morphology has been investigated.[117] Moreover, this platform can be used to investigate the mutual influence of two distinct signaling factor on many other processes where presentation of two ligands in controlled density and arrangement on an inert background is required.

In the second part the stable protein immobilization with the Co(III) mediated interaction between the chelator NTA and His-tagged proteins is in the focus. The approach involves the formation of monolayers by self-assembly that present NTA moieties at the interface. The NTA groups are then loaded with the appropriate metal ion and His_6-tagged protein is bound to the two open coordination sites. The preformed Co(II) complex is chemically oxidized to Co(III) using hydrogen peroxide. The resistance against competing ligands of the different Co(III), Co(II) and Ni(II) mediated complexes, the persistence of the Co(III) mediated interaction towards reducing agents and the protein functionality after chemical oxidation is considered. A fundamental difference in the Co(III), Co(II) and Ni(II) mediated NTA protein interaction is their behavior in the presence of high concentrations of competing ligands. Ligand exchange reactions with imidazole result in the unbinding of His_6-GFP on Ni(II) and Co(II) mediated interactions. Opposed to this, the Co(III) mediated interaction remains unaffected by the presence of imidazole due to its high thermodynamic and kinetic stability. A major concern of this immobilization strategy might be the potential conflict of the oxidation step with hydrogen peroxide and the sensitivity of many proteins towards oxidation. Exemplarily, the effect of H_2O_2 on the interaction of protein A and immunoglobulin is investigated. In this case, the oxidation step doesn't affect the interaction of the protein with immunoglobulin. Although, the conservation of the protein's functionality and activity has to be considered case by case, this method can still be applied to oxidation insensitive proteins. Furthermore, the chemical resistance of the Co(III) mediated interaction towards reducing agents is investigated. The Co(III) complexes prove excellently stable against ascorbic acid, TCEP, DTT and sodium sulfite. Thus, His-tagged proteins are stably immobilized on NTA presenting SAMs by the Co(III) mediated interaction. Moreover, this strategy serves as platform for the stable immobilization of oxidation insensitive proteins where higher thermodynamic and kinetic stability compared to the Ni(II) or Co(II) mediated interaction is required. The huge

libraries of His-tagged proteins as well as the large number of readily available His-tagged and NTA functionalized molecules and materials promise high application potential of this immobilization strategy.

In the third part of this study the Co(III) mediated interaction between His-tagged proteins and titanium dioxide nanoparticles functionalized with the chelator TETT is investigated. The complex is prepared in a two step procedure comprising first the formation of the labile $[Co^{II}(TETT)(His_6\text{-protein})]^n$ complex on the TiO_2 nanoparticles' surface and the subsequent oxidation to the corresponding Co(III) complex. The oxidation is mediated through the photoactivated radical formation by semiconducting TiO_2. The titanium dioxide nanoparticles are synthesized in a sequential process consisting of the preparation of oleic acid stabilized TiO_2 nanoparticles through hydrolysis of titanium tetraisopropoxide and a surface modification reaction with TETT. TiO_2-TETT nanoparticles are characterized by electron microscopy and DLS. Further, the accessibility of the chelating end groups for metal ion complexation is investigated. Colorimetric titration reveals an average loading capacity of about 1 mM $CoCl_2$ per 1 mg/mL TiO_2-TETT nanoparticles. On the other hand, the photoactivity of the TiO_2-TETT nanoparticles is proved with the loading of the nanoparticles with cobalt ions results in a lower hydroxy radical formation and the oxidation to Co(III) in the presence of two different UV light sources (254 nm and 365 nm, respectively). For the stable immobilization of a His-tagged protein on the TiO_2-TETT nanoparticels His_6-GFP is used as a model protein. The UV light illumination of the preformed $[Co^{II}(TETT)(His_6\text{-GFP})]^n$ results in the oxidation of the Co(II) centers to Co(III). Both fluorescence intensity measurements and indirect immunochemiluminescence detection reveal a higher stability of the Co(III) mediated TETT protein interaction compared to the equivalent Co(II) species. To test the applicability of this platform for a bioactive protein for targeted delivery, fluorescently labeled human transferrin-His_6 is immobilized on the TiO_2-TETT nanoparticles. As expected, a higher stability for the Co(III) mediated interaction is observed than in the case of Co(II). The investigation of the cellular uptake of the transferrin coated nanoparticles in two cell lines with distinct transferrin receptor expression level is aimed. In conclusion, the stable immobilization of His_6-tagged proteins on TiO_2 nanoparticles through the Co(III) mediated interaction is shown. Further, the applicability of this approach for the stable immobilization of other proteins is interesting as the photooxidation step restricts to oxidation insensitive proteins. Through immobilization of cell receptor specific ligands or cellular localization determining factors targeted delivery to certain types of cells or subcellular compartments might be achieved.

Chapter 4

Materials and Methods

4.1 Materials

4.1.1 Chemicals and supplies

The PEG precursors H_2N-PEG3000-alkyne, H_2N-PEG2000-OCH_3 and N^{ϵ}-azido-*L*-lysine hydrochloride are purchased from Iris Biotech GmbH (Marktredwitz, Germany), HS-$(CH_2)_{11}$-EG_3-NTA from ProChimia Surfaces Sp. z o. o. (Sopot, Poland), and 5/6-carboxyrhodamine 110-EG_3-azide and biotin-EG_3-azide from Jena Bioscience GmbH (Jena, Germany). The custom-made peptides cyclic(RGDfE)K(N_3)-NH_2, K(N_3)PHSRN and Ac-K(N_3)GGNGEPRGDTYRAYK(fluorescein)GG-NH_2 are manufactured by PSL Peptide Speciality Laboratories GmbH (Heidelberg, Germany) and cyclic[RGDfK(3-mercaptopropionyl-aminohexanoic acid)] by Peptides International, Inc (Louisville, USA). The diblockcopolymers polystyrene-*b*-poly-2-vinylpyridine are purchased from Polymer Source, Inc.(Dorval, Canada). The dialysis membranes Spectra/Por6 (MWCO 3.5 kDa), Spectra/Por7 (MWCO 3.5 kDa) and SpectraPor Float-A-Lyzer G2 (MWCO 100 kDa) are obtained from Spectrum Laboratories, Inc. (distributed by Sigma-Aldrich Chemie GmbH (Munich, Germany) or VWR International GmbH (Darmstadt, Germany)), single use micro DispoDialyzer (MWCO 5 kDa) from Harvard Apparatus (distributed by Sigma-Aldrich Chemie GmbH (Munich, Germany)), the nitrocellulose membrane Amersham Protran 0.45 µm NC and Amersham ECL prime Western blotting detection reagent from GE Healthcare Europe GmbH (Freiburg, Germany) and the Ni-NTA superflow cartridge (5 mL) from Quiagen GmbH (Hilden, Germany). Kanamycin monosulfate and isopropyl *β*-*D*-1-thiogalactopyranoside are purchased from Gold Biotechnology, Inc. (St. Louis, USA) and the pET His6 GFP TEV LIC cloning vector (1GFP) is a gift from Scott Gradia (Addgene plasmid # 29663). The antibodies anti-vinculin mouse IgG [hVIN-1], anti-bovine albumin rabbit antibody (whole antiserum) and anti-β-actin mouse IgG1 are purchased from Sigma-Aldrich Chemie GmbH (Munich, Germany), anti-paxillin rabbit IgG [Y113], anti-transferrin rabbit IgG and anti-transferrin receptor rabbit IgG from abcam plc (Cambridge, UK), anti-green fluorescent protein (anti-GFP) rabbit IgG fraction and Alexa Fluor 488 goat anti-mouse IgG (H + L) from Life

Technologies, Inc. (Eugene, USA), Alexa Fluor 647 goat anti-rabbit IgG (H + L) and Alexa Fluor 488 goat anti-rabbit IgG (H + L) from Molecular Probes (distributed by invitrogen detection technologies (Eugene, USA)), horesradish peroxidase (HRP) goat anti-rabbit IgG and HRP goat anti-mouse IgG from Santa Cruz Biotechnology, Inc. (Heidelberg, Germany). Protein A protein fragment with N-terminal His-tag (# ab52953) and recombinant human transferrin protein with C-terminal His-tag (# ab155698) are purchased from abcam plc (Cambridge, UK). NuPAGE® LDS sample buffer (4x), NuPAGE® sample reducing agent (10x), NuPAGE® Bis-Tris gel (4-12%), NuPAGE® MOPS SDS running buffer (20x), NuPAGE® transfer buffer (20x), and Novex® sharp prestained protein standard are purchased from Thermo Fischer Scientific Germany BV & Co KG (Braunschweig, Germany) and Halt™ protease and phosphatase single-use inhibitor cocktail (100x) from Thermo Scientific (Rockford, USA). Hydrogen peroxide (30%) is purchased from AppliChem GmbH (Darmstadt, Germany), ethyl acetate and toluene from Merck KGaA (Darmstadt, Germany), $CuSO_4 \cdot 5\ H_2O$ and magnesium sulfate from Grüssing GmbH Analytika (Filsum, Germany), acetic acid from J.T. Baker (Deventer, The Netherlands) and sodium azide from SERVA Electrophoresis GmbH (Heidelberg, Germany). $CaCl_2 \cdot 2\ H_2O$ and *para*-formaldehyde (PFA) are purchased from RiedeldeHaën (distributed by Sigma-Aldrich), $NiCl_2 \cdot 6\ H_2O$, trimethylamine *N*-oxide and 4-(2-pyridylazo)resorcinol from Fluka (distributed by Sigma-Aldrich) and *N*-(trimethoxysilylpropyl)ethylene diamine triacetic acid trisodium salt (TETT, 45% in water) from abcr GmbH (Karlsruhe, Germany). The following chemicals and supplies are purchased from Carl Roth GmbH & Co. KG (Karlsruhe, Germany): glass coverslips ((20 x 20) mm, (24 x 24) mm), molar sieve (3Å), tris(hydroxymethyl)aminomethane (Tris), NaOH, sodium dodecyl sulfate, lysogeny broth (LB) medium (Luria/Miller), agar-agar (kobe I), powdered milk (low fat), tween-20, Mowiol 4-88, 0.22 µm and 0.45 µm cellulose mixed ester (CME) syringe filters, methanol, ethanol, acetone and n-hexane. All other chemicals are purchased from Sigma-Aldrich (Munich, Germany).

Cell culture reagents including PBS tablets, Dulbecco's modified eagle medium (DMEM, high glucose, pyruvate, #41966), DMEM (high glucose, NEAA, no glutamine, #10938), *L*-glutamine (200 mM), penicillin streptomycin (10000 units/mL penicillin, 10000 µg/mL streptomycin) and 0.05% trypsin-EDTA are purchased from Gibco by life technologies (distributed by Thermo Fisher Scientific Germany BV & Co KG (Braunschweig, Germany)) and cell culture supplies from either nunc (distributed by Thermo Fisher Scientific Germany BV & Co KG (Braunschweig, Germany)) or Greiner Bio-One GmbH (Frickenhausen, Germany). WillCo-dish® glass bottom dishes are purchased from WillCo Wells B.V. (Amsterdam, The Netherlands). YFP-paxillin expressing rat embryonic fibroblasts (REF YFP-paxillin) and rat embryonic fibroblasts, wild type (REF52) are kindly provided by B. Geiger (Weizmann Institute of Science, Israel). Panc-1 cells are a gift of S. Kaufmann (University of Heidelberg, Germany). Human foreskin fibroblasts (hFF-1) are purchased from LGC Standards GmbH (Wesel, Germany).

Unless indicated otherwise, dd water is used in all experiments.

4.1.2 Equipment

Fluorescence imaging is performed using an Olympus IX inverted microscope (Olympus Deutschland GmbH, Hamburg, Germany) in combination with a Delta Vision RT system (Applied Precision Inc., Issaquah, USA), a cooled CCD camera (Photometrics, Tucson, USA) and process controlling through Resolve3D (Applied Precision Inc.,Issaquah, USA). The following two objectives are used for image acquisition: a 10x air lens (Neofluor 10x/0.3 phase contrast, Carl Zeiss AG, Jena, Germany) (for cell adhesion studies on cRGD functionalized PEG monolayers) and a 60x oil-immersion lens (PlanApo 60x/1.4, Olympus Deutschland GmbH, Hamburg, Germany) (for surface fluorescence intensity measurement and focal adhesion imaging). Furthermore, a Leica DM6000B microscope (Leica Microsystems GmbH, Wetzlar, Germany) equipped with a external light source EL6000 with a liquid optical fiber, a Leica DFC 365 FX camera, and process controlling by LAS AF 3.1.0 is used for fluorescence imaging. Images are acquired with a 10x air lens (HC PL APO 10x/0.40, Leica Microsystems GmbH, Wetzlar, Germany). Confocal imaging is performed with a LSM 880 (Carl Zeiss Microscopy GmbH, Jena, Germany) using a 63x/1.4 oil immersion objective (Carl Zeiss Microscopy GmbH, Jena, Germany) and the following light sources: UV diode (405 nm), Ar laser (488 nm) and HeNe laser (633 nm). Processing is controlled through the software ZEN black 2.0. Fluorescence samples at fixed time points are embedded with either Elvanol or Mowiol 4-88 containing 25 mg/mL 1,4-diazabicyclo[2.2.2]octane (DABCO) for stabilization.

Fluorescence intensity measurements and absorbance measurements in solution are performed in 96 well plates using a microplate reader Infinte M200 (Tecan Group Ltd, Männedorf, Switzerland) controlled by the software i-control 1.9. Detection of chemiluminescence is carried out with a Image Reader LAS3000 (Fujifilm Europe GmbH, Düsseldorf, Germany) and Amersham Imager 600 (GE Healthcare Europe GmbH, Freiburg, Germany).

X-ray photoelectron spectroscopie (XPS) measurements are performed with a Max 200 photoelectron spectrometer (Leybold-Heraeus, Cologne, Germany) in ultra high vacuum under pressures below 10^{-8} mbar. X-rays are generated by a magnesium anode which has a characteristic K_α radiation energy of 1253.6 eV. For the acquisition of the spectra emitted electrons are collected perpendicular to the sample surface with a hemispherical electron energy analyzer at constant pass energy of 96 eV and 48 eV for overview spectra and detailed spectra, respectively. Recorded spectra are normalized with respect to a spectrometer specific transmission function. Electrostatic charging of the samples is taken into account through calibration with respect to the C1s signal of ethylene glycol (286.4 eV) or the Si2p signal of the glass substrate (103.4 eV).[76] The spectra are analyzed with the software XPS Peak4.1.[118] Spectra are background corrected for signal quantification by subtracting the background according to Shirley and fitted by a symmetric Voigt function with a variable Gauß-Lorentz product function.

Quarz crystal microbalance with dissipation monitoring (QCM-D) mea-

surements are performed with a Q-Sense E-4 system (Q-Sense, Västra Frölunda, Sweden) equipped with flow chambers and a peristatic pump Reglo Digital MS-4/12 or IPC-N4 (Ismatec / Cole-Parmer GmbH, Wertheim, Germany). For the measurements either gold (Q-Sense, QSX 301) or SiO_2 (Q-Sense, QSX 303) QCM-D sensors are utilized.

Surfaces are thin film spin coated a spin coater WS-650Mz-23NPP (Laurell Technologies Corporation, North Wales, USA). The activation of gold nanostructed surfaces and QCM-D sensors is carried out with a 100-E plasma system (TePla, Kirchheim, Germany) and the gold nanostructed surfaces produced by BCMN are treated with a PS 210 microwave plasma system (PVA TePla AG, Kirchheim, Germany).

Scanning electron micrographs are acquired with a Leo 1530 or Ultra 55 (Carl Zeiss AG, Oberkochen, Germany); samples are previously covered with a carbon layer using a EM ACE200 vacuum coater (Leica Microsystems, Wetzlar, Germany).

Transmission electron micrographs are acquired with EM 912 Omega (Carl Zeiss Microscopy GmbH, Jena, Germany), or ARM200F (JEOL (Germany) GmbH, Freising, Germany). Lacey carbon films on 400 mesh copper grids (Plano GmbH, Wetzlar, Germany) are used for nanoparticle deposition.

Dynamic light scattering (DLS) and zeta potential measurements are performed on a Zetasizer Nano SZ (Malvern Instruments GmbH, Herrenberg, Germany) operated at a laser wavelength of 632.8 nm in combination with Rotilabo® single-use UV cells (Carl Roth GmbH & Co. KG, Karlsruhe, Germany) and folded capilary cells (Malvern Instruments GmbH, Herrenberg, Germany), respectively. For the determination of the size distribution by DLS five measurements per sample are acquired using the general purpose analysis method. Zeta potentials are quantified taking 3-5 measurements per sample and using the Smoluchowski approximation. All measurements are performed at room temperature (rt) using the predefined values for the refractive index and viscosity of water as dispersant. The number of scans pre measurement is set to automatic for both DLS and zeta potential measurements. Sample solutions are equilibrated for two minutes prior the measurement. For the TiO_2-TETT nanoparticles a refractive index of $n = 2.42$ and extinction coefficient of $\kappa = 0.0006$ at $\lambda = 632.8$ nm is assumed.[119]

For protein expression in *E. coli* a Minitron shaker (Infors AG, Bottmingen/Basel, Switzerland), a Excellla E24R incubator shaker (New Brunswick Scientific Co., Inc., Enfield, USA), a Omni Sonic Ruptor 400 ultrasonic homogenizer (Omni Imternational, Inc., Tulsa, USA) and a Avanti J-26XP centrifuge (Beckman Coulter, Inc., Brea, USA) along with a JA-10 or JA-25.5 rotor is used.Purification of TiO_2 nanoparticles is carried out with a Rotina R380 centrifuge (Andreas Hettich GmbH & Co.KG, Tuttlingen, Germany). For cell culture a 5702 R centrifuge (Eppendorf AG, Hamburg, Germany) is used. Sample preparation for Western blot is carried out with a 5417R centrifuge (Eppendorf AG, Hamburg, Germany). The Western blot is preformed with a XCell SureLock® Mini-Cell and XCell II™ blot module (Thermo Fisher Scientific Germany BV & Co KG, Braunschweig, Germany)

UV lamps used for photochemical oxidation are the UV hand lamp N-8K, 254 nm, 1 tube 8 W (Herolab GmbH Laborgeräte - made for Benda Laborgeräte, Wiesloch, Germany) and the VL-6.L, 365 nm, 1 tube 6 W (Vilber Lourmat Deutschland GmbH, Eberhardzell, Germany).

Fluorescence, chemiluminescence and SEM images are analyzed using ImageJ 1.48v.

4.2 Methods

4.2.1 Preparation of dual-functionalized biomimetic substrates using clickable PEG-alkyne

The experimental details of the subsequent section on the preparation of dual-functionalized biomimetic substrates by click reaction have been published by Schenk *et al.*.[74]

4.2.1.1 Synthesis of PEG-alkyne

The synthesis of $(CH_3CH_2O)_3$Si-PEG3000-alkyne (PEG-alkyne) is performed following the protocol for $(CH_3CH_2O)_3$Si-PEG2000-OCH_3 (PEG2000).[43] Amino-terminated PEG3000-alkyne (1 eq., 0.34 mmol) is suspended in 4 to 5 ml DMF under argon atmosphere and 3-(triethoxy)silylpropyl isocyanate (1.1 eq., 0.38 mmol) is added to the solution. After stirring the solution at rt for 24 h, it is cooled down to 0 °C and an excess of diethyl ether is added. The resulting suspension is stirred for 1 h at 0 °C before the precipitate is filtered out, washed with cold diethyl ether and dried under vacuum. The reaction yields a white powder (85%).
^{1}H-NMR [600MHz, $CDCl_3$]: δ (in ppm) = 6.28 (s, 1H, N*H*), 3.86 - 3.30 (m, 292H, O-CH_2 and N-CH_2), 3.67 (q, ^{4}J = 7.0 Hz, 6H, CH_3-CH_2), 3.15 (br s, 2H, CH_2-CH_2 -CH_2-NH), 2.49 (dt, ^{3}J = 7.3 Hz, ^{4}J = 2.4 Hz, 2H, C(=O)-CH_2-CH_2), 2.38 (t, ^{3}J = 7.3 Hz, 2H, C(=O)-CH_2-CH_2), 2.00 (t, ^{4}J = 2.6 Hz, 1H, C*H*), 1,58 (br s, 2H, Si-CH_2-CH_2), 1.20 (t, ^{3}J = 7.0 Hz, 9H, CH_3), 0.64 (br s, 2H, Si-CH_2).

4.2.1.2 PEGylation of glass and SiO_2 surfaces

The glass coverslips are cleaned in a freshly prepared 3:1 mixture of sulfuric acid and hydrogen peroxide (30%) for 1h, followed by thorough rinsing with water and sonication 3 times for 3 min each in fresh water. The glass coverslips are dried in a nitrogen stream. SiO_2 sensors for QCM-D are immersed in an aqueous solution of sodium dodecyl sulfate (3w/v%), washed with water thoroughly and dried in a nitrogen stream. Subsequently, the SiO_2 sensors are cleaned and activated in an oxygen plasma (0.4 mbar, 150 W, 45 min). Glass coverslips with an hexagonal array of gold nanoparticles are activated in oxygen plasma (0.4 mbar, 150 W, 10 min). For linking of the silyl ether terminated PEGs to the substrates, 0.25 mM solutions of both PEG-alkyne and PEG2000 in dry toluene (dried over 3 Å molar sieve) are prepared, mixed

in the desired ratio and supplemented with 25 µM triethyl amine. Surfaces are immersed into the PEG solution and are heated up to 80 °C under nitrogen atmosphere overnight. The surfaces are washed twice and sonicated for 5 min in first with ethyl acetate and then methanol. Then the surfaces are rinsed with methanol and dried in a nitrogen stream.

4.2.1.3 General procedure for surface modification through CuAAC

To functionalize the previously PEG coated surfaces by CuAAC the surfaces are incubated for 2 h in a moisture chamber with 100 - 200 µl freshly prepared reaction solution containing 100 mM ascorbic acid, 100 mM Tris buffer (pH 8.5), 150 µM azide-R (see below) and 1 mM $CuSO_4$ in water. Subsequently, the surfaces are rinsed with either water (and ethanol or methanol) or PBS and dried in a nitrogen stream. The azide containing reaction partners are used are 5/6-carboxyrhodamine 110-EG_3-azide, 3-azidomethyl-5-iodopyridine, Ac-K(N_3)GGNGEPRGDTYRAYK(fluorescein)GG-NH_2, N^{α},N^{α}-bis(carboxymethyl)-*L*-azido-lysine hydrochloride, biotin-EG_3-azide, cyclic(RGDfE)K(N_3)-NH_2 and K(N_3)PHSRN.

4.2.1.4 Surface fluorescence assay

Glass surfaces with different molar ratios of PEG-alkyne to PEG2000 (0, 25, 50, 75 and 100 mol% PEG-alkyne) are modified with a small fluorescent molecule, 5/6-carboxyrhodamine 110-EG_3-azide, with the CuAAC. Surfaces are mounted with Elvanol on a glass slide. The surface fluorescence intensity is measured with a fluorescence microscope taking 4 arrays of 5 x 5 images from each surface with the identical settings (60x oil immersion lens, 10% transmission, exposure time 0.25 s). Mean grey values are calculated with ImageJ and background corrected by subtracting the mean grey value of a glass surface without functionalization.

4.2.1.5 Synthesis of 3-azidomethyl-5-iodopyridine

1 eq. of 3-chloromethyl-5-iodopyridine (0.9 mmol) is dissolved in 5 ml DMF and 10 eq. (8.6 mmol) of sodium azide are added. The suspension is stirred for 24 h at rt and the product is extracted from the solution with water/ethyl acetate. The organic phase was dried over magnesium sulfate and evaporated under reduced pressure to yield the product (57%).
^{1}H-NMR [300MHz, $CDCl_3$]: δ (in ppm) = 8.81 (d, ^{4}J = 1.8 Hz, 1H, ArH), 8.50 (d, ^{4}J = 1.6 Hz, 1H, ArH), 8.01 (d, ^{4}J = 1.9 Hz, 1H, ArH), 4.36 (s, 2H, CH_2).

4.2.1.6 Quantification of CuAAC reaction on the surface by XPS

Glass coverslips with different molar ratios of PEG-alkyne to PEG2000 (0, 25, 50, 75, 100 mol% PEG-alkyne) are modified with 3-azidomethyl-5-iodopyridine by the click reaction.The N1s signal before and after click reaction on pure

PEG-alkyne surfaces is compared. The surfaces are analyzed by XPS on the basis of overview spectra and detailed spectra of the I 3d, the C 1s and the N 1s region. The N1s signal is fitted to one nitrogen species before the CuAAC and four chemically different nitrogen species after CuAAC, respectively. In the latter case, the relative area under the curve of the fit for N=**N**-N, C-**N**-N and C-**N**=C is fixed to 1:2:1 according to the chemical structure of the reaction product.

4.2.1.7 Chymotrypsin assay

To quantify the ligand density of ligand coupled to the PEG-alkyne by CuAAC a method adopted from the chymotrypsin assay established by Barber *et al.*[77] is used. PEG coated glass substrates with varying mol ratios of PEG-alkyne to PEG2000 (0, 25, 50, 75, 100 mol% PEG-alkyne) are functionalized with a fluorescently labeled peptide with a α-chymotrypsin cutting site, K(N_3)GGNGEPRGDTYRAYK(fluorescein)GG, by CuAAC. The immobilized peptide is enzymatically digested by immersing the surface in a 2 ml solution of 1.25 µg/ml α-chymotrypsin (from bovine pancreas) in 30 mM Tris (pH 8.0), 50 mM $CaCl_2$ and 10 µM HCl and incubating it for 16 h at 30 °C and 20 rpm. Afterward the samples are removed and washed with PBS. The amount of the released fluorescent label by the α-chymotrypsin digestion is quantified by fluorescent intensity measurements. Each 200 µl solution from the samples are measured in a black 96-well plate in a microplate reader and 4 x 4 measurements are taken per well. A reference curve is generated from 10µM Ac-K(N_3)GGNGEPRGDTYRAYK(fluorescein)GG-NH_2 treated under the same conditions as the surfaces (1.25 µg/ml α-chymotrypsin in 30 mM Tris (pH 8.0), 50 mM $CaCl_2$, 10 µM HCl stirred at 30 °C and 20 rpm for 16 h). The peptide solution is diluted with 30 mM Tris (pH 8.0), 50 mM $CaCl_2$ to a fluorescein concentration range from 0 - 375nM (0, 25, 50, 75, 125, 250, 375 nM fluorescein). Enzymatically treated surfaces as well as undigested control samples are mounted with Mowiol and the surface fluorescence intensity is analyzed under a fluorescence microscope. On each surface 4 arrays of 5 x 5 images are acquired with the same settings (60x oil immersion lens, 5% transmission, exposure time 0.04 s). The mean grey values determined with ImageJ are background corrected by subtracting the value for a glass sample and normalized to an autofluorescent standard for comparison.

4.2.1.8 Biotin-streptavidin binding monitored by QCM-D

SiO_2 sensors are passivated with a mixture of PEG2000 and PEG-alkyne in varying densities (0, 25, 50, 75, 100 mol% PEG-alkyne) and functionalized with biotin-EG_3-azide. QCM-D measurements are performed with a constant flow rate of 10 µl/min and at 25 °C. The sensors are initially equilibrated in PBS for 30 min. 5 µg/ml streptavidin in PBS is washed over to the sensor surfaces for 1 h before washing again with PBS for 20 - 30 min. The frequency change in the 7th frequency is calculated based on the resonance frequency before the

addition of streptavidin (averaged over 5 min, 25. - 30. min) and in the washing step after the streptavidin binding (averaged over 5 min, 110. - 115. min).

4.2.1.9 Protein repellent properties of PEG-alkyne

SiO_2 sensors are coated with a PEG-alkyne monolayer, mounted into the QCM-D chamber and equilibrated with PBS. The measurement is performed with a constant flow rate of 10 µl/min at 25 °C. Following solutions are consecutively directed over the sensors: PBS for 30 min, 0.01 w/v% bovine serum albumin (BSA) in PBS for 10 min, PBS for 5 min, 0.1 w/v% BSA in PBS for 10 min, PBS for 5 min, 1 w/v% BSA in PBS for 10 min, PBS for 5 min, 5 w/v% BSA in PBS for 10 min, and PBS for 10 min.

4.2.1.10 Synthesis of N^{α},N^{α}-bis(carboxymethyl)-*L*-azido-lysine hydrochloride[1, 2]

To a cooled solution of bromoacetic acid (4 eq., 4.8 mmol) in 5 ml 1.5 M NaOH, a solution of N^{ϵ}-azido-*L*-lysine hydrochloride (1 eq., 1.2 mmol) in 3 ml 1.5 M NaOH is added dropwise. The reaction mixture is stirred overnight at rt and additional 2 h at 50 °C before it is cooled down to 0 °C. The reaction solution is acidified with concentrated HCl to pH 1 and the volume of the solution is decreased to 1 - 2 mL under reduced pressure. The residue is overlayed with acetone, shaken gently and the organic phase is removed. The addition of acetone and collection of the organic phase is repeated three times. The combined organic layers are dried with $MgSO_4$, filtered and evaporated under reduced pressure.
^{1}H-NMR [400MHz, D_2O]: δ (in ppm) = 4.20 (s, 1H, CH_2-C*H*), 4.17 (s, 4H, N-CH_2-COOH), 3.32 (t, ^{3}J = 6.3 Hz, 2H, N_3-CH_2), 2.07 - 1.86 (m, 2H, CH_2-CH), 1.73 - 1.46 (m, 4H, CH2-CH_2-CH_2-CH_2)

4.2.1.11 Investigation of surface retained Cu ions after CuAAC

For this study five distinctly coated glass surfaces are prepared: I. PEG-alkyne, II. PEG-alkyne exposed to CuAAC reaction conditions without complementary reaction partner (azide-R), III. PEG-alkyne reacted with N^{α},N^{α}-bis(carboxymethyl)-*L*-azido-lysine hydrochloride (azide-NTA) and IV. PEG-alkyne functionalized with azide-NTA and additionally loaded with Cu^{2+} ions. To remove Cu ions complexed by NTA groups on the surface after the click reaction with azide-NTA, samples are washed in an aqueous solution of 25 mM EDTA in 50 mM Tris (pH 7.4) and 300 mM NaCl . To load the immobilized NTA groups with Cu^{2+} ions the surface is treated with 100 mM $CuSO_4$(aq), and then washed with a solution of 50 mM Tris (pH 7.4) buffer containing 300 mM NaCl and dried in a nitrogen stream.

4.2.1.12 Rat embryotic firoblast adhesion on cRGD functionalized surfaces

PEG monolayers on glass surfaces with 0, 0.01, 0.1, 1, 10 or 100 mol% PEG-alkyne ratio are modified by the CuAAC reaction with cyclic(RGDfE)K(N_3)-NH_2 (azide-cRGD). The samples and control samples, which haven't been modified by CuAAC, are treated with 70% ethanol for 5 min for sterilization and subsequently washed with PBS three times. REF YFP-paxillin cells cultured in serum-free media since the previous day are seeded onto the samples in a density of ca. 5000 cells/cm^2. After 4 h cultivation the cells are fixed with a 4 w/v% PFA in PBS solution (filtered through a 0.22 µm CME filter) for 20 min at rt. After washing with PBS, the samples are stored at 4 °C in PBS overnight. Afterward cells are permeabilized using 0.1 vol% Triton X-100 in PBS for 5 min at rt. Unspecific interactions are blocked by treating the samples with 1 w/v% BSA in PBS for at least 10 min at rt. Next, the surfaces are incubated with 200 µl of a solution consisting of 2 µg/ml TRITC-conjugated phalloidin in 1 w/v% BSA in PBS for 1h at rt in a moisture chamber. The samples are washed twice with PBS and mounted with Mowiol containing DAPI (1 µg/ml). 4 arrays of 5 x 5 fluorescence images of each sample are taken and analyzed using ImageJ. The number of cells per mm^2 and the spreading area of the cells is quantified based on the DAPI stained cell nuclei and the TRITC-phalloidin stained actin cytosceleton, respectively.

4.2.1.13 Preparation of gold nanostructured surfaces

Gold nanostructured surfaces are prepared by BCMN.[33, 34, 36] Briefly, a diblockcopolymer, polystyrene-*b*-poly-2-vinylpyridine (PS-*b*-P2VP) is dissolved in an aprotic solvent (toluene or *o*-xylene) to a final concentration higher than the critical micelle concentration. The formed micelles are loaded with gold ions by adding $HAuCl_4$ to the solution. The solution with gold loaded diblockcopolymer micelles is spin coated or dipp coated on freshly cleaned glass substrates. The polymer is removed and the gold ions are reduced to elementary gold nanoparticles by hydrogen plasma treatment (0.3 mbar, 600 W, 45 min).

Nanostructured surfaces used in this work are prepared with the polymer PS(110000)-*b*-P2VP(70500) (numbers in brackets specify the molecular weights in the individual polymer blocks).

solvent	polymer concentration	loading rate*	interparticle distance
o-xylene	4 mg/ml	0.3	54 ± 12 nm
o-xylene	2.4 mg/ml	0.4	100 ± 15 nm

* The loading rate is specified by the ratio of the added gold ions to the 2-vinylpyridine units.

4.2.1.14 Dual fluorescent labeling of gold nanostructured surfaces with intermediate PEG-alkyne

The PEG-alkyne monolayer on a gold nanostructured glass surface (interparticel distance: 54 ± 12 nm) is modified by the CuAAC reaction with biotin-EG_3-azide. Then, the gold nanoparticles are functionalized with a solution containing 250 µM HS-$(CH_2)_{11}$-EG_3-NTA (HS-NTA, thiol-NTA, stock solution: 5 mM in ethanol) and 250 µM $NiCl_2$ (stock solution: 100 mM in water) diluted in 50 mM Tris (pH 7.4), 300 mM NaCl (Tris-NaCl buffer). The surface is incubated with 250 µl of this solution for 1 h at rt in a moisture chamber and then washed in Tris-NaCl buffer for 10 min. Next, the sample is incubated with 250 µl Atto565-streptavidin (5 µg/ml in Tris-NaCl buffer) for 1 h at rt in a moisture chamber and washed again in Tris-NaCl buffer for 5 min. Finally, the sample is incubated with 250 µl ca. 10 µM His_6-GFP in Tris-NaCl buffer for 1 h, washed three times for 5 min each in Tris-NaCl buffer and mounted with Mowiol. The dual staining of the surface with two fluorophores is analyzed with a fluorescence microscope.

4.2.1.15 Influence of cRGD and PHSRN density on REF cell adhesion

Gold nanostructured surfaces (interparticle distance: 100 ± 15 nm) are coated with a PEG monolayer containing various molar ratios of PEG-alkyne (0, 0.1, 1 and 10 mol% PEG-alkyne). The clickable PEG between the gold nanoparticles is functionalized with K(N_3)PHSRN through CuAAC reaction. The gold nanoparticles are modified with cyclic[RGDfK(3-mercaptopropionyl-aminohexanoic acid)] (HS-cRGD) by incubating the samples with 200 µl 25 µM HS-cRGD in water for 2 h at rt in a moisture chamber. The prepared surfaces are washed several times in PBS and stored in PBS overnight at 4 °C. REF cells are cultured in serum-free media for 3.5 h and seeded onto the samples (previously treated with sterile PBS) at a density of 2000 or 5000 cells/cm^2. Cells are cultured on the surfaces for 4 h at 37 °C and 5% CO_2. For fixation of the cells samples are treated with 4 w/v% PFA in PBS (filtered through a 0.22µm CME filter) for 20 min at rt, then washed three time in PBS and stored overnight in PBS at 4 °C. To permeabilize the cells the samples are immersed in 0.1 vol% Triton-X 100 in PBS for 5 min at rt followed by a blocking step with 1 w/v% BSA in PBS for 30 min. Optionally samples are incubated with anti-vinculin mouse IgG (1:200 dilution in 1 w/v% BSA in PBS) and anti-paxillin rabbit IgG (1:200 dilution in 1 w/v% BSA in PBS) for 1 h at rt in a moisture chamber and washed in PBS (2 x 10 min). Hereon, the cells are stained with Alexa Fluor 488 goat anti-mouse IgG (5 µg/ml), Alexa Fluor 647 goat anti-rabbit IgG (5 µg/ml) and/or TRITC-phalloidin (2 µg/ml) for 1 h in a moisture chamber at rt. Finally, samples are washed in PBS (2 x 10 min) and mounted with Mowiol containing DAPI (1 µg/ml). For the quantification of the number of adherent cells on the surface 12 images per sample are taken under a fluorescence microscope and analyzed using ImageJ. The number of cells per mm^2 is determined based on the DAPI stained cell nuclei and the

TRITC-phalloidin dyed actin.

4.2.1.16 Cell culture

Rat embryonic fibroblasts (REF52) and rat embryonic fibroblasts expressing yellow fluorescent protein (YFP) labelled paxillin (REF YFP-paxillin) are cultured in DMEM (high glucose, NEAA, no glutamine) medium supplemented with 10% fetal bovine serum (FBS), 1% *L*-glutamine and 1% penicillin streptomycin at 37 °C and 5% CO_2. The medium is filtered (0.22 µm CME filter) before adding the antibiotics. Upon reaching of 80-100% confluence cells are rinsed with sterile PBS (3x) and detached by 0.05% trypsin-EDTA treatment for about 3 min. Cells are sedimented by centrifugation (3-5 min, 800-1000 rpm) and resuspended in fresh media at the desired density.

4.2.2 Co(III) as mediator ion to immobilize His-tagged proteins on NTA functionalized surfaces

4.2.2.1 Recombinant expression of His_6-GFP in *E. coli*

For the heat-shock transformation of the His_6-GFP plasmid into *E. coli*, 0.5 µl plasmid (∼100 ng/µl) and 50 µl chemical competent *E. coli* BL21(DE3)* are mixed and incubated on ice for 20 min. The mixture is heated up to 42 °C for 1 min, put back on ice for a few minutes and supplemented with 950 µl LB-medium. After letting the bacteria grow for 1 h at 37 °C while shaking (200 rpm), the suspension is plated onto an agar plate containing kanamycin (50 µg/ml) for antibiotic selection and incubated overnight at 37 °C. A starter culture is prepared by inoculating a bacteria colony into 10 ml LB-medium with 50 µg/ml kanamycin and shaking the culture (200 rpm) overnight at 37 °C. The starter culture is transferred into 1 l LB-medium with 50 µg/ml kanamycin and incubated at 37 °C, 200 rpm until an optical density of $A_{600nm} = 0.8$ is reached. Protein production is induced by the addition of 500 µl 1 M isopropyl β-*D*-1-thiogalactopyranoside (IPTG) to the suspension and incubation of the culture for additional 4 h while shaking at 37 °C. The bacteria are separated from the medium by centrifugation (8 min, 6000 rpm, 4 °C) and the pellet is stored at -20 °C. For the protein purification the pellet is resuspended in 15 ml 50 mM Tris buffer (pH 7.4) and 300 mM NaCl (Tris-NaCl buffer), supplemented with 150 µl phenylmethylsulfonyl fluoride (PMFS, 100 mM in methanol) and lysed with a probe sonicator (10 min, 50% pulse, 40%power). Soluble proteins and bacterial debris are separated by centrifugation (18000 rpm, 20 min, 4 °C). The supernatant is filtered through a 0.45 µm CME syringe filter and purified using a Ni^{2+}-NTA column. The protein solution is applied twice onto the Ni^{2+}-NTA column, which is hereinafter flushed with 10 ml Tris-NaCl buffer and 20 ml Tris-NaCl buffer with 12.5 mM imidazole to remove unspecifically bound protein. The protein is eluted from the column with 10 ml 250 mM imidazole in Tris-NaCl buffer and dialyzed against Tris-NaCl buffer at 4 °C for 1 d exchanging the buffer solution 2 times meanwhile. Aliquots of the protein solution are

stored at -80 °C. Protein concentration is determined by UV-vis spectroscopy ($\epsilon_{280\ nm}$ = 18490 $M^{-1}cm^{-1}$, $\epsilon_{485\ nm}$ = 83300 $M^{-1}cm^{-1}$).

4.2.2.2 Formation of metal ion loaded NTA SAMs on gold

The QCM-D experiments are performed at 25°C and a flow rate of 100 µL/min if not otherwise indicated. First, gold coated sensors are equilibrated in Tris-NaCl buffer for 10 min. A stock solution of 2 mM HS-$(CH_2)_{11}$-EG_3-NTA in ethanol is diluted to a final concentration of 50 µM in Tris-NaCl buffer and applied to the sensor for 20-25 min (optionally, the pump flow is stopped a few minutes after injection). Excessive thiol is removed in a 10 min washing step with Tris-NaCl buffer. For the loading of the NTA groups with the appropriate metal ion 100 mM $CoCl_2$ or $NiCl_2$ in Tris-NaCl buffer is washed over the sensor for 5 min. Another washing step with Tris-NaCl buffer for 5-20 min follows.

4.2.2.3 Co(III), Co(II) and Ni(II) mediated immobilization of His_6-GFP on NTA presenting SAM

NTA SAMs on gold are formed and loaded with either Co^{2+} or Ni^{2+} ions as described in section 4.2.2.2. The sensors are incubated with 5 µM His_6-GFP in Tris-NaCl buffer for 20 min (the pump flow is stopped a few minutes after injection) followed by a washing step with Tris-NaCl buffer for 10 min. For the oxidation of Co(II) to Co(III), cobalt ion loaded sensors are incubated with 10mM H_2O_2 in Tris-NaCl buffer for 30 min. For comparison, the Ni(II) and Co(II) interaction is considered. These sensors are kept in Tris-NaCl buffer meanwhile. A washing step with Tris-NaCl buffer for 10 min is followed by 250 mM imidazol in Tris-NaCl buffer for 10 min and an additional wash in Tris-NaCl buffer for 10-15 min.

4.2.2.4 Long-term stability of the Co(III) and the Ni(II) mediated interaction between NTA and His_6-GFP

The QCM-D measurements are performed on gold coated sensors with a flow rate of 100 µL/min at 37 °C. Metal ion loaded NTA SAMs on gold are formed according to section 4.2.2.2. Next, the sensors are incubated with 5 µM His_6-GFP in Tris-NaCl buffer until equilibrium is reached (the flow is stopped a few minutes after the injection). The sensor is washed with Tris-NaCl buffer and either oxidized by applying 10 mM H_2O_2 in Tris-NaCl buffer for 30 min (samples with Co/textsuperscript2+ ions) or remained in Tris-NaCl buffer (samples with Ni^{2+} ions). Tris-NaCl buffer is directed over the sensor for 16 h. Optionally, 250 mM imidazole in Tris-NaCl buffer is passed over the sensor before rinsing again with Tris-NaCl buffer. The resonance frequencies before His_6-GFP addition (averaged over a period of 2 min), 5 min after the oxidation step (and corresponding time points for Ni^{2+}) (averaged over 5 min) and after 15.9 h washing with buffer (averaged over 5 min) are detemined and the average change in resonance frequency per hour ($\Delta(\Delta f_n/n)/\Delta t$) as well as the

relative change in resonance frequency per hour (normalized to the amount of initially bound protein) is calculated.

4.2.2.5 Interaction of surface immobilized protein A with anti-BSA antibody

The interaction of protein A with anti-BSA antibody is monitored by QCM-D using a constant flow rate of 20 µL/min at 25 °C. A NTA functionalized SAM is formed and loaded with Co^{2+} or Ni^{2+} ions as described above (4.2.2.2). The sensors are incubated with 71 µg/ml His-tagged protein A fragment in Tris-NaCl buffer for 25 min followed by a washing step with Tris-NaCl buffer for 15 min. For the Co(III) mediated immobilization the sensor is treated with 10 mM H_2O_2 in Tris-NaCl buffer for 30 min and washed with Tris-NaCl buffer for 10 min, while sensors with Co(II) or Ni(II) mediated interaction are kept in Tris-NaCl buffer for the same time frame. A stock solution of 3.0 mg/mL anti-BSA antibody is diluted in Tris-NaCl buffer to a final concentration of 0.3 mg/mL and the sensors are incubated with the primary antibody solution for 90 min (the flow is stopped 25-30 min after injection). After a washing step with Tris-NaCl buffer for 35 min, the sensors are treated with 250 mM imidazole in Tris-NaCl buffer for 10 min and rinsed again with Tris-NaCl buffer for 15 min. Finally, the sensors are incubated with 50 mM EDTA (pH 7.4) in Tris-NaCl buffer for 10 min and subsequently washed with Tris-NaCl buffer for 35 min.

4.2.2.6 Effect of reducing agents on Co(III) mediated His_6-GFP immobilization

The experiment is performed at 25 °C and a constant flow rate of 20 µL/min. A monolayer of thiol-NTA on gold is formed by self-assembly and the NTA moieties are loaded with Co^{2+} ions according to the above mentioned protocol (4.2.2.2). A solution of 5 µM His_6-GFP in Tris-NaCl buffer is guided over the sensors for 25 min (optionally the flow is stopped 20 min after injection) followed by a washing step with Tris-NaCl buffer for 10-15 min. The sensors are incubated with 10 mM H_2O_2 in Tris-NaCl buffer for 30 min. Subsequently, the surfaces are washed with Tris-NaCl buffer for 15 min, 250 mM imidazole in Tris-NaCl buffer for 10-30 min, and Tris-NaCl buffer for additional 15-25 min. The sensors are incubated with a 1 mM solution of one of the following reducing agents - ascorbic acid (pH 7.4), TCEP (pH 7.4), DTT or sodium sulfite - in Tris-NaCl buffer for 30 min, followed by a washing step with Tris-NaCl buffer for 5 min, 250 mM imidazole in Tris-NaCl buffer for 10 min and Tris-NaCl buffer for another 15 min. This sequence is repeated with 10 mM and 100 mM reducing agent. Finally, the sensors are treated with 50 mM EDTA (pH 7.4) in Tris-NaCl buffer for 10 min and rinsed again with Tris-NaCl buffer for 45 min.

4.2.3 Stable immobilization of His-tagged proteins on TiO_2-TETT nanoparticles for targeted delivery

4.2.3.1 Synthesis of TETT coated TiO_2 nanoparticles

TETT-coated TiO_2 nanoparticles are synthesized in a two step procedure, which involves first the formation of oleic acid stabilized TiO_2 nanoparticles and hereinafter a surface modification reaction.[110] For the synthesis of oleic acid stabilized TiO_2 nanoparticles 35 g oleic acid (technical grade, 90%) is dried at 120 °C under nitrogen stream for 1 h and cooled down to 100 °C. Titanium(IV) isopropoxide (1 eq., 2 mmol) is added to the oleic acid and the mixture is stirred for 5 min. Subsequently, 2 ml of 2 M trimethylamine *N*-oxide (2 eq., 4 mmol) aqueous solution is added rapidly and the reaction mixture is refluxed for ca. 15 h at 100 °C. The precipitated nanoparticles are extracted by centrifugation (3900 g, 20 min), washed 2-3 times with methanol and dried under vaccum.

For the surface modification in a two-phase reaction, 100 mg oleic acid stabilized TiO_2 nanoparticles are suspended in 10 ml hexane, supplemented with 10 µl acetic acid and sonicated for 10 min. 1.2 ml TETT (45% in water) is added slowly to the suspension under vigorously stirring and the reaction mixture is heated up to 60 °C for 3 d. The two phases are separated by centrifugation (3900 g, 5 min) and the aqueous phase, which contains the highly water-dispersible TETT coated TiO_2 nanoparticles, is washed twice with hexane before it is dialyzed against 2 l deionized water in a regenerated cellulose dialysis membrane (MWCO 3.5 kDa) for 4 d exchanging the water four times meanwhile.

4.2.4 Optical characterization of TiO_2-TETT nanoparticles by SEM

Glass coverslips ((20 x 20) mm^2) are cleaned in a 3:1 mixture of sulfuric acid and hydrogen peroxide (piranha solution) for ca. 1 h and hereinafter rinsed with water. The coverslips are sonicated three times for 3 min in fresh water and dried in a nitrogen stream. TiO_2-TETT nanoparticels are dispersed in water to a final concentration of 5 mg/ml. 20 µl nanoparticle solution are spin coated (8000 rpm, 45 s) onto each surface.

4.2.5 TEM imaging of TiO_2-TETT nanoaprticles

An aqueous dispersion of TiO_2-TETT nanoparticles is applied to a lacey carbon film on 400 mesh copper grid. The TiO_2-TETT nanoparticles on the dried grid are visualized by TEM.

4.2.6 Optical characterization of TiO_2-TETT nanoparticles by DLS

The following solutions are prepared:

I. 1 mg/ml TiO_2-TETT in 10 mM Tris (pH 7.4)
II. 1 mg/ml TiO_2-TETT, 1 mM $CoCl_2$, in 10 mM Tris (pH 7.4)

For UV light exposure (254 nm and 365 nm, respectively) 1.2 ml of the appropriate solution is transferred into a 10 ml beaker, positioned under the UV light (at a distance of ca. 6 cm) and illuminated for 3 h. The size distribution of the nanoparticles is determined by DLS.

4.2.7 Zeta potential of TiO_2-TETT nanoparticles

For the determination of the zeta potential for the TiO_2-TETT nanoparticles the same solutions as for the size distribution measurements by DLS are used. 1 mL of the nanoparticle solution (with or without UV treatment) is transferred into a folded capillary cell and the zeta potential is measured.

4.2.8 Colorimetric detection of Co^{2+} ions

The absorbance is measured at $\lambda = 508$ nm with a plate reader using a 96-well plate containing each 200 µl solutions of 50 µM 4-(2-pyridylazo)resorcinol in 10 mM Tris buffer (pH 7.4) and varying $CoCl_2$ concentrations (0 µM, 2.5 µM, 5 µM, 10 µM, 15 µM, 20 µM, 25 µM, 30 µM, 40 µM, 50 µM, 75 µM, and 100 µM $CoCl_2$).

4.2.8.1 Titration of TiO_2 nanoparticles with Co^{2+}-ions

The absorbance at $\lambda = 508$ nm is measured for 200 µl solutions that contain a final concentration of 1 mg/ml TiO_2-TETT nanoparticles, 50 µM 4-(2-pyridylazo)resorcinol in 10 mM Tris buffer (pH 7.4) and different concentrations of $CoCl_2$ (0, 200 µM, 400 µM, 500 µM, 600 µM, 700 µM, 800 µM, 900 µM, 1.00 mM, 1.10 mM, 1.20 mM, 1.30 mM, 1.40 mM, 1.50 mM, 1.60 mM, 1.70 mM, 1.80 mM, and 2.00 mM $CoCl_2$).

4.2.8.2 Photoactivity of TETT coated TiO_2 nanoparticles

To prove the photoactivity of the TETT coated TiO_2 nanoparticles three different solutions in 20 mM Tris buffer (pH 7.4) are prepared and exposed to either ambient light or UV light for different incubation times.

I. 2 mg/ml TiO_2-TETT, 2 mM terephthalic acid (TA)
II. 2 mg/ml TiO_2-TETT, 2 mM $CoCl_2$, 2 mM TA
III. 2 mM $CoCl_2$, 2 mM TA

For each condition 1.1 ml of the corresponding solution is filled into a 10 ml beaker and treated with ambient or UV light. At different time points (t = 0/15/30/60/90/120/180 min) 100 µl of the different solutions are removed and mixed with either 100 µl water (solution I. and II.) or 100 µl 2 mg/ml TiO_2 nanoparticles (solution III.), respectively. The photoactivity is quantified by measuring the fluorescence of formed 2-hyroxyterephthalic acid (2-HTA, $\lambda_{ex} = 315$ nm, $\lambda_{em} = 425$ nm) and the absorbance of Co^{3+}-species ($\lambda = 550$nm). To quantify the produced amount of 2-HTA a standard with concentrations ranging from 0

to 50 µM 2-HTA (0 µM, 1 µM, 5 µM, 10 µM, 20 µM, and 50 µM 2-HTA) with 1 mg/ml TiO_2-TETT nanoparticles in 10 mM Tris buffer (pH 7.4) is used.

4.2.8.3 Immobilization of His-tagged GFP onto TETT coated TiO_2 nanoparticles by photooxidation of cobalt(II) complexes

A 1 ml solution of 2 mg/ml TiO_2-TETT, 2 mM $CoCl_2$ and 2 µM His_6-GFP in 20 mM Tris buffer (pH 7.4) with 200 mM NaCl is either exposed to ambient light or UV light for 3 h. As a dialysis control 2 µM His_6-GFP in 20 mM Tris buffer (pH 7.4) with 200 mM NaCl is used. Next, 450 µl of each solution is mixed with 450 µl H_2O and 450 µl 200 mM imidazole, respectively. The diluted solutions are dialyzed against the corresponding buffer solutions (10 mM Tris buffer (pH 7.4) with 100 mM NaCl without or with 100 mM imidazole) for 44 h using a cellulose ester dialysis device (MWCO 100 kDa). The concentration of the remaining protein is quantified by fluorescence intensity measurements using a plate reader (λ_{ex} = 480 nm, λ_{em} = 510 nm) and an indirect immunochemiluminescence assay as described below.

4.2.8.4 Fluorescent labeling of transferrin-His_6 with Atto647N-NHS ester

200 µg of human transferrin protein with C-terminal His-tag are dissolved in 200 µL H_2O to a final concentration of 1mg/mL protein in PBS. 20 µL $NaHCO_3$ (stock solution: 1 M in H_2O, pH 8.0) and 2.22 µL Atto647N-NHS (stock solution: 10 mg/mL in DMSO) are added and the solution is stirred for 2 h at rt. The reaction mixture is dialyzed (MWCO 5 kDa) against 500 mL PBS overnight at 4 °C.

4.2.8.5 Preparation of transferrin coated TiO_2-TETT nanoparticles

A solution of 1 mg/ml TiO_2, 1 mM $CoCl_2$ and 0.5 µM transferrin-Atto647N in 10 mM Tris (pH 7.4) and 100 mM NaCl is prepared. A 800 µl aliquot of this solution is transferred into a 10 ml beaker, covered with a quartz glass slide, placed under the UV lamp (in a distance of ca. 6 cm) and illuminated with 254 nm UV light for 3 h. Further, a 0.5 µM transferrin-Atto647N in 10 mM Tris (pH 7.4) and 100 mM NaCl is prepared. 550 µl of each the protein loaded nanoparticle solutions (either treated with UV light or not) or the protein solution are transferred into a cellulose ester dialysis device (MWCO 300 kDa) and dialyzed jointly against 2 l 10mM Tris (pH 7.4) and 100 mM NaCl for 44 h at 4 °C under continuous stirring. The protein concentrations of the solutions before and after dialysis are analyzed by fluorescence intensity measurements and an indirect immunochemiluminescence assay. For fluorescence intensity measurements each 200 µl solution and buffer are pipetted in a white 96-well plate measured in the plate reader (λ_{ex} = 644 nm, λ_{em} = 669 nm).

4.2.8.6 Protein quantification by indirect immunochemiluminescence assay

Drops of 5 µl of each protein solution are applied onto a nitrocellulose membrane. Non-specific adsorption is blocked by soaking the membrane in 5 w/v% powdered milk (low fat) in Tris buffered saline containing tween 20 (TBS-T: 50 mM Tris (pH 8.0), 150 mM NaCl, 0.1 vol% tween 20) for 30 min or 3 w/v% BSA in TBS-T for 1 h. Incubation of the nitrocellulose membrane with the primary antibody overnight in 3 w/v% powdered milk (low fat) in TBS-T at 4°C or 1 w/v% BSA in TBS-T at rt is followed by three washing steps with TBS-T for at least 5 min. Subsequently, the membrane is incubated with the secondary antibody HRP-conjugated goat anti-rabbit IgG buffer for 1 h at rt. A further washing step in TBS-T (three times for at least 5 min) follows. Protein signals are detected with a chemiluminescence imager using the ECL prime Western blotting detection reagent kit. Therefore, a 1:1 mixture of the solutions A and B of the kit is applied on the membrane for some seconds to minutes, the excessive solution is removed and the chemiluminescence detected. For the analysis of His_6-GFP protein solutions powdered milk (low fat) is used as blocking agent in combination with the primary antibody anti-GFP rabbit IgG at a final concentration of 2 µg/ml and 0.1 µg/ml HRP-conjugated goat anti-rabbit IgG. Quantification of transferrin-Atto647N is carried out using BSA as blocking agent, 0.5 µg/ml anti-transferrin rabbit IgG and 0.08 µg/ml HRP-conjugated goat anti-rabbit IgG.

4.2.8.7 Expression level of transferrin receptor in hFF-1 and panc-1 cells

To determine the expression level of the transferrin receptor in hFF-1 and panc-1 cells, 100000 cells are plated in a cell culture dish (3.5 cm diameter) and cultured overnight. Radio-immunoprecipitation assay (RIPA) buffer is supplemented with EDTA (100x, final concentration 5 mM) and protease and phosphates inhibitor cocktail (100x) to obtain the lysis buffer. A solution of 200 µl lysis buffer is added to the cell culture dish and samples are frozen at -80 °C for several days. Cell lysates are centrifuged (13000 rpm, 30 min at 4 °C) and the supernatant is used for a sodium dodecyl sulfate polyacrylamide gel electrophoresis (SDS-PAGE). 13 µl of the supernatant from each cell lysate are added to 7 µL of a 10:4 mixture of NuPAGE® LDS sample buffer (4x) and NuPAGE® sample reducing agent (10x). Samples are heated up to 95 °C for 10 min. The NuPAGE® Bis-Tris gel (4-12%) is loaded with 10 µL Novex® sharp pre-stained protein standard and 20 µL denatured sample solution, respectively. The SDS-PAGE is performed in NuPAGE® MOPS SDS running buffer at 200 V for 50 min. Next, the proteins bands (separated according to their size) are transferred from the Bis-Tris gel to a nitrocellulose membrane using the XCell II™ blot module. The transfer is performed in transfer buffer by applying 30 V for 75 min. The nitrocellulose membrane is blocked with 3 w/v% BSA in TBS-T for 1 h at rt and incubated overnight with 1 µg/mL anti-transferrin receptor rabbit IgG in 1 w/v% BSA in TBS-

T. The membrane is washed three times in TBS-T for 5 min each, followed by the incubation with 0.08 µg/mL HRP-conjugated goat anti-rabbit IgG in 1 w/v% BSA in TBS-T for 1 h. After a further washing step, the protein bands are detected with a chemiluminescence imager using the ECL prime Western blotting detection reagent kit. To detection the β-actin expression levels the nitrocellulose membrane is soaked in TBS-T for 30 min followed by the incubation with the primary antibody anti-β-actin (1 µg/mL in 1 w/v% BSA in TBS-T for 1 h) and the secondary antibody HRP-conjugated goat anti-mouse IgG (0.08µg/mL in 1 w/v% BSA in TBS-T) as well as the detection of the protein signals according to the before mentioned description.

4.2.8.8 Investigation of the cellular uptake of transferrin-Atto647N loaded TiO_2 nanoparticles in hFF-1 and panc-1

hFF-1 and panc-1 cells are seeded into WillCo-dish® glass bottom dishes at a density of 10000 cells/cm^2 and 25000 cells/cm^2, respectively and cultured overnight at 37 °C and 5% CO_2. The cells are starved in serum free medium for several hours before transferrin decorated TiO_2-TETT nanoparticles are added to the medium with a 1:100 dilution. After 15 h cultivation cells are fixed with 4 w/v% PFA in PBS for 20 min at rt. A washing step with PBS is followed by permeabilization with 0.1 vol% Triton X-100 in PBS for 5 min and blocking of unspecific interaction though incubation with 3 w/v% BSA in PBS for 1 h. The primary antibody anti-transferrin receptor rabbit IgG is diluted in 1 w/v% BSA in TBS-T to a final concentration of 2 µg/mL and applied to the samples for 1 h. The samples are washed three times 5 min in PBS followed by the incubation with the secondary antibody Alexa Fluor 488 goat anti-rabbit IgG (4 µg/mL) and DAPI (1 µg/mL) in 1w/v% BSA in PBS for 1 h. After a further washing step samples are embedded in Mowiol.

4.2.8.9 Cell culture

Human foreskin fibroblasts (hFF-1) and panc-1 are cultured at 37 °C and 5% CO_2 in DMEM (high glucose, pyruvate) medium supplemented with 15% and 10% FBS, respectively . The DMEM medium supplemented with FBS is filtered (0.22 µm CME filter) before adding 1% penicillin streptomycin. Splitting of cells includes rinsing of the cells with sterile PBS (3x), detaching of the cells with 0.05% trypsin-EDTA for ca. 3 min, centrifugation of the cell suspension (3 min, 800 rpm) and resuspension in the appropriate culture media at the desired density.

Bibliography

[1] P. K. Bae, K. N. Kim, S. J. Lee, H. J. Chang, C. K. Lee, and J. K. Park. The modification of quantum dot probes used for the targeted imaging of his-tagged fusion proteins. *Biomaterials*, 30(5):836–42, 2009.

[2] A. Lascaux, G. Delahousse, J. Ghostin, J.-P. Bouillon, and I. Jabin. Second generation calix[6]trenamides - highly selective graftable receptors for neutral guests and contact ion pairs. *European Journal of Organic Chemistry*, pages 5272–5278, 2011.

[3] E. S. Redeker, D. T. Ta, D. Cortens, B. Billen, W. Guedens, and P. Adriaensens. Protein engineering for directed immobilization. *Bioconjugate Chemistry*, 24(11):1761–1777, 2013.

[4] K. Hauff, C. Zambarda, M. Dietrich, M. Halbig, A. L. Grab, R. Medda, and E. A. Cavalcanti-Adam. Matrix-immobilized bmp-2 on microcontact printed fibronectin as *in vitro* tool to study bmp-mediated signaling and cell migration. *Frontiers in Bioengineering and Biotechnology*, 3(62), 2015.

[5] G. Maheshwari, A. Wells, L. G. Griffith, and D. A. Lauffenburger. Biophysical integration of effects of epidermal growth factor and fibronectin on fibroblast migration. *Biophysical Journal*, 76(5):2814–2823, 1999.

[6] M. Poujade, E. Grasland-Mongrain, A. Hertzog, J. Jouanneau, P. Chavrier, B. Ladoux, A. Buguin, and P. Silberzan. Collective migration of an epithelial monolayer in response to a model wound. *Proceedings of the National Academy of Sciences of the USA*, 104(41), 2007.

[7] F. Rusmini, Z. Zhong, and J. Feijen. Protein immobilization strategies for protein biochips. *Biomacromolecules*, 8(6):1775–1789, 2007.

[8] J. D. Watson and F. H. C. Crick. Molecular structure of nucleic acids: a structure for desoxyribose nucleic acid. *Nature*, 171, 1953.

[9] E. P. Diamandis and T. K. Christopoulos. The biotin-(strept)avidin system: principles and applications in biotechnology. *Clinical Chemistry*, 37(5), 1991.

[10] S. Chevalier, C. Cuestas-Ayllon, V. Grazu, M. Luna, H. Feracci, and J. M. de la Fuente. Creating biomimetic surfaces through covalent and oriented binding of proteins. *Langmuir*, 26(18):14707–14715, 2010.

[11] H. C. Kolb, M. G. Finn, and K. B. Sharpless. Click chemistry: diverse chemical function from a few good reactions. *Angewandte Chemie - International Edition*, 40(11):2004–2021, 2001.

[12] A. Keppler, M. Kindermann, S. Gendreizig, H. Pick, H. Vogel, and K. Johnsson. Labeling of fusion proteins of O^6-alkylguanine-DNA alkyltransferase with small molecules in vivo and in vitro. *Methods*, 32(4):437–444, 2004.

[13] G. V. Los, L. P. Encell, M. G. McDougall, D. D. Hartzell, N. Karassina, C. Zimprich, M. G. Wood, R. Learish, R. F. Ohana, M. Urh, D. Simpson, J. Mendez, K. Zimmerman, P. Otto, G. Vidugiris, J. Zhu, A. Darzins, D. H. Klaubert, R. F. Bulleit, and K. V. Wood. HaloTag: A novel protein labeling technology for cell imaging and protein analysis. *ACS Chemical Biology*, 3(6):373–382, 2008.

[14] S. E. Ochsenhirt, E. Kokkoli, J. B. McCarthy, and M. Tirrell. Effect of RGD secondary structure and the synergy site PHSRN on cell adhesion, spreading and specific integrin engagement. *Biomaterials*, 27(20):3863–3874, 2006.

[15] X. Chen, P. Sevilla, and C. Aparicio. Surface biofunctionalization by covalent co-immobilization of oligopeptides. *Colloids and Surfaces B: Biointerfaces*, 107:189–197, 2013.

[16] J. Lee, I. Choi, and W.-S. Yeo. Preparation of gradient surfaces by using a simple chemical reaction and investigation of cell adhesion on a two-component gradient. *Chemistry - A European Journal*, 19(18):5609–5616, 2013.

[17] M. A. Azagarsamy and K. S. Anseth. Bioorthogonal click chemistry: An indispensable tool to create multifaceted cell culture scaffolds. *ACS Macro Letters*, 2(1):5–9, 2013.

[18] Y. Ma, J. Zheng, E. F. Amond, C. M. Stafford, and M. L. Becker. Facile fabrication of "dual click" one- and two-dimensional orthogonal peptide concentration gradients. *Biomacromolecules*, 14(3):665–671, 2013.

[19] H. Cai, D. Depoil, M. Palma, M. P. Sheetz, M. L. Dustin, and S. J. Wind. Bifunctional nanoarrays for probing the immune response at the single-molecule level. *Journal of Vacuum Science & Technology B*, 31(6):06F902, 2013.

[20] D. Delcassian, D. Depoil, D. Rudnicka, M. Liu, D. M. Davis, M. L. Dustin, and I. E. Dunlop. Nanoscale ligand spacing influences receptor triggering in T cells and NK cells. *Nano Letters*, 13:5608–5614, 2013.

[21] G. A. Hudalla and W. L. Murphy. Immobilization of peptides with distinct biological activities onto stem cell culture substrates using orthogonal chemistries. *Langmuir*, 26(9):6449–6456, 2010.

[22] D. G. Castner, K. Hinds, and D. W. Grainger. X-ray photoelectron spectroscopy sulfur 2p study of organic thiol and disulfide binding interactions with gold surfaces. *Langmuir*, 12(21):5083–5086, 1996.

[23] Y. Xue, X. Li, H. Li, and W. Zhang. Quantifying thiol-gold interactions towards the efficient strength control. *Nature Communications*, 5:4348, 2014.

[24] H. Grönbeck, A. Curioni, and W. Andreoni. Thiols and disulfides on the Au(111) surface: the headgroup - gold interaction. *Journal of the American Chemical Society*, 122(16):3839–3842, 2000.

[25] D. Krüger, H. Fuchs, R. Rousseau, D. Marx, and M. Parrinello. Interaction of short-chain alkane thiols and thiolates with small gold clusters: Adsorption structures and energetics. *The Journal of Chemical Physics*, 115(10):4776–4786, 2001.

[26] J. C. Love, L. A. Estroff, J. K. Kriebel, R. G. Nuzzo, and G. M. Whitesides. Self-assembled monolayers of thiolates on metals as a form of nanotechnology. *Chemical Reviews*, 105(4):1103–1170, 2005.

[27] H. Häkkinen. The gold-sulfur interface at the nanoscale. *Nature Chemistry*, 4(6):443–455, 2012.

[28] C. D. Bain, E. B. Troughton, Y.-T. Tao, J. Evall, G. M. Whitesides, and R. G. Nuzzo. Formation of monolayer films by the spontaneous assembly of organic thiols from solution onto gold. *Journal of the American Chemical Society*, 111(1):321–335, 1989.

[29] S. Herrwerth, W. Eck, S. Reinhardt, and M. Grunze. Factors that determine the protein resistance of oligoether self-assembled monolayers - internal hydrophilicity, terminal hydrophilicity, and lateral packing density. *Journal of the American Chemical Society*, 125(31):9359–9366, 2003.

[30] S. I. Jeon, J. H. Lee, J. D. Andrade, and P. G. de Gennes. Protein surface interactions in the presence of polyethylene oxide: I simplified theory. *Journal of Colloid and Interface Science*, 142(1), 1991.

[31] G. A. Hudalla and W. L. Murphy. Chemically well-defined self-assembled monolayers for cell culture: toward mimicking the natural ECM. *Soft Matter*, 7(20):9561–9571, 2011.

[32] C. H. Minsky, B. B.and Antoni and H. Boehm. Controlled immobilization strategies to probe short hyaluronan-protein interactions. *Scientific Reports*, 6(21608), 2016.

[33] J. P. Spatz, S. Mössmer, C. Hartmann, and M. Möller. Ordered deposition of inorganic clusters from micellar block copolymer films. *Langmuir*, 16(6):407–415, 2000.

[34] T. Lohmüller, D. Aydin, M. Schwieder, C. Morhard, I. Louban, C. Pacholski, and J. P. Spatz. Nanopatterning by block copolymer micelle nanolithography and bioinspired applications. *Biointerphases*, 6(1):MR1–MR12, 2011.

[35] H. Boehm. *Micromechanical properties and structure of the pericellular coat of living cells modulated by nanopatterned substrates*. PhD thesis, Ruprecht-Karls-University Heidelberg, 2008.

[36] R. Glass, M. Möller, and J. P. Spatz. Block copolymer micelle nanolithography. *Nanotechnology*, 14(10):1153–1160, 2003.

[37] J. C. Meiners, H. Elbs, A. Ritzi, J. Mlynek, and G. Krausch. Chemically functionalized surfaces from ultrathin block-copolymer films. *Journal of Applied Physics*, 80(4):2224–2227, 1996.

[38] M. Arnold, V. C. Hirschfeld-Warneken, T. Lohmüller, P. Heil, J. Blümmel, E. A. Cavalcanti-Adam, M. López-García, P. Walther, H. Kessler, B. Geiger, and J. P. Spatz. Induction of cell polarization and migration by a gradient of nanoscale variations in adhesive ligand spacing. *Nano Letters*, 8(7):2063–2069, 2008.

[39] V. C. Hirschfeld-Warneken, M. Arnold, A. Cavalcanti-Adam, M. López-García, H. Kessler, and J. P. Spatz. Cell adhesion and polarisation on molecularly defined spacing gradient surfaces of cyclic RGDfK peptide patches. *European Journal of Cell Biology*, 87(8-9):743–750, 2008.

[40] J. Bansmann, S. Kielbassa, H. Hoster, F. Weigl, H. G. Boyen, U. Wiedwald, P. Ziemann, and R. J. Behm. Controlling the interparticle spacing of Au-salt loaded micelles and Au nanoparticles on flat surfaces. *Langmuir*, 23(20):10150–10155, 2007.

[41] G. Kästle, H.-G. Boyen, F. Weigl, G. Lengl, T. Herzog, P. Ziemann, S. Riethmüller, O. Mayer, C. Hartmann, J. P. Spatz, M. Möller, M. Ozawa, F. Banhart, M. G. Garnier, and P. Oelhafen. Micellar nanoreactors - preparation and characterization of hexagonally ordered arrays of metallic nanodots. *Advanced Functional Materials*, 13(11):853–861, 2003.

[42] B. Alberts, A. Johnson, J. Lewis, M. Raff, K. Roberts, and P. Walter. *Molecular biology of the cell*. Garland Science, 5 edition, 2007.

[43] J. Blümmel, N. Perschmann, D. Aydin, J. Drinjakovic, T. Surrey, M. Lopez-Garcia, H. Kessler, and J. P. Spatz. Protein repellent properties of covalently attached PEG coatings on nanostructured SiO2-based interfaces. *Biomaterials*, 28(32):4739–4747, 2007.

[44] M. Arnold, E. A. Cavalcanti-Adam, R. Glass, J. Blümmel, W. Eck, M. Kantlehner, H. Kessler, and J. P. Spatz. Activation of integrin function by nanopatterned adhesive interfaces. *ChemPhysChem*, 5(3):383–388, 2004.

[45] E. A. Cavalcanti-Adam, A. Micoulet, J. Blümmel, J. Auernheimer, H. Kessler, and J. P. Spatz. Lateral spacing of integrin ligands influences cell spreading and focal adhesion assembly. *European Journal of Cell Biology*, 85(3-4):219–224, 2006.

[46] E. A. Cavalcanti-Adam, T. Volberg, A. Micoulet, H. Kessler, B. Geiger, and J. P. Spatz. Cell spreading and focal adhesion dynamics are regulated by spacing of integrin ligands. *Biophysical Journal*, 92(8):2964–2974, 2007.

[47] M. Arnold, M. Schwieder, J. Blümmel, E. A. Cavalcanti-Adam, M. López-Garcia, H. Kessler, B. Geiger, and J. P. Spatz. Cell interactions with hierarchically structured nano-patterned adhesive surfaces. *Soft Matter*, 5(1):72–77, 2009.

[48] J. A. Opsteen and J. C. M. van Hest. Modular synthesis of block copolymers via cycloaddition of terminal azide and alkyne functionalized polymers. *Chemical Communications*, pages 57–59, 2005.

[49] W. H. Binder and R. Sachsenhofer. 'Click' chemistry in polymer and materials science. *Macromolecular Rapid Communications*, 28(1):15–54, 2007.

[50] N. D. Gallant, K. A. Lavery, E. J. Amis, and M. L. Becker. Universal gradient substrates for click biofunctionalization. *Advanced Materials*, 19(7):965–969, 2007.

[51] M. D. Best. Click chemistry and bioorthogonal reactions: unprecedented selectivity in the labeling of biological molecules. *Biochemistry*, 48(28):6571–6584, 2009.

[52] F. Himo, T. Lovell, R. Hilgraf, V. V. Rostovtsev, L. Noodleman, K. B. Sharpless, and V. V. Fokin. Copper(I)-catalyzed synthesis of azoles. DFT study predicts unprecedented reactivity and intermediates. *Journal of the American Chemical Society*, 127(1):210–216, 2005.

[53] A. Makarem, R. Berg, F. Rominger, and B. F. Straub. A Fluxional Copper Acetylide Cluster in CuAAC Catalysis. *Angewandte Chemie - International Edition)*, 54(25):7431–7435, 2015.

[54] L. Jin, D. R. Tolentino, M. Melaimi, and G. Bertrand. Isolation of bis(copper) key intermediates in Cu-catalyzed azide-alkyne "click reaction". *Science Advances*, 1(5):e1500304, 2015.

[55] J. E. Hein and V. V. Fokin. Copper-catalyzed azide-alkyne cycloaddition (CuAAC) and beyond: new reactivity of copper(I) acetylides. *Chemical Society Reviews*, 39(4):1302–1315, 2010.

[56] N. J. Agard, J. A. Prescher, and C. R. Bertozzi. A strain-promoted [3+2] azide-alkyne cycloaddition for covalent modification of biomolecules in living systems. *Journal of the American Chemical Society*, 126(46):15046–15047, 2004.

[57] L. Zhang, X. Chen, P. Xue, H. H. Y. Sun, I. D. Williams, K. B. Sharpless, V. V. Fokin, and G. Jia. Ruthenium-catalyzed cycloaddition of alkynes and organic azides. *Journal of the American Chemical Society*, 127(46):15998–15999, 2005.

[58] J. Porath, J. Carlsson, I. Olsson, and G. Belfrage. Metal chelate affinity chromatography, a new approach to protein fractionation. *Nature*, 258(5536):598–599, 1975.

[59] E. Hochuli, H. Döbeli, and A. Schacher. New metal chelate adsorbent selective for proteins and peptides containing neighbouring histidine residues. *Journal of Chromatography A*, 411:177–184, 1987.

[60] E. Hochuli, W. Bannwarth, H. Döbeli, R. Gentz, and D. Stüber. Genetic approach to facilitate purification of recombinant proteins with a novel metal chelate adsorbent. *Nature Biotechnology*, 6(11):1321–1325, 1988.

[61] S. Knecht, D. Ricklin, A. N. Eberle, and B. Ernst. Oligohis-tags: mechanisms of binding to Ni^{2+}-NTA surfaces. *Journal of Molecular Recognition*, 22(4):270–279, 2009.

[62] L. Nieba, E. Nieba-Axmann, A. Persson, M. Hämäläinen, F. Edebratt, A. Hansson, J. Lidholm, K. Magnusson, A. F. Karlsson, and A. Plückthun. Biacore analysis of histidine-tagged proteins using a chelating nta sensor chip. *Analytical Biochemistry*, 252:217–228, 1997.

[63] A. N. Kapanidis, Y. W. Ebright, and R. H. Ebright. Site-specific incorporation of fluorescent probes into protein: hexahistidine-tag-mediated fluorescent labeling with (Ni^{2+}:nitrilotriacetic acid)$_n$-fluorochrome conjugates. *Journal of the American Chemical Society*, 123(48):12123–12125, 2001.

[64] S. Lata, A. Reichel, R. Brock, R. Tampé, and J. Piehler. High-affinity adaptors for switchable recognition of histidine-tagged proteins. *Journal of the American Chemical Society*, 127(29):10205–10215, 2005.

[65] S. Lata, M. Gavutis, R. Tampé, and J. Piehler. Specific and stable fluorescence labeling of histidine-tagged proteins for dissecting multi-protein complex formation. *Journal of the American Chemical Society*, 128(7):2365–2372, 2006.

[66] H. Block, B. Maertens, A. Spriestersbach, N. Brinker, J. Kubicek, R. Fabis, J. Labahn, and F. Schäfer. Immobilized-metal affinity chromatography (IMAC): a review. In *Methods in Enzymology*, volume 463, pages 439–473. Academic Press Inc, 2nd revised edition, 2009.

[67] C. You, S. Wilmes, O. Beutel, S. Löchte, Y. Podoplelowa, F. Roder, C. Richter, T. Seine, D. Schaible, G. Uze, S. Clarke, F. Pinaud, M. Dahan, and J. Piehler. Self-controlled monofunctionalization of quantum dots for multiplexed protein tracking in live cells. *Angewandte Chemie - International Edition*, 49:4108–4112, 2010.

[68] C. You and J. Piehler. Mulivalent chelators for spatially and temporally controlled protein functionalization. *Analytical and Bioanalytical Chemistry*, 406:3345–3357, 2014.

[69] Erwin Riedel. *Anorganische Chemie*. Walter de Gruyter, Berlin, 6 edition, 2004.

[70] Lutz H. Gade. *Koordinationschemie*. Wiley-VCH, Weinheim, 1 edition, 1998.

[71] L. Helm and A. E. Merbach. Inorganic and bioinorganic solvent exchange mechanisms. *Chemical Reviews*, 105(6):1923–1959, 2005.

[72] H. Ogino and K. Ogino. Redox potentials and related parameters of cobalt(III/II) complexes containing aminopolycarboxylates. *Inorganic Chemistry*, 22(15):2208–2211, 1983.

[73] J. Bond and D. B. Hobson. The stability constants of cobalt(III) chelates of polyaminopolycarboxylic acids. *Journal of the Chemical Society A: Inorganic, Physical, Theoretical*, pages 2155–2157, 1969.

[74] F. C. Schenk, H. Boehm, J. P. Spatz, and S. V. Wegner. Dual-functionalized nanostructured biointerfaces by click chemistry. *Langmuir*, 30(23):6897–6905, 2014.

[75] A. C. Gouget-Laemmel, J. Yang, M. A. Lodhi, A. Siriwardena, D. Aureau, R. Boukherroub, J.-N. Chazalviel, F. Ozanam, and S. Szunerits. Functionalization of azide-terminated silicon surfaces with glycans using click chemistry: XPS and FTIR study. *Journal of Physical Chemistry C*, 117(1):368–375, 2013.

[76] C. D. Wagner. *Handbook of x-ray photoelectron spectroscopy: a reference book of standard data for use in x-ray photoelectron spectroscopy*. Physical Electronics Division, Perkin-Elmer Corp., Eden Prairie, Minnesota, USA, 1979.

[77] T. A. Barber, G. M. Harbers, S. Park, M. Gilbert, and K. E. Healy. Ligand density characterization of peptide-modified biomaterials. *Biomaterials*, 26(34):6897–6905, 2005.

[78] U. Hersel, C. Dahmen, and H. Kessler. RGD modified polymers: biomaterials for stimulated cell adhesion and beyond. *Biomaterials*, 24(24):4385–4415, 2003.

[79] G. Le Saux, A. Magenau, T. Böcking, K. Gaus, and J. J. Gooding. The relative importance of topography and RGD ligand density for endothelial cell adhesion. *PloS one*, 6(7):e21869, 2011.

[80] D. Aydin, I. Louban, N. Perschmann, J. Blümmel, T. Lohmüller, E. A. Cavalcanti-Adam, T. L. Haas, H. Walczak, H. Kessler, R. Fiammengo, and J. P. Spatz. Polymeric substrates with tunable elasticity and nanoscopically controlled biomolecule presentation. *Langmuir*, 26(19):15472–15480, 2010.

[81] G. Maheshwari, G. Brown, D. A. Lauffenburger, A. Wells, and L. G. Griffith. Cell adhesion and motility depend on nanoscale RGD clustering. *Journal of Cell Science*, 113(10):1677–1686, 2000.

[82] S. F. M. van Dongen, P. Maiuri, E. Marie, C. Tribet, and M. Piel. Triggering cell adhesion, migration or shape change with a dynamic surface coating. *Advanced Materials*, 25(12):1687–1691, 2013.

[83] S. P. Massia and J. A. Hubbell. An RGD spacing of 440 nm is sufficient for integrin $\alpha_v\beta_3$-mediated fibroblast spreading and 140 nm for focal contact and stress fiber formation. *Journal of Cell Biology*, 114(5):1089–1100, 1991.

[84] S. V. Graeter, J. Huang, N. Perschmann, M. López-García, H. Kassler, J. Ding, and J. P. Spatz. Mimicking cellular environments by nanostructured soft interfaces. *Nano Letters*, 7(5):1413–1418, 2007.

[85] T. W. Jensen, B.-H. Hu, S. M. Delatore, A. S. Garcia, P. B. Messersmith, and W. M. Miller. Lipopeptides incorporated into supported phospholipid monolayers have high specific activity at low incorporation levels. *Journal of the American Chemical Society*, 126(46):15223–15230, 2004.

[86] G. A. Hudalla and W. L. Murphy. Using "click" chemistry to prepare SAM substrates to study stem cell adhesion. *Langmuir*, 25(10):5737–5746, 2009.

[87] N. Orgovan, B. Peter, S. Bösze, J. J. Ramsden, B. Szabó, and R. Horvath. Dependence of cancer cell adhesion kinetics on integrin ligand surface density measured by a high-throughput label-free resonant waveguide grating biosensor. *Scientific Reports*, 4:4034, 2014.

[88] S. Aota, M. Nomizu, and K. M. Yamada. The short amino acid sequence Pro-His-Ser-Arg-Asn in human fibronectin enhances cell-adhesive function. *The Journal of Biological Chemistry*, 269(40):24756–24761, 1994.

[89] S. D. Redick, D. L. Settles, G. Briscoe, and H. P. Erickson. Defining fibronectin's cell adhesion synergy site by site-directed mutagenesis. *The Journal of Cell Biology*, 149(2):521–527, 2000.

[90] Y. Feng and M. Mrksich. The synergy peptide PHSRN and the adhesion peptide RGD mediate cell adhesion through a common mechanism. *Biochemistry*, 43(50):15811–15821, 2004.

[91] J. L. Eisenberg, J. L. Piper, and M. Mrksich. Using self-assembled monolayers to model cell adhesion to the 9th and 10th type III domains of fibronectin. *Langmuir*, 25(24):13942–13951, 2009.

[92] S. V. Wegner, F. C. Schenk, and J. P. Spatz. Cobalt(III)-mediated permanent and stable immobilization of histidine-tagged proteins on NTA-functionalized surfaces. *Chemistry - A European Journal*, 22(9):3156–3162, 2016.

[93] S. V. Wegner and J. P. Spatz. Cobalt(III) as a stable and inert mediator ion between NTA and His6-tagged proteins. *Angewandte Chemie - International Edition*, 52(29):7593–7596, 2013.

[94] W. Maret and B. L. Valle. Cobalt as probe and label of proteins. *Methods in Enzymology*, 226:52–71, 1993.

[95] H. E. Wart. Introduction of exchange-inert metal ions into enzymes. *Methods in Enzymology*, 158:95–110, 1988.

[96] M. D. Hall, T. W. Failes, N. Yamamoto, and T. W. Hambley. Bioreductive activation and drug chaperoning in cobalt pharmaceuticals. *Dalton Transactions*, pages 3983–3990, 2007.

[97] S. Shao, J. Geng, H. A. Yi, S. Gogia, S Neelamegham, A. Jacobs, and J. F. Lovell. Functionalization of cobalt porphyrin-phospholipid bilayers with his-tagged ligands and antigens. *Nature Chemistry*, 7:438–446, 2015.

[98] K. T. Thurn, E. M. B. Brown, A. Wu, S. Vogt, B. Lai, J. Maser, T. Paunesku, and G. E. Woloschak. Nanoparticles for applications in cellular imaging. *Nanoscale Research Letters*, 2(9):430–441, 2007.

[99] H. Zhang, C. Wang, B. Chen, and X. Wang. Daunorubicin-TiO_2 nanocomposites as a "smart" pH-responsive drug delivery system. *Internatioanl Journal of Nanomedicine*, 7:235–242, 2012.

[100] T. Rajh, L. X. Chen, K. Lukas, T. Lui, M. C. Thurnauer, and D. M. Tiede. Surface restructuring of nanoparticles: an effizient route for ligand-metal oxide crosstalk. *The Journal of Physical Chemistry B*, 106:10543–10552, 2002.

[101] P. D. Cozzoli, A. Kornowski, and H. Weller. Low-temperature synthesis of soluble and processable organic-capped anatase TiO_2 nanorods. *Journal of the American Chemical Society*, 125(47):14539–14548, 2003.

[102] R. W. Cheyne, L. Smith, T. A. D. Trembleau, and A. C. Mclaughlin. Synthesis and characterisation of biologically compatible tio$_2$ nanoparticles. *Research Letters*, 6(423), 2011.

[103] K. T. Thurn, T. Paunesku, A. Wu, E. M. B. Brown, B. Lai, S. Vogt, J. Maser, M. Aslam, V. Dravid, R. Bergan, and G. E. Woloschak. Labeling tio$_2$ nanoparticles with dyes for optical fluorescence microscopy and determination of tio$_2$-dna nanoconjugate stability. *Small*, 5(11):1318–1325, 2009.

[104] A. L. Linsebigler, G. Lu, and J. T. Yates Jr. Photocatalysis on TiO_2 surfaces: principles, mechanisms, and selected results. *Chemical Reviews*, 95(3):735–758, 1995.

[105] M. A. Henderson. A surface science perspective on TiO_2 photocatalysis. *Surface Science Reports*, 66(6-7):185–297, 2011.

[106] A. Fujishima, X. Zhang, and D. A. Tryk. TiO_2 photocatalysis and related surface phenomena. *Surface Science Reports*, 63(12):515–582, 2008.

[107] D. B. Hamal and K. J. Klabunde. Valence state and catalytic role of cobalt-ions in cobalt TiO_2 nanoparticle photocatalysts for acetaldehyde degradation under visible light. *The Journal of Physical Chemistry C*, 115(35):17359–17367, 2011.

[108] Q. He, Z. Zhang, J. Xiong, Y. Xiong, and H. Xiao. A novel biomaterial - Fe_3O_4:TiO_2 core-shell nano particle with magnetic performance and high visible light photocatalytic activity. *Optical Materials*, 31(2):380–384, 2008.

[109] C. Dette, M. A. Pérez-Osorio, C. S. Kley, P. Punke, C. E. Partick, P. Jacobson, F. Giustino, S. J. Jung, and K. Kern. TiO_2 anatase with a bandgap in the visible region. *Nano Letters*, 14:6533–6538, 2014.

[110] Y. Qin, L. Sun, X. Li, Q. Cao, H. Wang, X. Tang, and L. Ye. Highly water-dispersible TiO_2 nanoparticles for doxorubicin delivery: effect of loading mode on therapeutic efficacy. *Journal of Materials Chemistry*, 21(44):18003–18010, 2011.

[111] W. J. Geary, G. Nickless, and F. H. Pollard. The metal complexes of some azo and azomethine dyestuffs: Part I. Spectra in water, and dioxan/water in the wavelength range 320-600mμ. *Analytica Chimica Acta*, 26:575–582, 1962.

[112] W. J. Geary, G. Nickless, and F. H. Pollard. The metal complexes of some azo and azomethine dyestuffs: Part II. Determination of stability constants, and preparation of solid complexes. *Analytica Chimica Acta*, 27:71–79, 1962.

[113] K. A. McCall and C. A. Fierke. Colorimetric and fluorimetric assays to quantitate micromolar concentrations of transition metals. *Analytical Biochemistry*, 284(2):307–315, 2000.

[114] J. C. Barreto, G. S. Smith, N. H. P. Strobel, P. A. McQuillin, and T. A. Miller. Terephthalic acid: a dosimeter for the detection of hydroxyl radicals *in vitro*. *Life Sciences*, 56(4):89–96, 1995.

[115] K. Ishibashi, A. Fujishima, T. Watanabe, and K. Hashimoto. Quantum yields of active oxidative species formed on TiO_2 photocatalyst. *Journal of Photochemistry and Photobiology A: Chemistry*, 134(1-2):139–142, 2000.

[116] Y. Nosaka, S. Komori, K. Yawata, T. Hirakawa, and A. Y. Nosaka. Photocatalytic ·OH radical formation in TiO_2 aqueous suspension studied by several detection methods. *Physical Chemistry Chemical Physics*, 5(20):4731–4735, 2003.

[117] E. Baha-Schwab. *Directing osteogenic signaling and differentation by surfaces modified with adhesive proteins and immobilized bone morphogenetic protein 2*. Phd thesis, Heidelberg, 2015.

[118] Raymund W.M. Kwok. XPSPeak 4.1.

[119] G. E. Jellison Jr., L. A. Boatner, J. D. Budai, B. S. Jeong, and D. P. Norton. Spectroscopic ellipsometry of thin film and bulk anatase (TiO_2). *Journal of Applied Physics*, 93(12):9537–9541, 2003.

Eidesstattliche Versicherung

gemäß § 8 der Promotionsordnung der Naturwissenschaftlich-Mathematischen Gesamtfakultät der Universität Heidelberg

1. Bei der eingereichten Dissertation zu dem Thema **"Chemical modification strategies for the preparation of bioactive interfaces"** handelt es sich um meine eigenständig erbrachte Leistung.

2. Ich habe nur die angegebenen Quellen und Hilfsmittel benutzt und mich keiner unzulässigen Hilfe Dritter bedient. Insbesondere habe ich wörtlich oder sinngemäß aus anderen Werken übernommene Inhalte als solche kenntlich gemacht.

3. Die Arbeit oder Teile davon habe ich bislang nicht an einer Hochschule des In- oder Auslands als Bestandteil einer Prüfungs- oder Qualifikationsleistung vorgelegt.

4. Die Richtigkeit der vorstehenden Erklärungen bestätige ich.

5. Die Bedeutung der eidesstattlichen Versicherung und die strafrechtlichen Folgen einer unrichtigen oder unvollständigen eidesstattlichen Versicherung sind mir bekannt.

Ich versichere an Eides statt, dass ich nach bestem Wissen die reine Wahrheit erklärt und nichts verschwiegen habe.

Heidelberg, den 7th March, 2016

Franziska C. Schenk